THE IDENTIFICATION OF THE MECHANISMS OF LRBA DEFICIENCY DEPENDENT DEFECTS IN REGULATORY T-CELL FUNCTION

by

PEGAH ZAHEDIMARAM

Submitted to the

Graduate School of Engineering and Natural Sciences

in partial fulfillment of

the requirements for the degree of

Doctor of Philosophy

Sabanci University

July 2022

ABSTRACT

THE IDENTIFICATION OF THE MECHANISMS OF LRBA DEFICIENCY DEPENDENT DEFECTS IN REGULATORY T-CELL FUNCTION

Pegah Zahedimaram

Molecular Biology, Genetic, and Bioengineering, PhD Thesis, 2022

Thesis supervisor: Selim Çetiner

Keywords: lipopolysaccharide-responsive beige like anchor protein (LRBA), Cytotoxic T-lymphocyte-associated protein-4 (CTLA-4), CRISPR/Cas9, Biotinylation, Mass Spectrometry

Primary immunodeficiencies are a very diverse group of disorders characterized by recurring infections. Loss of function mutations in the gene encoding LRBA (lipopolysaccharide-responsive beige like anchor protein) were recently identified to cause PID which is associated with autoimmunity. Several studies have shown that the LRBA molecule regulates CTLA-4 cell surface expression. Besides CTLA-4, LRBA has been claimed to have an effect on the vesicular trafficking of epidermal growth factor receptor (EGFR) and cell surface expression of FasL in the plasma membrane.

In this study, the main objective was to discover the defects caused by LRBA deficiency in T-cells. For this purpose, the Jurkat leukemic T-cell line was used as the model cell line and the CRISPR/Cas9 system was used to knock-out (KO) this protein in the Jurkat cell line. The differentially expressed proteins on the surface of WT and KO Jurkat cells were assessed by the means of cell surface biotinylation coupled with mass spectrometry (MS) analysis. CD3, CD4, PVRIG, NOTCH3, CD1d, and Sema7A were found to be downregulated and CD53, CD148, CD154, CD134, A33, and CD70 to be upregulated in LRBA negative cell lines. We identify the decrease in CD3 and CD4 seemed to be most significant and relevant to the loss of LRBA. As expected, endogenous CTLA-4 expression was also decreased in our LRBA KO cell lines. Additionally, CTLA-4 protein overexpression could not rescue CTLA4 expression to WT levels in LRBA KO Jurkat

cell lines indicating the dominant phenotype obtained by LRBA loss. This study identifies alternative targets of the LRBA protein and delineates the mechanism of surface CTLA4 expression, potentially identifying new targets that can be used to cure immunodeficiencies resulting from LRBA loss.

ÖZET

DÜZENLEYİCİ T-HÜCRE FONKSİYONUNDA LRBA EKSİKLİĞİNE BAĞLI HATALARIN MEKANİZMALARININ BELİRLENMESİ

Pegah Zahedimaram

Moleküler Biyoloji, Genetik ve Biyomühendislik, Doktora Tezi, 2022

Tez Danışmanı: Selim Çetiner

Anahtar Kelimeler: lipopolisakkarit duyarlı bej benzeri çapa proteini (LRBA), Sitotoksik T-lenfosit ile ilişkili protein-4 (CTLA-4), CRISPR/Cas9, Biyotinilasyon, Kütle Spektrometrisi

Primer immün yetersizlik (PİY) sendromları tekrar eden enfeksyonlara neden olan hastalık grubudur. lipopolysaccharide-responsive beige like anchor protein (LRBA) proteinini kodlayan gendeki foksiyon kaybı mutasyonlarının otoimünite ile ilişkilendirilmiş PİY sendromlarına neden olduğu belirlenmiştir. LRBA molekülünün CTLA-4 proteininin hücre yüzeyindeki ifadesini kontrol ettiği belirlenmiştir. CTLA-4 proteini yanında LRBA proteininin epidermal büyüme faktörü reseptörü (EGFR) ve FasL proteinlerinin hücre yüzeyinde ifade edilmesini kontrol ettiği bilinmektedir.

Bu çalışmanın ana hedefi T lenfositlerde LRBA eksikliğinin yol açtığı bozuklukların keşfidir. Bu amaç ile Jurkat T lenfosit lösemi hücre hattı model olarak kullanılmış ve CRISPR/Cas9 sistemi aracılığı ile LRBA proteini bu hücrelerden silinmiştir. Mutant ve yabanıl tip Jurkat hücrelerinin yüzeyde ifade ettiği proteinlerdeki değişiklikler yüzey biyotinilasyonu ve kütle spektrometresi ile analiz edilmiştir. LRBA ifade etmeyen hücrelerin yüzeylerinde CD3, CD4, PVRIG, NOTCH3, CD1d, ve Sema7A proteinlerinin azaldığı ve CD53, CD148, CD154, CD134, A33, ve CD70 proteinlerinin de arttığı belirlenmiştir. LRBA kaybında CD3 ve CD4 proteinlerinin azalması en önemli fark olarak ortaya çıkmaktadır. Beklenildiği gibi endojen CTLA-4 proteininin yüze ifadesi de mutant hücrelerde azalmaktadır. Ek olarak CTLA-4 proteininin mutant hücrelerde yüksek seviyede eksojen olarak ifadesi, CTLA-4 yüzey seviyelerini yabanıl tip hücrelerdeki

seviyeye ulaştıramadığı da gözlemlenmiştir. Bu bulgu LRBA kaybının dominan bir fenotip olduğunu göstermektedir. Bu çalışma LRBA proteininin alternatif hedeflerini keşfetmiş ve CTLA-4 yüzey ifadesinin mekanizmasını ortaya çıkarmıştır. Yeni LRBA hedeflerinin bulunması bağışıklık sistemi bozukluğu hastalıklarının teşhis ve tedavisinde kullanılabilecektir.

To my dearest,

Navid

ACKNOWLEDGEMENTS

I would like to express my sincere gratitude to Professor Batu Erman for his thoughtful comments and recommendations on this dissertation. His faith in science has always paved the way to find better solutions and more professional answers to obstacles in our investigations. Learning to think the same way was always what I was trying to learn during my Ph.D., which I hope I have accomplished to some extent. I considerably recognize the help of Dr. Tolga Sütlü, that I started my Ph.D. in his lab, and the foundation of whatever I know about molecular biology was built in his lab.

I am so honored to have both as my supervisors. I have learned practical lessons not only in science but in life from them while witnessing how they stand for what they think is right, and I am so happy to be on their side as much as possible.

I would like to thank my committee members, Prof. Dr. Selim Çetiner, Dr. Christopher Mayack, and Dr. Ögun Adebali, for their valuable time, interest, and constructive suggestions.

I am so grateful to our collaborators at Marmaray university, Prof. Dr. Safa Bariş and Mehmet Cihangir Çatak, also Prof. Dr. Nurhan Özlu, Buşra Akarlar, and Ali Yurtseven from Koç university, for their contribution in MS data acquisition and analysis.

I was so lucky to make the best friends during my Ph.D. that each of them profoundly affected my research in different ways. I want to specially thank Dr. Sarah Barakat my dearest sister and friend for all her physical and mental help during the most difficult parts of my Ph.D., also Ecem Ultanir for her direct help in this project, and all our current and previous lab members, Dr. Görkem Odabaş, Dr. Sinan Öcal, Melike Gezen, Buşra Şimşek, Alp Ertunga Eyupoğlu, İzem Devecioglu, Ege Ezen, Mustafa Tunçay, Berkay Engin, Canberk Yeşilada, Selen Balkan, Dr. Sofia Piepoli, Gülin Baran, Melike Berksöz, Seden Bedir, Liyne Noğay, Hasan Güneş Diridiri. My dear friends in Sutlu lab group, Mert Kaya Aras, Elif Çelik, Ebru Zeynep Ergün, Zeynep Sena Karahan, Gözde Özcan, Dr Başak Ozata, Dr. Didem Özkazanç, Dr. Cevriye Pamukçu, Dr. Ayhan Parlar, Dr Esen Doğan, Dr. Ece Canan Sayitoğlu, Lolai Ikromzoda, and Aydan Saraç. My research and lab work were more productive, efficient, and enjoyable with their support and assistance.

My dearest Navid, my love, friend, and husband, earns the most memorable thank you for his never-ending support. He has always been the source of my energy and motivation

in difficult and challenging moments. His wisdom has been a great help in dealing with tight spots. He is the miracle of my life, and I feel so proud and lucky to have him in my life.

I have the best parents ever, Maman Goli and Baba Mohammad Azize ghalbam, that always have been there for me, and their pure love and kindness have always been my motivation to go on no matter what. I also like to thank my parents-in-law, Maman Soosan and Baba Mohammad Joon, for their love and warm words whenever I needed them. I also appreciate the support of my brother and sister, Pedram and Setareh Joon, and all other family members who have encouraged me in my life and career.

I will never forget the joyful memories of my friends: Naeimeh Rajabalizadeh, Arash Ebrahimi, Meysam Rafiei, Mahsa Nourani, Negar Farhadi, Ehsan Khoshniat, Nasim Barzegar, Faraz Tehranizadeh, Mehri Ahmadian, Ali Azizi, Ali Asgharpour, Ali Barzegar, Sina Rastani, Deniz Mortazavi, Asal Ghaffari, Amin Ahmadi, Sirous Khabbaz, Araz Sheibani, Pozhhan Mokhtari, Zohreh Aliabadi, Mohammad Dabbagh, Kaveh Rahimzadeh, Amin Bagherzadeh, Yasaman Karimian, Saeedeh Ahmadi, and Madine Rastgoo, I am grateful to them for all fun memories they made for me.

This study was supported by The Scientific and Technological Research Council of Turkey with the grant number: 318S202.

Table of Contents

LIST OF FIGURES

LIST OF TABLES

LIST OF SYMBOLS AND ABBREVIATIONS

α	Alpha
β	Beta
μ	Micro
A	Amper
Ab	Antibody
AKAP	A kinase anchor protein
ALPS	Autoimmune Lymphoproliferative Syndrome
Amp	Ampicillin
AP1	Activator Protein 1
Arf	ADP-ribosylation factor)-1
BCL-6	B-Cell Lymphoma 6
BDCP	BEACH domain-containing proteins
BEACH	Beige and Chediak-Higashi
BGL	Beige-Like Protein
bp	Base pair
Cas	CRISPR-associated
CCR7	C-C Motif Chemokine Receptor 7
CD	Cluster of Differentiation
CHAI	CTLA-4 Haploinsufficiency with Autoimmune Infiltration
CHS	Chediak-Higashi syndrome
Con-A	Concanavalin A-like
CRISPR	Clustered Regularly Interspaced Short Palindromic Repeats

CTLA-4	Cytotoxic T-Lymphocyte Antigen-4
CVID	Common Variable Immunodeficiency
CXCR5	C-X-C chemokine receptor type 5
DBD	DNA Binding Domain
DC	Dendritic Cell
DMEM	Dulbecco's Modified Eagle Medium
DMSO	Dimethylsulfoxide
DNA	Deoxyribonucleic Acid
DSB	Double Strand Break
DUF1088	Unknown Function 1088
E. Coli	Escherichia Coli
EGFR	Epidermal Growth Factor Receptor
ERK1/2	Extracellular Signal-Regulated Kinases
FBS	Fetal Bovine Serum
FOXP3	Forkhead Box P3
GC	Germinal Cell
GFP	Green Flourescent Protein
GO	Gene Ontology
GOF	Gain of Function
h	Hour
HBS	HEPES-Buffered Saline
HDR	Homology-Directed Repair
ICOS	Inducible T-cell Costimulator
IFN-γ	Interferon-γ
IL-4	Interleukin-4
indel	Insertion Deletion
IRF4	Interferon Regulatory Factor 4

Kan	Kanamycin
KEGG	Kyoto Encyclopedia of Genes and Genomes
KO	Knock Out
LATAIE	LRBA deficiency with autoantibodies, Treg defects, autoimmune infiltration, and enteropathy
LB	Luria Broth
LRBA	Lipopolysaccharide responsive beige-like anchor protein
min	Minute
mRNA	Messenger RNA
NHEJ	Non-Homologous End Joining
NK	Natral Killer cell
NKG2D	Natural Killer Group 2D
NLS	Nuclear Localization Signal
OD	Optical Density
PAM	Protospacer Adjacent Motif
PBS	Phosphate Buffered Saline
PC	Plasma Cell
PCR	Polymerase Chain Reaction
PD-1	Programmed cell death protein 1
PH	Pleckstrin homology
PRDM1	B lymphocyte-induced maturation protein-1
qPCR	quantitative polymerase chain reaction
Rab	Ras-associated binding
RNA	Ribonucleic Acid
RNA-Seq	RNA Sequencing
RT-PCR	Reverse transcription polymerase chain reaction
SDS-PAGE	Sodium Dodecyl Sulfate Polyacrilamide Gel Electrophoresis

TALEN	Transcription Activator-Like Effector Nuclease
TCR	T-Cell Receptor
Tfh-cell	T-follicular helper cell
Th- cell	T-helper cell
WD40	Tryptophan and aspartic acid repeats
WDFY3	WD and FYVE zinc finger domain containing protein 3
WT	Wild Type
ZF	Zinc Finger

1. INTRODUCTION

1.1. Lipopolysaccharide responsive beige-like anchor protein (LRBA) gene discovery

Lipopolysaccharides are bacterial antigens that induce B lymphocytes that promote B cell maturation and release of inflammatory cytokines. A gene-trapping method was used to discover new genes involved in immune cell maturation, which led to the identification of several LPS-responsive genes. [1]

Chediak-Higashi syndrome (CHS) patients suffer from a severe kind of immunodeficiency which is characterized by advanced neurologic dysfunction, hypopigmentation, and a bleeding sensitivity. These patients have distinct defects in the function of immune cells, including T cell cytotoxicity, NK cell killing, granulocytes function, and monocyte chemotaxis. CHS and beige (the name for the CHS disease in mice) lysosomes exhibit abnormalities in protein sorting. Moreover, CHS patients' T cells or beige macrophages lack regular CTLA-4 and class II surface expression, respectively [2,3,4].

cAMP-dependent protein kinase A (PKA) consists of two catalytic and two regulatory subunits. As AKAPs and their R binding sites do not share any sequence homology, their functions differ but their structures do not. The RI and RII binding sides of the amphipathic helix, created by AKAPs and PKA, bind together through the hydrophobic pocket built by two subunits of PKA. By doing so, cAMP activates PKA, releasing its subunits and phosphorylating substrates at a specific subcellular location. Subcellular structures associated with AKAPs include dendrites, vesicles, endoplasmic reticulum, mitochondria, plasma membranes, and nuclear membranes [5,6].

Lipopolysaccharide responsive beige-like anchor protein (LRBA), identified as a novel LPS-inducible gene in mice and humans, which has homology to the domains of the chs1/beige and AKAP genes [7]. It has been determined that the murine Lrba gene has a high degree of similarity to a human partial cDNA sequence, Beige-Like Protein encoding

cDNA (BGL), which has 7.3 kb. Other cDNA sequences were obtained from human lung, brain, and kidney cDNA libraries [7].

1.2. LRBA characteristics

LRBA is a member of the WDL-BEACH-WD40 (WBW) gene family that can physically associate with different vesicular compartments in cells [7].The gene that encodes this protein is found on human chromosome 4q31.3 and consists of 750,839 bp separated by 58 exons. The protein has a molecular mass of 319 kDa and contains 2,863 amino acids, which is the only described isoform, and other isoforms are mapped computationally in Fig.1-1. The sequence analysis of LRBA cDNA from a mouse B lymphocyte library indicated that there are three distinct transcripts of 9903, 9396, and 8854 bp encoding lrba-α (2856 aa), lrba-ß (2792 aa), lrba-ɣ (2779 aa), respectively. Based on homology search all these isoforms have BEACH domain while lba-α has 5 WD repeats, lba-ß has 3 WD repeats and lba-ɣ misses the WD repeats. The same study experimentally showed that the expression level of the three transcripts were different in the cell lines and tissues of their study, concluding that these different transcripts may have diverse functions in specific tissues [7].

By reverse transcription polymerase chain reaction (RT-PCR) and quantitative polymerase chain reaction (qPCR), transcripts of this protein have been detected in lymph nodes, bone marrow, spleen, fetal liver, placenta, kidney, and pancreas. In functional studies, lipopolysaccharides (LPS), which are carbohydrate-linked lipids derived from Gram-negative bacteria's outer membranes and cells walls, are observed to trigger LRBA expression. The innate immune system recognizes LPS as a harmful agent and responds accordingly. The expression of LRBA in several cancer tissues increases significantly when LRBA is involved in this LPS-dependent innate immune response [7,8].

In a northern-blot analysis of LPS-stimulated murine macrophage cell line RAW264, LRBA mRNA was detected using a probe directed against the LRBA BEACH domain. Furthermore, in the same cell line, using electron microscopy, LRBA was seen in the endoplasmic reticulum, plasma membrane, clathrin-related endocytic vesicles, and nucleus [7]. These findings imply that LRBA plays a role in innate immune responses and by multiple functions in different subcellular regions of the cell. Likely different domains

of this large protein are responsible for different functions, most of which have not been identified.

1.3. Protein domains and structure of LRBA

Domains within proteins are structural and/or functional units. A specific interaction or function is usually assigned to them. A protein's function is often predicted by analyzing its domains. When larger groups of proteins share the same domain(s), hypotheses about their functions can be generated.

LRBA has several domains, the most well-studied of which is the BEACH domain (beige and Chediak-Higashi). This domain, which is made up of 280 amino acids, is conserved in several proteins collectively known as BEACH domain-containing proteins (BDCP) and is mostly found near the C-terminus (Fig.1-2) [9]. The BDCPs also contain the ConA-like domain (concanavalin A-like), the PH domain (Pleckstrin homology), and the WD40 domain (tryptophan and aspartic acid repeats). There is a common DUF1088 domain between LRBA and the paralog neurobeachin (NBEA), suggesting that these two proteins may have unique functions not found in other members of the BDCP (Fig. 1-2) [10]. A protein called neurobeachin (Nbea) controls membrane protein trafficking at the tubulovesicular endomembrane and at the postsynaptic plasma membrane. It is unknown what role Nbea plays in the central nervous system, although it is required for induced transmission at neuromuscular junctions [11].

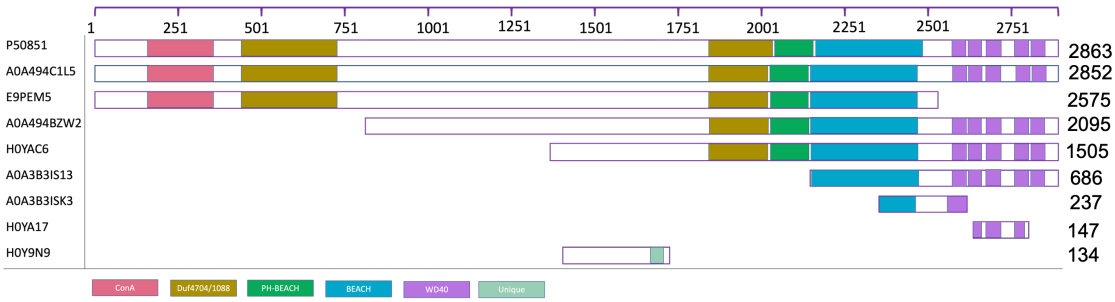

Figure 1-1. Isoforms of the LRBA protein. Isoform alignment and the specific domains they cover. Isoform with 2863 amino acids is the only described one, and the rest are predicted computationally. The numbers next to the sequences indicate the number of amino-acids.

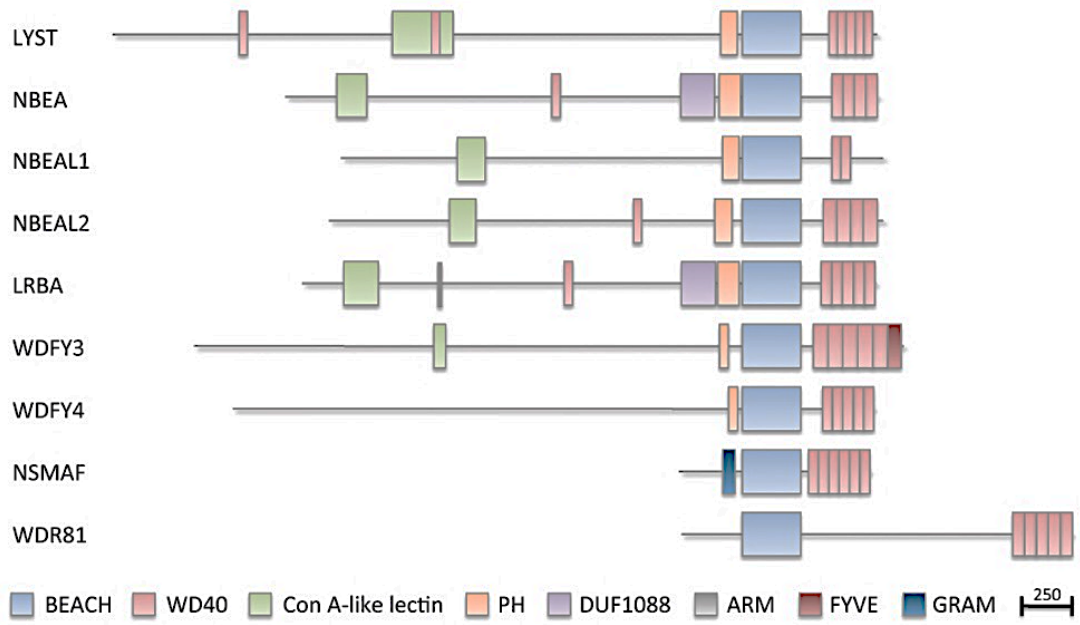

Figure 1-2. Schematic representation of protein domains that exist in human BDCPs. The alignment of BEACH domain and other known domains, including ConA like lectin, DUF1088, ARM, FYVE, and GRAM in all nine BDCPs. LYST: lysosomal trafficking regulator, NBEA: neurobeachin, NBEAL: neurobeachin-like, WDFY: WD and FYVE zinc finger domain containing protein, NSMAF: neutral sphingomyelinase activation-associated factor, WDR81: WD repeat domain 81[9] .

1.3.1. BEACH domain

LYST (lysosomal trafficking regulator) has a conserved 'BEACH' domain that is mutated in Chediak–Higashi syndrome (CHS). Beige refers to the CHS mouse model and CH is an acronym for Beige and Chediak-Higashi [12]. A BEACH domain has also been identified in eight other human proteins (Fig.1-2). Repeats of the WD sequence often follow or precede Beach domains, lectin binding domains resembling concanavalin A, and PH-like domains [9].

As a result of their insufficient length, several hydrophobic segments in BEACH do not meet the standard criteria for being classified as b-strands. Proteins with the BEACH are located at the C-terminus (Fig.1-2). One large insertion can be seen between the BEACH domains of LYST and other members of the family [9,13].

1.3.2. PH domain

It should also be noted that many BDCPs have a PH domain that is a 100 amino acid stretch right before the BEACH domain region (Fig.1-2) [14]. PH domains are found in a wide variety of proteins implicated in intracellular signaling or forming part of the cytoskeleton. A PH domain can bind to biological membranes through phospholipid binding , and some PH domains can bind proteins as well[15,16]. It may be possible that PH domains enable their host proteins to target the cytosolic surface of membranes, which allows them to be localized to the appropriate compartment within the cell. The three-dimensional structures of PH domains in some proteins are remarkable due to their low sequence homology, but their sequence homology in some proteins may make them difficult to identify [17].

In studies of PH-like and BEACH domains in NBEA 18 or LRBA 13 amino acid segments, the PH-like domains had a similar fold to classical PH domains and were strongly interacted with their BEACH domains. According to these studies, NSMAF has a PH-like domain that precedes the BEACH domain, and one or both of these domains may function as one. Fig.1-2 shows that NSMAF contains a membrane-associated domain called GRAM, not PH. A BDCP BEACH/PH-like domain is hypothesized to interact with a partner (possibly a peptide segment). It appears that some PH-like domains in BDCPs don't have a strong affinity for phospholipids due to structural blocks at the binding site. They lack positively charged side chains on their surfaces that may be needed to bind the highly negatively charged phospholipids [17,18,13]. The biochemical analysis of LRBA and NBEA 13 revealed that there is no binding between phospholipids and their PH-BEACH domains, but NSMAF binds them.

1.3.3. WD Domains

A WD40 repeat (also known as a WD or β-transducin repeat) is a 40-amino acid structural motif that frequently ends in a tryptophan and aspartic acid (W- D) dipeptide. A WD protein domain is formed by combining several of these repeats. WD-containing proteins contain 4–16 repeating units that are thought to form a circularized -propeller structure,

though WD domains containing fewer than seven WD40 repeats may be less stable. WD-repeat proteins are involved in a wide range of cellular functions, including cell cycle regulation, transcription regulation, signal transduction, autophagy, and apoptosis. Among the familiar application of WD-repeat proteins, vesicle trafficking is the most important [19,20]. These proteins are considered multiprotein complex assembly coordinators, with WD domains acting as a scaffold for heteromeric protein involvement. PH and WD domains are frequently found together in the same protein or as binding partners. The sequences outside the repeats determine the specificity of the WD-repeat proteins [17].

1.3.4. Concanavalin A-like lectin binding domain

Six of the nine BDCPs have a Concanavalin A (ConA)-like lectin domain, though the instance in LYST is difficult to identify because of a huge (WD40 domain) insertion (Fig.1-2). Lectins bind carbohydrates, and the ConA-like lectin domain is found in a wide domain of proteins with small series of similarity and a wide range of functions. It was proposed that the ConA-like lectin domain in BDCPs may be involved in oligosaccharide binding related to protein crowd and organizing in parallel to the secretory pathway, particularly in relation to vesicle fusion machinery components [14].

1.4. Function of the LRBA protein

1.4.1. LRBA Function and LRBA deficiency in immune check point signaling

By haphazardly placing genes and somatically mutating them, the immune system can distinguish specific molecular structures within pathogens, providing long-term protection against recurrence. This receptor diversity process, however, creates lymphocytes that react to self-antigens. In order to control these auto-reactive cell clones, two main mechanisms have been developed: The first is called central tolerance, which involves removing self-reactive B and T cells from the bone marrow and thymus.

Peripheral tolerance involves eliminating self-reactive immune cells that bypass central tolerance. After an immune response against a pathogen has been initiated, peripheral tolerance also plays an important role in maintaining immune homeostasis, a balance of

costimulatory and inhibitory signals (also called immune checkpoints) that determines the durability of the T cell immune response. Invading pathogens or self-antigens can cause tissue damage, autoinflammatory and autoimmune diseases if an immune response is not controlled. Genetic mutations have been linked to a number of immunodeficiency and immune dysregulation syndromes [21].

The CTLA-4 receptor protein is found on the plasma membrane of activated T cells. By binding to CD86 and CD80 on the surface of antigen-presenting cells instead of CD28, which is a costimulatory molecule, it regulates homeostasis and peripheral immunological tolerance [22]. CTLA-4 is found first in intracellular compartments like the Golgi apparatus, endosomes, secretory granules, and lysosomes. CTLA-4 migrates to the cell membrane after TCR activation, but is continuously endocytosed via clathrin-coated vesicles. In lysosomes, CTLA-4 molecules are rapidly degraded after endocytosis [23,24]. CTLA-4 has two tyrosine motifs in its cytoplasmic tail, Y201VKM and Y218FIP. There are two intracellular proteins called AP-1 and AP-2 that bind to the Y201VKM motif (clathrin-associated adapter). The AP-2 protein mediates CTLA-4 internalization from the cell surface to endosomes and lysosomes, while AP-1 controls its trafficking from the Golgi apparatus to endosomes and lysosomes [23]. CTLA-4 vesicular trafficking to the plasma membrane is dependent on LRBA, according to a study. By maintaining intracellular CTLA-4 levels for immediate mobilization to the surface membrane, LRBA maintains intracellular levels (Fig.1-3). CTLA-4 degradation in lysosome compartments is accelerated when LRBA is lacking, resulting in decreased levels both intracellularly and on the surface [25].

Finally, silencing AP-1 but not AP-2 partially rescues the loss of CTLA-4 in LRBA deficient cells by interacting with CTLA-4's cytoplasmic tail, specifically the Y201VKM motif [25]. Foxp3 + CD4 + cells from LRBA-deficient mouse spleens have lower CTLA-4 levels [26]. In Hela and Jurkat cells transduced with CTLA-4, CTLA-4 was found in several compartments marked by Rab5, Rab7, and Rab11. Inhibiting dominant-negative Rab5 increased CTLA-4 surface expression while reducing internalization and degradation. Also, it was discovered that constitutively active Rab11 increased CTLA-4 surface expression, while DN Rab11 decreased it, suggesting CTLA-4 is similar to recycling receptors like EGFR. A study of CTLA04 trafficking revealed that LRBA deficiency significantly impaired CTLA-4 recycling and degradation in Jurkat cells, which was not

corrected by expressing CA Rab11. Further, CTLA-4 co-localization with Rab11 decreased when LRBA was lacking, suggesting LRBA is upstream of Rab11 and is required to deliver CTLA-4 to Rab11 recycling compartments. [27].

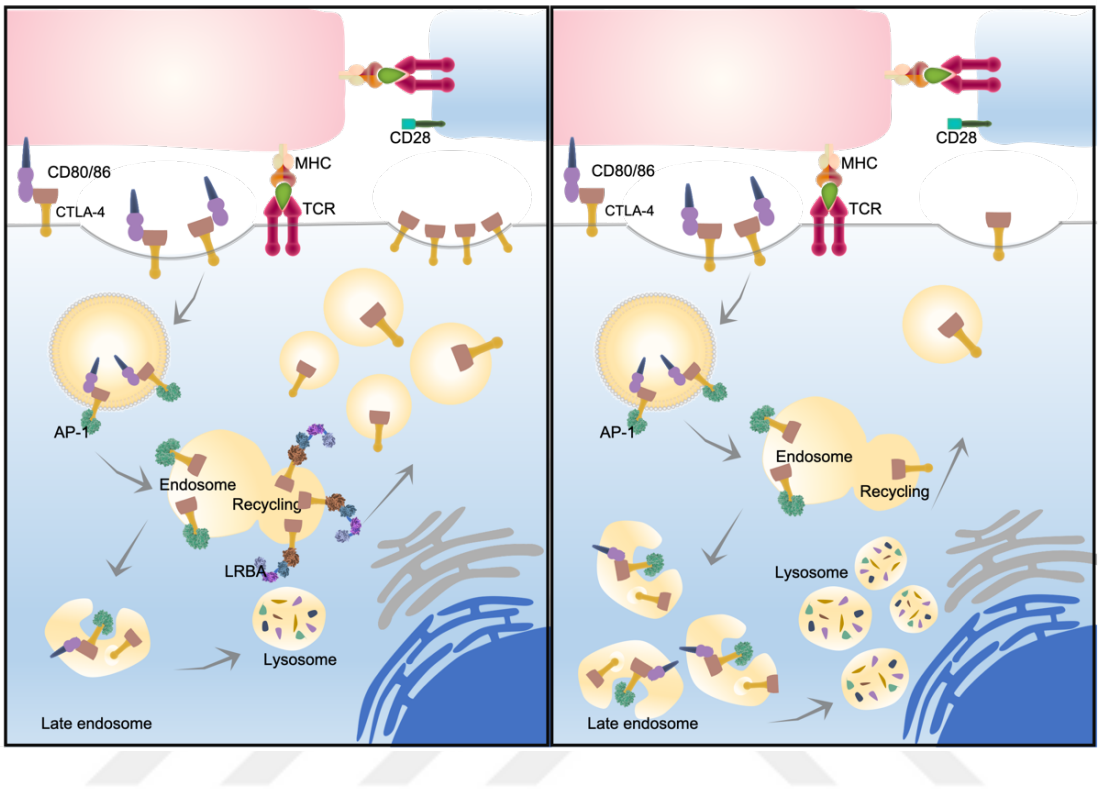

Figure 1-3 LRBA regulates CTLA-4 recycling to the cell surface. LRBA and AP-1 proteins have been discovered to bind to CTLA-4's tail, which results in different fates for CTLA-4. LRBA may direct CTLA-4 recycling to the plasma membrane, whereas AP-1 may facilitate CTLA-4 trafficking to lysosomal compartments, where it is degraded.

1.4.2. LRBA deficiency and T helper cells distribution

From naive precursors, there are distinct subsets of effector CD4+ T cells that can be distinguished by their expression of various transcription factors, production of certain cytokines, and the functions of specific effectors that facilitate the clearing of pathogenic threats and reinforce the ability of the mammalian immune system to generate robust, efficient, and specific immunity [28]. IL-4, IL-5, and IL-13 are produced by Th1 cells, which protect the host against intracellular bacterial and viral infections; Th17 cells produce IL-17A, IL-17F, IL-22, IL-26, and CCL20 and play a big role in immunity against fungi and bacteria [29]. A distinction between immune responses is immunological memory, which is accomplished by generating long-lived plasma cells (PCs) and memory B cells that

produce high-affinity antibodies (Abs) continuously or when the initiating pathogen is reintroduced. As a result, they neutralize and/or eliminate infectious pathogens, preventing severe and recurring diseases [30–32].

In response to foreign Ags, germinal centers (GCs) form transiently in secondary lymphoid tissues, where they make long-lived PCs and memory B cells. It's caused by cognate interactions between Ag-specific B cells, CD4+ T cells, and accessory cells, which cause responding B cells to grow and change their Ig genes. Memory B cells or PCs can only differentiate from GC B cells that compete for Ag, cell-cell interactions, and cytokines provided by CD4+ T cells, dendritic cells (DCs), and follicular DCs [30,32–34]. This kind of serological memory can protect the host for a long time, even forever [35]. In order to ensure high-affinity B cells, differentiation of activated B cells into memory cells and PC, and quantity and quality of the Ab response, CD4+ T cell assistance is crucial at different stages of GC reactions. The CD4+ T cells involved in this process are called T follicular helper cells (Tfh). Tonsil Tfh cells are CD4+ T cells that express the B cell zone homing chemokine receptor CXCR5 but not the T cell zone chemokine receptor CCR7 [36,37].

Instead of CXCR5 expression, Tfh cells have features like the transcriptional repressor BCL-6, the cytokine IL-21, the chemokine CXCL13, and a group of molecules involved in T cell/B cell interaction — CD40L, ICOS, SLAM receptors, SAP, and PD-1. By coordinating and regulating chemokines, chemokine receptors, cytokines, and cognate receptor/ligand pairs, Tfh cells are exactly positioned within B-cell follicles and GCs to provide survival and helper signals for B cell differentiation. IL-21 is the most common B-cell helper cytokine derived from Tfh. In fact, IL-21 activates key transcriptional regulators such as BCL6, PRDM1 (encoding Blimp1), XBP1, and IRF4 in human and murine B cells, resulting in proliferation, Ig class switching, and PC differentiation. In the peripheral blood of healthy donors, there are also circulating Tfh (cTfh) cells that are CD4+CXCR5+ memory T cells. A number of key differences exist between cTfh cells and genuine Tfh cells in secondary lymphoid tissues (e.g., cTfh cells express less Bcl-6, ICOS, and PD-1), but it is widely accepted that cTfh cells function and develop like Tfh cells [37].

CXCR3+CCR6- PD-1hi IFN+ cTfh1 were also significantly elevated in patients with LRBA deficiency and CTLA4 haploinsufficiency. A biomarker of

autoimmunity/inflammation, soluble CD25, positively correlated with cTfh cell proportions in LRBA-deficient patients, while CTLA4 expression on Tregs was inversely correlated with cTfh proportions in either genotype and healthy donors. [38,39]. In order to limit human Tfh cell differentiation (Fig.1-4.B), CTLA-4 expression must be intact. Abatacept (soluble CTLA-4 Fc, which blocks the interaction between B7 and CD28, which reduces immune cell activity) is another evidence for this finding for people with LRBA or CTLA-4 deficiencies. As a result of his treatment, the proportion of cTfh cells and PD-1 expression decreased significantly in cases without a severe and prolonged disease course [39]. There's a link between chronic inflammation and abnormal T helper cells, particularly Th1, Th17, and Th22 cells. Also, an imbalance between anti-inflammatory (e.g., IL10) and pro-inflammatory (e.g., IL10) cytokines can lead to immune homeostasis dysregulation and autoimmune and inflammatory diseases.[40]. As a result of Treg cells' profound lack of CTLA4 expression, patients with LRBA deficiency have dysregulated T follicular helper (TFH) cells (a phenotype associated with autoimmune diseases). There's no intrinsic abnormality in TFH cells in LRBA deficient patients, but rather Treg cells fail to control TFH cells' differentiation and suppress effector T cells. Aside from impressing effector T cells with CTLA4, Tregs also produce immunosuppressive cytokines like TGF, IL35, and IL10 [37,40].

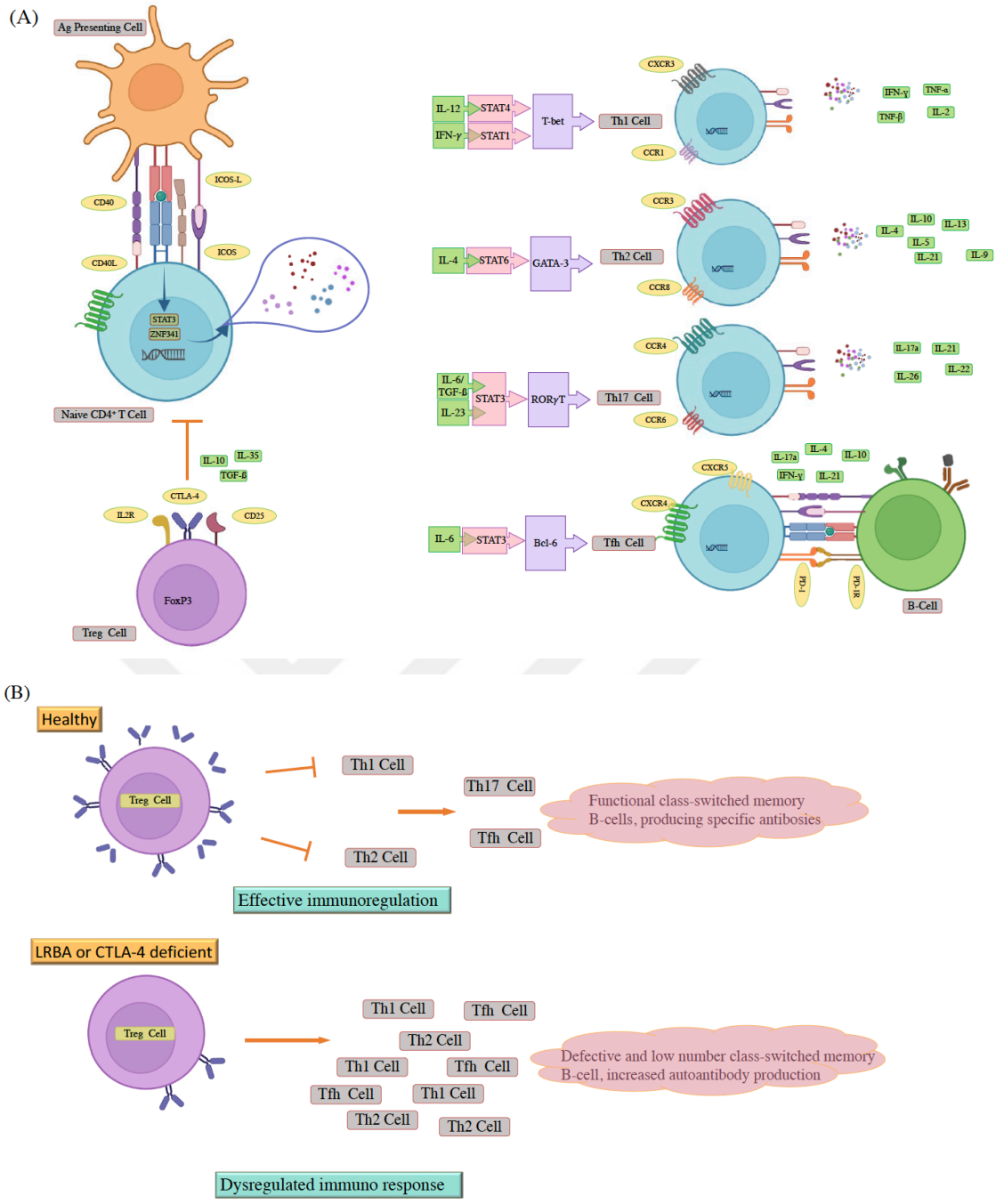

Figure 1-4. Tfh cell differentiation and functionally distinct subset specialization. A) After interacting with APC, naive CD4+ cells are stimulated for differentiation into Th1, Th2, Th17, Tfh, and Treg cells. Tfh cells provide helper signals for cognate B cell differentiation into long-lived memory B cells or Ig-secreting plasma cells. B) High expression of CTLA-4 in Treg cells leads to a low frequency of Tfh cells and control of autoimmunity, while low expression of CTLA-4 results in a high number of Tfh cells and autoimmunity.

1.4.3. LRBA effect on endosomal trafficking

Other studies support the idea that LRBA plays a role in vesicular trafficking in addition to CTLA-4. In dominant negative LRBA mutants, EGFR expression and phosphorylation were reduced, which is expressed in a wide range of tissues and interacts with EGF, TGF, and other ligands. Phosphorylation of this receptor activates signaling pathways for proliferation, differentiation, cell growth, migration, and apoptosis prevention [8]. As with CTLA-4 in lymphocytes, expression of EGFR on the cell surface is regulated by clathrin-mediated endocytosis, which either destroys it or recycles it. Inhibitions to this receptor's vesicular trafficking lead to abnormal localization, increased signaling, and cancer [41]. There's no evidence that LRBA and EGFR physically interact, but AP-2 facilitates endocytosis and EGFR trafficking via endocytic pathways [42].

In LRBA deficient patients, apoptosis mediated by Fas was decreased [43]. By binding to Fas ligands, Fas receptors induce apoptosis via the extrinsic pathway (FasL), which leads to FasL internalization, like EGFR, which triggers apoptosis. The plasmatic level of FasL in LRBA-deficient patients isn't known, but elevated serum FasL in these patients suggests that LRBA deficiency, like CTLA-4, could affect FasL's trafficking to the plasmatic membrane or lysosomes [44].

In mice lacking LRBA, ERK1/2 and AKT are phosphorylated poorly in natural killer (NK) cells stimulated with anti-NKG2D or anti-NKp46 antibodies, resulting in a significant decrease in IFN-gamma production. This study didn't determine the expression levels of these receptors in LRBA-deficient mice, but there's some evidence that NKG2D and DAP10 may get degraded after exposure to certain ligands, and clathrin may help [45,46,47].

It's not clear how LRBA modulates cellular receptors, despite these studies. The transport seems to be through clathrin-coated vesicles, from which the receptors are released into early endosomes, where they're either degraded by lysosomal enzymes or recycled to the cell surface. This type of trafficking is thought to require AP-1. By binding to Arf-1 (ADP-ribosylation factor)-1 and more specifically to Arf-6 in recycling endosomes, and other protein complexes, AP-1 is found in the Golgi apparatus and endosomes. The recycling of receptors is also dependent on vesicular compartments and their proteins,

such as Arf, phospholipase D, and Rab. This and another study mention earlier suggest that Rab11 and Bchs might control vesicle trafficking in Drosophila [27,48].

1.4.4. LRBA role in autophagy

As a lysosomal degradation mechanism, autophagy destroys damaged organelles and microorganisms, then recycles macromolecules. This process creates a double membrane phagophore near the target, which elongates and surrounds it to mature with the assimilation of a cytosolic charge later, forming the autophagosome. In order for autophagosomes to form an amphisome, they need to be fused with early or late endosomes. By fusing with lysosomes, mature autophagosomes degrade their contents with lysosomal proteases and hydrolytic enzymes [49].

It has been shown that several LRBA homologous genes are associated with autophagy. The protein encoded by WDFY3 (WD and FYVE zinc finger domain containing protein 3) colocalizes with markers associated with autophagosomes [50]. In addition, P62 interacts with the PH-BEACH domain as well [51]. A protein known as P62 occurs at autophagosome formation sites and interacts with proteins such as LC3 (microtubule-associated protein 1A / 1B-light chain 3) and ubiquitinated proteins. It has been shown that LC3 can be recruited to the autophagosome membrane by conjugating it with phosphatidylethanolamine, thus promoting autophagic influx [49]. As a result of immortalizing B cells from LRBA deficient patients, we were able to determine that starvation resulted in a significant reduction in autophagy influx, as well as an increased Golgi apparatus, autophagosome accumulation, and centrioles when compared to healthy cells [52]. It is possible that LRBA is found in endocytic vesicles, thereby facilitating the fusion of autophagosomes and late endosomes, leading to the formation of the amphisome, considering that both cell surface receptor trafficking and autophagy require endocytic vesicles as well. In a similar way to CTLA-4, LRBA is believed to compete with clathrin adapter proteins in lymphocytes in order to regulate autophagy in lymphocytes [10]. There is also an interaction between LRBA and LC3 in silico [53].

1.4.5. LRBA role in apoptosis

Cells undergo apoptosis as a way to regulate their growth and development. At one time, it was believed that caspases were proteases that executed apoptosis. However, now it has been discovered that partial destabilization of the lysosomal membrane, along with the release of hydrolytic enzymes, can activate caspases to initiate and complete apoptosis [54,55]. There is evidence that lysosomal destabilization contributes to apoptosis in germinal centers derived from tonsils [55]. As a result of increasing lysosomal damage in these cells, caspase 8 cleavage occurred in the cytoplasm, as well as the DNA being cleaved by cathepsin B. P53 caused lysosomal destabilization and negatively regulated the promoter of LRBA [8]. As a tumor suppressor gene, P53 encodes a nuclear transcription factor that either facilitates DNA repair or induces apoptosis [56]. The possibility exists that if p53 did not have LRBA, lymphocytes might apoptose in the absence of LRBA. Although we do not know exactly how p53 causes lysosomal destabilization or LRBA prevents apoptosis, we know that autophagy and apoptosis play an important role in cell fate. Under certain conditions, autophagy can assist cells in surviving and preventing apoptosis [57].

As a result of increasing autophagy, for example, we are able to make cells survive in the absence of nutrients and growth factors by inhibiting apoptosis. It has been proposed that autophagy occurs because the autophagosome damages the mitochondria, which prevents cytochrome C from reaching the cells. In other cases, autophagy may result in cell death, either dependently or independently of apoptosis. There are also some proteins that act both as autophagy triggers and as apoptosis [57]. As a result of the cleavage of proteases, these autophagic proteins either positively or negatively regulate mitochondrial apoptosis [15]. Apoptosis and autophagy defects have been observed in LRBA-deficient cells. This phenotype may be caused by changes in mitochondrial clearance or increased protease cleavage.

1.5. LRBA deficiency as a primary immune deficiency disease

Primary immunodeficiencies are a very diverse group of disorders that are generally inherited in a Mendelian pattern. According to recent reports, LRBA defects are one of the most common autosomal recessive defects causing common variable immunodeficiency (CVID), and they are also implicated in autoimmune

lymphoproliferative syndrome (ALPS)-like (ALPS-like) disease [58]. Because LRBA plays an important role in modulating the expression of CTLA-4 on the surface of cells, it is known that LRBA deficiency causes a loss of regulatory T cells (Tregs). A complicated disease called LATAIE (LRBA deficiency with autoantibodies, Treg defects, autoimmune infiltration, and enteropathy) is very rare. As with CHAI (CTLA-4 Haploinsufficiency with Autoimmune Infiltration), LATAIE is caused by heterozygous, deleterious mutations in the CTLA4 gene that are deleterious. There is a higher incidence of this disease at younger ages, and it usually appears at a younger age [59].

According to a systematic review of data collected from different publications, 102 patients initially showed signs of autoimmunity and 27% had chronic diarrhea, based on the data collected. The majority of patients were diagnosed with common variable immunodeficiency (43%), or autoimmune disorders (28%) as their primary diagnoses [60]. There were fewer switched-memory B cells and plasmablasts in most patients, but CD21low B cells were higher in 78% of patients. T-cell counts were normal in 80% of patients, but Treg count decreased in 66%. As a result of this review, it is confirmed that patients with LRBA deficiency have abnormal B-cell counts, mostly switched-memory B cells and plasmablasts. CD4+ and CD8+ cell numbers were significantly reduced in 22% of patients and 11% of them.ctively.

A patient with LRBA deficiency may experience different symptoms and complications even when more than one family member has the same mutation. In LRBA deficiency, no genotype-phenotype correlation has been found (except for severe mutations and enteropathy), meaning that there may be unknown modifier genes or environmental factors that determine or influence phenotypic outcomes [60]. With mutations spread throughout LRBA protein, there were 93 homozygous cases and 16 compound heterozygous cases. Even though predicting complications would help clinical management, identifying genetic defects in immune disorders didn't give a more precise classification of LRBA deficiency. Most LRBA mutations don't produce protein. As a result of the mutations, transcribed mRNA or translated proteins can get unstable, degrade fast, or end up truncated and useless. Generally, nonsense and indel mutations are more harmful to the protein than missense and splicing mutations, except for enteropathy. There was no connection between clinical and laboratory findings and mutation type and location except for enteropathy. Three patients have been reported to have residual LRBA

protein expression. It has been shown that the closer the mutation is to the gene's 5' end, the more likely it is that protein expression will be suppressed. According to some studies, LRBA protein expression may reduce disease severity. However, there is not much evidence to support that at present [58,60].

1.6. Jurkat cell line

It was only in the mid-1980s that T-cell biologists realized a relatively new field of study called signal transduction could be applied to the study of how antigenic stimuli activate T cells. Over the past two decades of extensive research, almost all of the key components of T-cell receptor signaling have been identified, localized, and partially characterized. It was in the early days of TCR signaling research that immunologists had access to mouse and human T-cell lines capable of mounting biologically relevant responses to TCR stimulation. Among the T-cell lines included within this legendary group were HPB-ALL and HuT-78 T-cell lines, as well as EL4, which is from mice (LBRM-33) origins. Although all of these cell lines produced significant findings, Jurkat, a human leukemic T-cell line, was the most famous and historic [61].

A 14-year-old boy with acute lymphoblastic leukemia was found to have a Jurkat cell line, which was isolated from his blood in 1977. Our modern understanding of multiple signaling pathways is based on the Jurkat cell line, which has laid the foundation for our understanding of TCR signaling. The Jurkat cell line paved the way for our understanding of TCR signaling. However, as Jurkat became increasingly popular as a model T-cell line, some abnormalities in the cell line began to emerge [62].

Because PTEN and INPP5D (SHIP) were not present in Jurkat cells, PI3K signaling was abnormal. Gene expression defects were the first sign of trouble in Jurkat cells. This study proposes that the loss of these two phosphatidylinositol signaling central regulators is responsible for activating PI3K signaling, which is a major regulator of downstream TCR signaling. Jurkat is still widely used in biomedical research, despite the decline in Jurkat publications over the next decade [61,62].

In 1987, Snow and Judd published the first karyotypes of Jurkat, which revealed it to be hypotetraploid, with fewer than four times as many chromosomes as haploid [63]. After a few years, it was discovered that the Jurkat cell line contained four distinct p53 alleles, which confirmed that it was tetraploid [64]. Recent research has confirmed Jurkat

tetraploidy. According to the German Collection of Microorganisms and Cell Cultures (DSMZ), the Jurkat karyotype has been defined as a hypotetraploid flat karyotype with 7.8 percent polyploidy. An in situ hybridization study conducted in 2013 found mosaicism in cultures with tetraploid backgrounds [65]. It is important to point out that in addition to the damaged genes PTEN and INPP5D, there are other genes that are damaged in the Jurkat cell line that have an effect on T-cell receptor signaling, and CTLA-4 is the most relevant gene for the current study.

For the first time ever, it has been found that CTLA4 mRNA does not appear to be expressed or induced in Jurkat T cells. There is still no explanation for this. Recent studies have found CTLA4 protein, and the transcript is less abundant in Jurkat cells compared to peripheral blood mononuclear cells. This suggests that CTLA4 protein accumulates in the cytosol, which suggests that CTLA4 protein accumulates [66]. According to a genome-wide study on Jurkat cells, codon 20 is changed to a stop codon because of a homozygous, stop-gained, single nucleotide substitution at codon 20. Approximately half of the reads in this study were affected by this mutation, which may explain the lower expression of CTLA4 in Jurkat cells, but other mechanisms may also be involved [62].

1.7. CRISPR/Cas9 technology

Engineers are able to construct biological systems and organisms in various fields of basic science, medicine, and biotechnology. There are currently a number of tunable sequence-specific endonucleases on the market, including zinc-finger nucleases (ZFNs), transcription activator-like effector nucleases (TALENs), and RNA-guided Clustered Regularly Interspaced Short Palindromic Repeats (CRISPR) and the CRISPR-associated protein (Cas), that can be used to edit genomes in a wide variety of species. Using the first two approaches, endonuclease catalytic domains are attached to modular DNA-binding proteins in order to induce targeted double-stranded breaks (DSBs) in specific genomic regions. On the other hand, CRISPR/Cas utilizes small RNAs to guide a nuclease to pair with the target DNA through Watson-Crick base pairing (Fig. 1-5), making it extremely simple to design, highly specific, efficient, and a good candidate for high-throughput gene editing and multiplexing [67].

As an important component of the adaptive immune system in prokaryotes, CRISPR loci are found within plasmids or viral DNA (called "spacers") that are infected by microorganisms within an array of short palindromic repeat sequences. It is an enzyme that recognizes the common sequence close to the spacer using the protospacer adjacent motif (PAM). Cas9 is a nuclease protein found in streptococcus thermophilus. By using this motif, the protein binds to a common sequence close to the spacer. The CRISPR RNA (crRNA) duplexed with the transactivating CRISPR RNA (tracrRNA) is used to guide Cas9 proteins to target DNA. For the genome editing (Fig. 1-5.A), a modified synthetic crRNA and tracrRNA (sgRNA) is used [68,69].

Basically, there are two components to this gene editing system. The first component is the Cas9 protein, which consists of RuvC (cleaves the non-complementary strand of DNA) and HNH (cleaves the complementary strand). In the target DNA, these domains cause double-stranded breaks (DSBs). A single guide RNA (sgRNA) bearing a scaffold sequence for attaching to Cas9 and a 20 base pair spacer sequence complementary to the target gene and close to the PAM sequence is the second component of effective gene editing. There is an sgRNA that tells the CRISPR/Cas9 complex where to go, which then uses either non-homologous end-joining (NHEJ) or homology-directed repair (HDR) to fix DNA (Fig. 1-5.B).

NHEJ occurs in the majority of cell types, and it involves random insertion and deletion of base pairs at the cut site. Frameshift mutations are common in this error-prone mechanism, resulting in premature stop codons and/or polypeptides that are not functional. In addition to the effectiveness of gene disruption in genetic knockout experiments and functional genomic CRISPR screens, this pathway might also prove useful in the clinic if gene disruption offers a chance to treat a disease. As another pathway, error-free HDR, uses the homologous DNA strand as a template to fix damaged DNA, and it has the potential to be used in clinical applications. Using an exogenous donor template and the CRISPR/Cas9 machinery, this pathway can be tested experimentally in cells [67].

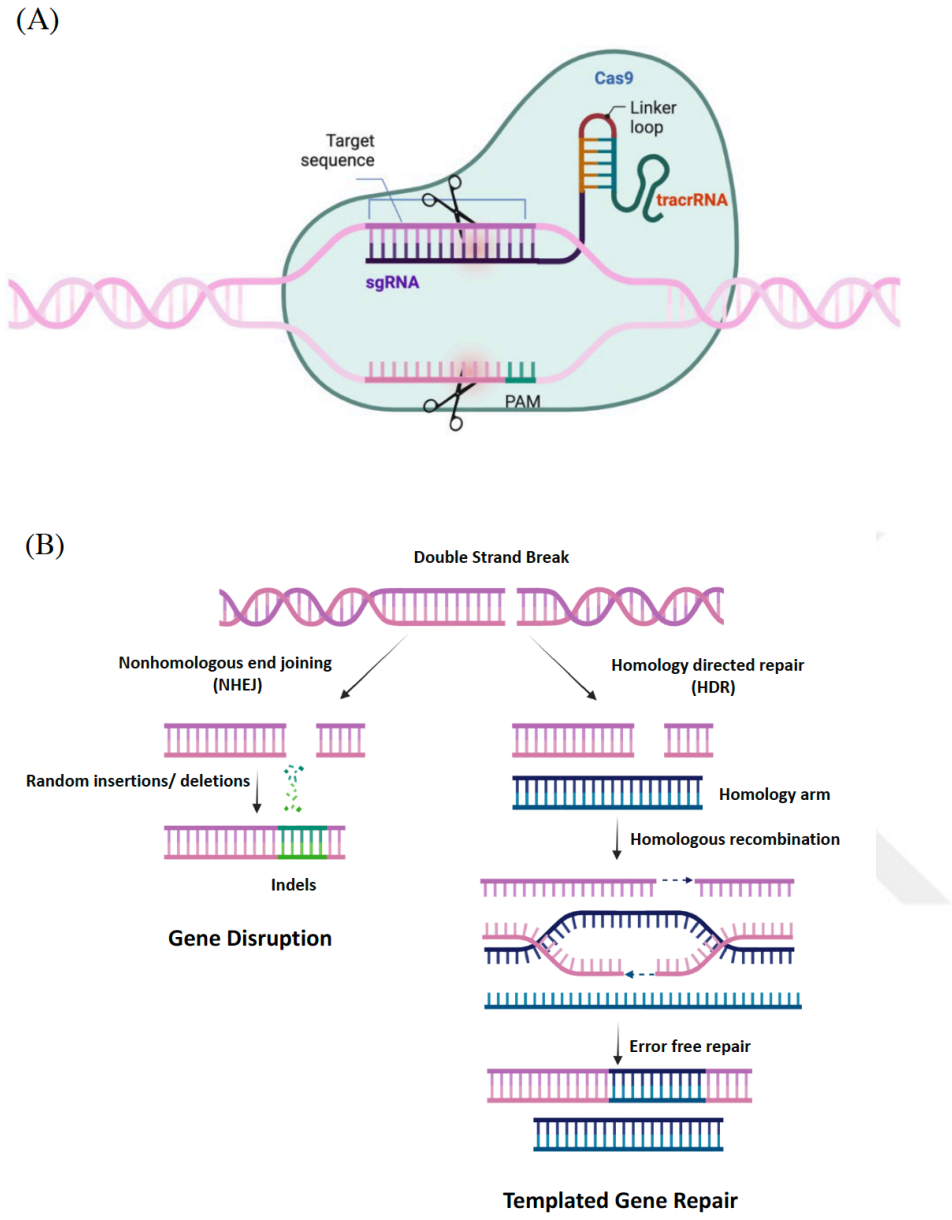

Figure 1-5. Schematic representation of RNA guided Cas9 genome editting. A) The Cas9 neclease targets the DNA by a 20-nt long sgRNA that is paired with DNA upstream of a required 5'-NGG adjacent motif (PAM). The whole process results in DSB almost 3 bp upstream of the PAM. B) DSB repair mechanism falls in two different ways of nonhomologeous end joining (NHEJ) or homology directed repair (HDR).

2. AIM OF THE STUDY

In this study our main objective was to identify membrane proteins that directly or indirectly have an interaction with LRBA protein. In the first part of the study, we generated the LRBA KO cell lines targeting different exons of the LRBA gene. The presence of CRISPR/Cas9 induced nonsense mutations and the absence of protein expression in these cell lines were verified by DNA sequencing, T7 endonuclease assays, western blotting and flow cytometry. In the second part of the study, we performed surface biotinylation on both WT and one of the single clonal KO cell lines to label and isolate membrane proteins for MS analysis. The differentially expressed proteins were analyzed with flow cytometry in all generated KO cell lines for further confirmation. Finally we, over expressed CTLA-4 cDNAs in WT and LRBA KO Jurkat cell lines to generate a model cell line which has a more T-regulatory cell-like features.

3. MATERIALS AND METHODS

3.1. Materials

3.1.1. Chemicals

Appendix A lists all the chemicals.

3.1.2. Equipment

In appendix B the used facilities are listed.

3.1.3. Buffers and Solutions

Tris-Borate -EDTA (TBE) Buffer: In 1 L of ddH_2O, 54 g Tris-base, 27.5 g boric acid, and 20 ml 0.5M EDTA (pH 8.00) were dissolved to make 1 L of 5X stock solution. The solution is kept at room temperature (RT) and diluted 1 to 10 with ddH_2O to make a 0.5X TBE working solution.

Agarose Gel: 1 g of agarose powder was heated in 100 ml 0.5X TBE buffer to make 100 ml 1 percent w/v gel. The solution was treated with 0.002 percent (v/v) ethidium bromide.

Phosphate-buffered Saline (PBS): 10X DPBS was diluted 1:10 with ddH_2O to make 1X working solution. The solution was filter-sterilized when required.

Calcium chloride ($CaCl_2$) Solution: 60 mM CaCl2, 15% Glycerol, and 10 mM PIPES (pH 7.0) were mixed with ddH_2O to make a total volume of 500 ml. The solution was sterilized with a filter and stored at 4°C.

Triton X-100 Lysis Buffer: For 10 ml buffer add 0.5ml Triton X-100 20% (2 ml Triton X-100 + 8 ml ddH_2O), 0.5 ml Tris-HCl 1 M (pH 7.4), 0.3 ml NaCl 5 M, 0.04 ml EDTA 0.5 M (pH 8), 1 protease inhibitor (Roche complete mini EDTA free) tablet, and 8.7 ml ddH_2O. Aliquoted and kept in -20 °C.

Tris-Glycine buffer: For 1 L 10X buffer, 30.3 gr Tris-base, 144 gr Glycine and 10 gr SDS was mixed in the ddH_2O and the final volume was made up to 1 liter. The pH of buffer should be around 8.3 and no need for pH adjustment.

Tricine Buffer: For 1 L 1X buffer, 8.95 gr Tricine, 6.06 gr Tris-Base and 1 gr SDS was mixed in ddH_2O and the final volume was made up to 1 liter. The pH should of this solution should be around 8.24 and no need for further adjustments.

Tris-Acetate Buffer: 18 gr Tris-base was dissolved in 80 ml ddH_2O, then the pH was adjusted to 7 by adding Acetic Acid gradually, and the final volume was made up to 100 ml with ddH_2O.

Tris-base (0.5 M) Buffer: 6 gr Tris-base was dissolved in 80 ml ddH_2O, then the pH was adjusted to 6.8 using 6N HCl and final volume was made up to 100 ml with ddH_2O.

Transfer Buffer: For 1 L 1X solution 100 ml Tris-Glycine 10X, 100 ml Methanol, and 3.75 ml SDS 10% was mixed and the final volume was made up to 1 liter with ddH_2O.

Protein loading buffer: for 10 ml 4X stock solution, 2 ml Tris-HCl 1M (pH 6.8), 1 gr SDS, 4 ml Glycerol 100%, 0.4 ml β-mercaptoethanol 14.7 M, 8 mg bromophenol Blue, and the volume was adjusted to 10 ml with ddH_2O. The solution was aliquoted and kept at -20 °C.

SDS Separating gel: For 8 ml 3% Tris-Acetate separating gel, 0.6 ml Acrylamide 40%, 5.2 ml ddH2O, 2ml Tris-Acetate 1.5M (pH 7), 80 µl SDS 10 %, 80 µl APS 10 %, 8 µl TEMED were mixed. (For 8 % gel, 1.6 ml Acrylamide 40% and 4.2 ml ddH_2O was mixed with the same amount of the rest of the materials)

SDS Stacking gel: For 8 ml 3% Tris-base separating gel, 0.6 ml Acrylamide 40%, 5.2 ml ddH2O, 2ml Tris-base 0.5M (pH 6.8), 80 µl SDS 10 %, 80 µl APS 10 %, 8 µl TEMED were mixed.

PBS-Tween20 (PBS-T) solution: for 500 ml 1X solution 0.25 ml tween20 was added to 500 ml PBS 1X solution.

Blocking Buffer: To make 20 ml 5% skimmed milk, 1 gr skimmed milk was dissolved in 20 ml PBS-T 1X and vortexed well.

Antibody dilution buffer: Primary antibodies for western blot were diluted in 5% BSA buffer in PBS-T 1X, treated with sodium azide to the final concentration of 0.03 %. Secondary antibodies were diluted freshly in 5% skimmed milk buffer in PBS-T 1X.

3.1.4. Growth Media

Luria Broth (LB): 20 g LB powder was dissolved in 1 L ddH_2O and autoclaved at 121°C for 15 minutes to make 1 L 1X LB media. Kanamycin at a final concentration of 50 g/ml or ampicillin at a final concentration of 100 g/ml was added to the liquid medium just before use for selection.

LB-Agar: 20 g LB powder and 15 g bacterial agar powder were dissolved in 1 L ddH_2O and autoclaved at 121°C for 15 minutes to make 1X agar medium in 1L. The autoclaved LB agar is then mixed with the antibiotic of choice in the desired ratio. Kanamycin (50 g/ml) or ampicillin (100 g/ml) were added to the prepared medium just before filling the petri dishes. The sterile plates were kept at 4 °C.

RPMI: Jurkat cells were cultivated in RPMI1640 growth medium with 10% heat-inactivated fetal bovine serum (FBS), 25mM HEPES, 2mM L-Glutamine, 1mM Sodium Pyruvate ,0.1mM MEM non-essential amino acid solution, 1% PenStrep (100 U/mL Penicilium and 100 µg/mL Streptomycin)

DMEM: 293FT cells were cultured in DMEM with 10% heat-inactivated fetal bovine serum, 2mM L-Glutamine, 1mM Sodium Pyruvate, 0.1mM MEM Non-essential amino acid solution, and 25mM HEPES solution.

Freezing medium: All cell lines were frozen in heat-inactivated fetal bovine serum containing 6% DMSO (v/v).

3.1.5. Commercial Molecular Biology Kits

Appendix C shows the molecular biology kits.

3.1.6. Enzymes

Restriction and modifying enzymes, polymerase enzymes, enzyme buffers, and PCR reagents were from either New England Biolabs (NEB) or Fermentas.

3.1.7. Antibodies

Appendix D lists all the used antibodies.

3.1.8. Plasmids and oligonucleotides

Plasmids and oligonucleotides which are used are in Table 3-1 and Table 3-2, respectievely.

Plasmid name	Purpose of use	Source
lentiCRISPRv2	Mammalian expression plasmid for the CRISPR/Cas9 system with puromycin resistance gene	Addgene (#52961)
LeGO-iG2 Puro	Lentiviral construct for eGFP expression with IRES	Addgene (#27341)

pMDLg/pRRE	Virus production/packaging plasmid (Gag/Pol)	Addgene (#12251)
pRSV-REV	Virus production/packaging plasmid (Rev)	Addgene (#12253)
phCMV-VSV-G	Virus production/packaging plasmid (Env)	Addgene (#8454)

Table 3-1. Plasmids used in this study.

Oligo name	SEQUENCE (5’ to 3’)	Purpose of use
LRBA-gRNA-1-Exon2-Top	caccgGACAATGCACCCCCTTCAGT	LentiCRISPRv2 cloning
LRBA-gRNA-1-Exon2-Bot	aaacACTGAAGGGGGTGCATTGTCc	LentiCRISPRv2 cloning
LRBA-gRNA-3-Exon6-Top	caccgTATGGCCATTTGGCTATAGG	LentiCRISPRv2 cloning
LRBA-gRNA-3-Exon6-Bot	aaacCCTATAGCCAAATGGCCATAc	LentiCRISPRv2 cloning
LRBA-Exon 42-5'-Top	caccgGTATATGCCAAGATCTAATG	LentiCRISPRv2 cloning

LRBA-Exon 42-5'-Bot	aaacCATTAGATCTTGGCATATACc	LentiCRISPRv2 cloning
LRBA-Exon 42-3'-Top	caccgTGTTTGCCATAAAGATCTCC	LentiCRISPRv2 cloning
LRBA-Exon 42-3'-Bot	aaacGGAGATCTTTATGGCAAACAc	LentiCRISPRv2 cloning
Ctla-4 Fwd- EcorI Legoig2puro	tctattcGAATTCATGGCTTGCCTTGGATTTCAGCGGCACAAGG	LegoiG2purp cloning
Ctla-4 Rev- NotI-Legoig2puro	tagtctgGCGGCCGCTCAATTGATGGGAATAAAATAAGGCTGAAATTGC	LegoiG2purp cloning
LRBA-Exon2-fwd	TCCAATAGGGTTTGGCGTTGT	Genomic DNA PCR for Exon2 of LRBA CRISPR target site
LRBA-Exon2-rev	TGACCAGACCATTAGAGAAGGT	Genomic DNA PCR for Exon2 of LRBA CRISPR target site
LRBA-Exon6-fwd	TCTAAACCAAGCGGTAAAGCC	Genomic DNA PCR for Exon6 of LRBA CRISPR target site
LRBA-Exon6-rev	GATCATGTACCTTTTGTGGCTTG	Genomic DNA PCR for Exon6 of LRBA

		CRISPR target site
LRBA-Exon42-fwd	TGTATGTAAAAGCATTATTGGGCA	Genomic DNA PCR for Exon42 of LRBA CRISPR target site
LRBA-Exon42-rev	AAATGCAGCCACCTTCCAGA	Genomic DNA PCR for Exon42 of LRBA CRISPR target site

Table 3-2. List of oligonucleutides.

3.1.9. DNA and Protein Molecular Weight Markers

DNA ladders and protein molecular weight markers which are used are in Appendix E.

3.1.10. DNA Sequencing

Sequencing service was commercially provided by Macrogen, Europe.

(https://dna.macrogen-europe.com).

3.1.11. Software, Computer-Based Programs, and Websites

The software used in this project are shown in Table 3-3.

SOFTWARE, PROGRAM, WEBSITE NAME	WEBSITE, COMPANY	APPLICATION
CLC Main workbench V.7	QIAGEN Bioinformatics	Primer design, molecular cloning, sequence data analysis, sequence alignment
BD Accuri C6 software	BD Biosciences	Collecting flow cytometry data
FlowJo V.10	FlowJo, LLC	analyzing flow cytometry data
NCBI BLAST	https://blast.ncbi.nlm.nih.gov/Blast	DNA sequence alignment tool
Ensembl Genome Browser	http://www.ensembl.org	Human genome sequence information
CRISPR Design, Zhang Lab, MIT	http://crispr.mit.edu	sgRNA design and off target analysis for CRISPR
CRISPOR	http://crispor.tefor.net/	sgRNA design and off target analysis for CRISPR

Addgene	https://www.addgene.org/	Plasmids map and information
G:Profiler	https://biit.cs.ut.ee/gprofiler/gost	Gene ontology studies of proteins
SAINT (Significance Analysis of INTeractome)	http://saint-apms.sourceforge.net/Main.html	Mass spectrometry data analysis

Table 3-3. The list of programs, websites and software used here and the purpose of their uses.

3.2. Methods

3.2.1. Bacterial Cell Culture

Bacterial culture growth: The Escherichia coli (E. coli) DH5 strain was grown overnight at 37°C in Luria Broth (LB), shaking at 250 rpm. Glycerol was added to the overnight grown culture to a final concentration of 10% in 1 mL in a cryo-vial for long-term storage of bacterial cells at -80°C. Bacteria were spread on LB/agar-containing petri dishes with glass beads and incubated overnight at 37°C without shaking to obtain single colonies. Prior to any application, all growth media were supplemented with or without a selective antibiotic.

Preparation of competent bacteria: A single E.coli DH5α colony was selected from an LB/agar petri dish (incubated overnight without antibiotic selection). In a 200 mL flask, the colony was inoculated in 50 mL LB without any selective antibiotics and incubated at 37°C overnight, shaking at 250 rpm. The following day, 4 mL of this overnight culture was diluted in 400 mL LB medium in a 2 L flask and incubated at 37°C, shaking at 250 rpm, until the optical density (at 590 nm) reached 0.375. The culture was then transferred

into 50 ml polypropylene tubes (8 in total) and incubated on ice for 10 minutes before being centrifuged at 1600 g for 10 minutes at 4°C. Each pellet was resuspended in 10 mL of ice-cold CaCl2 solution and centrifuged at 1100 g for 5 minutes at 4°C. The pellets were resuspended in 10mL of ice-cold CaCl2 solution and incubated for 30 minutes on ice. After a final centrifugation at 1100 g for 10 minutes at 4°C, the pellets were resuspended in 2mL of ice-cold CaCl2 solution and pooled in a single polypropylene tube (16 ml bacterial solution in total). This solution was dispensed into 1.5ml centrifuge tubes in 200L aliquots. Competent cells were immediately frozen in liquid nitrogen and stored at -80°C for future use. The transformation efficiency of competent cells (typically 107-108 cfu/g) was tested using pUC19 plasmid transformation at various plasmid DNA concentrations.

Transformation of competent bacteria: In order to do transformation, DH5α competent cells were thawes on ice. Plasmid was added to competent cell and incubated on ice for 30 minutes. Subsequently, the cells were exposed to 42 °C heat shock for 90 seconds followed by immediate 30 seconds incubation on ice. Then 800 µl of LB was added and cells were incubated at 37°C for 45 minutes. The cells were centrifuged for 1 minute at 13,000 rpm, and the pellet was resuspended in 100 µl LB before being spread on Petri dishes. Plates were incubated overnight at 37 °C without shaking.

Plasmid DNA isolation: Plasmid DNA was isolated using either the alkaline lysis protocol from Molecular Cloning: A Laboratory Manual (Sambrook et al), Commercial Macherey-Nagel Mini or Midiprep Kits, or the Qiagen Mini-Midiprep Kits according to the manufacturer's instructions. A UV- or a NanoDrop- spectrophotometer was used to determine the concentration and purity of the isolated DNA.

3.2.2. Mammalian Cell Culture

Maintenance of cell lines: HEK293FT cells were kept in DMEM medium, in sterile tissue culture flasks, and in an incubator which was kept at 37°C and 5% CO_2. The cells where split with 1:10 ratio in fresh DMEM medium whenever reached to over 80% confluency.

Jurkat cells were kept in RPMI medium under the same condition and every 2-3 days they were split with 1:3 or 1:5 ratio in fresh RPMI medium.

In order to freeze cells, they were resuspended in freezing medium and kept for at least 24 hours at -80°C before being transferred to nitrogen tank for long term storage. While thawing the cells were washed from freezing medium immediately and resuspended in fresh complete medium.

Lentivirus production: On the first day, $5x10^6$ HEK293 cells were seeded in a 10 cm poly-D-lysine coated tissue culture plates. Next day, cells were co-transfected with the master mix containing, 3.75 µg of pMDLg/pRRE, 2.5 µg of pRSV-REV, 1.25 µg of phCMV-VSV-G, and 7.5 µg of gene of interest plasmid, 25 µM Chloroquine, and 0.1M $CaCl_2$. 10 hours later, the medium was changed with a fresh DMEM medium and virus was collected, filterd and stored at -80°C after 36 hours for further use.

Lentiviral transduction of Jurkat cells: $1x10^6$ of cells were resuspended in 1ml fresh RPMI medium and 5 ml of virus was added in the presence of a final concentration of 8 g/ml of protamine sulfate. The cells were kept in an incubator at 37°C and 5% CO_2 overnight. Next day, the virus was washed out through centrifugation (300g, 3minutes) and replaced by fresh RPMI medium. The cells were kept in culture for 10 days to grow before starting puromycin selection (1ug/ml). The expression of any protein of interest was checked through flow cytometry before and after puromycin selection.

Generation of single-cell clones: conditioned medium was made in advance by taking the medium of healthy, untreated Jurkat cell medium when grown to $1x10^6$ cell/ml, centrifuge, filter and keep at 4°C for short term and at -20 for longer than 1 week storage. The cells were counted, and calculation was done to have 100 cells/ml in the fresh RPMI medium. To seed 0.5 cell/well in a 96-well plate, take 1ml of 100 cells/ml and mix with 10 ml of conditioned medium and 9 ml of fresh RPMI medium and plate 100 µl of this dilution in each well. 15 plates was made from each condition and plates were checked to mark the wells with single colonies after 2 weeks and one week after that the wells with single colonies were transferred to 24 well plates and later expanded to 6 well plates. Cells in 6 well plate were screened for the presence of LRBA protein with intracellular staining and flow cytometry analyses. The colonies that showed decreased expression were transferred to flask to be freezed and further analyzed.

sgRNA design and off-target analysis: sgRNA for CRISPR targeting human LRBA gene were designed by "Zhang Lab" CRISPR desining tool, (www.crispr.mit.edu). For each sgRNA off-targets were also considered.

Phosphorylation and annealing of oligonucleotide pairs: Top and bottom single stranded oligonucleotides were synthesized separately in the complementary form, with flanking sides to be ligated in pLentiCRISPRv2 plasmid after digestion with BsmbI restriction enzyme. The selected sgRNA sequences were synthesized by Sentebiolab Company (sentebiolab.com.tr).

Following reaction mixture and thermocycler parameteres were used to anneal top and bottom strand after diluting oligoes to 100 µM.

sgRNA Top Oligonucleotide	1 µl
sgRNA Bottom Oligonucleotide	1 µl
10X T4 Ligase Buffer	1 µl
T4 PNK Enzyme	1 µl
ddH2O	To 10 µl

37°C	30 minutes
95°C	5 minutes
Ramp down to 25°C	5°C/minute

LentiCRISPRv2 plasmid digestion and dephosphorylation: The following reaction mixture was incubated at 37°C for 2 hours to digest LentiCRISPR plasmid with BsmBI enzyme.

lentiCRISPRv2 plasmid	5 µg
10X 3.1 Buffer (NEB)	3 µl
DTT (10 mM)	5 µl
BsmBI (10,000 U/ml) (NEB)	3 µl
ddH2O	To 30 µl

Dephosphorylation of digested plasmid:

lentiCRISPRv2 BsmBI digestion reaction	30 µl
10X RSAP Buffer	5 µl
RSAP (20,000 U/ml)	3 µl
ddH2O	50 µl

After gel purification of 12 kb band of digested dephosphorylated plasmid, ligation reaction was done by incubating following mixture at room temperature for 1 hour.

BsmBI digested lentiCRISPRv2 plasmid	50 ng
Oligonucleotide duplex (1:200 dilution)	1 µl
10X T4 Ligase Buffer (NEB)	2 µl
T4 Ligase (400,000 U/ml) (NEB)	1 µl
ddH2O	To 10 µl

Transformation of LentiCRISPRv2 plasmid: Ligation reaction from previous section was transformed into DH5α competent cells and then the isolated plasmid DNA from single bacterial colonies were sent for sanger sequencing to confirm the sequence of ligated sgRNA. The sequencing primer is binding to the human U6 promoter in the plasmid.

Generating LentiCRISPRv2 expressing cell lines: Jurkat cells were either transduced with lentivirus containing lentiCRISPRv2 plasmid following the protocol mentioned in 3-2-2 section or they were transfected using Neon transfection kit. For Neon transfection, in first day, $2x10^6$ cells were resuspended in the mixture of 100 µl HBS buffer and 5 µg plasmid DNA. Cells were transfected using a 100 µl golden Neon tip and the following transfection conditions: Pulse: 1350 V, Pulse width: 10 ms, Pulse number: 3 pulses. $40x10^6$ cells were tranfected intotal and each $4x10^6$ cells were seeded in10 ml fresh RPMI in 10 cm plates. Next day, cells were pooled and seeded to $0.5x10^6$ cells in fresh RPMI medium. For half of the cells puromycine selection was started and the other half was kept growing without any selection. After 4 days the puro selected cells were collected and resuspended in fresh RPMI medium without puromycin and kept in culture for two weeks to grow before doing further analyses to check the KO efficiency.

3.2.3. Determination Genome Targeting Efficiency

T7 endonuclease I assay: The T7 Endonuclease I (T7EI) enzyme was used to assess the efficiency of CRISPR/Cas9-mediated genome targeting. T7EI's endonuclease activity recognizes and cleaves non-perfectly matched DNA. PCR products are generated from gDNA of clonal cell lines whose genomes were targeted using the CRISPR/Cas9 system in the first step of this assay. The PCR products are denatured, re-annealed, and digested with the T7EI enzyme in the second step. To determine mutations in the genome, digested fragments are analyzed.

T7 Endonuclease I (T7EI) enzyme was used to determine CRISPR/Cas9 mediated genome targeting efficiency. T7EI recognizes and cleaves non-perfectly matched DNA by its endonuclease activity. In the first step of this assay, PCR products are produced from gDNA of clonal cell lines whose genome was targeted using CRISPR/Cas9 system.

Targeted exons were amplified by Q5 DNA polymerase using forward and reverse primers mentioned in 3.1.8 section with optimum annealing temperature which was determined after performing gradient PCR for each pair of primer.

5X Q5 HF Buffer (NEB)	5 µl
10 mM dNTPs	0.5 µl
10 µM forward primer	1.25 µl
10 µM reverse primer	1.25 µl
Template DNA	20 ng
Q5 HF Polymerase (2,000 U/ml) (NEB)	0.25 µl
ddH2O	To 25 µl

Thermocycler conditions for amplifying DNA:

Initial Denaturation	98 °C	30 seconds
30 cycles	98 °C	10 seconds
	50-72 °C	20 seconds
	72 °C	20 seconds
Final Extension	72 °C	2 minutes
Hold	4 °C	∞

T7EI digestion reaction:

PCR Reaction	10 µl

10X Buffer 2 (NEB)	2 µl
ddH2O	To 19.5 µl

Thermocycler conditions to denature and anneal the PCR product:

Initial temperature	Denaturation 95°C	5 minutes
Annealing	Ramp down to 85°C	2°C/second
	Ramp down to 25°C	0.1°C/second
Hold	4°C	∞

T7EI enzyme was used to digest annealed PCR products. WT genomic DNA was used as a negative control and transfected or infected genomic DNA was used as a positive control.

The following mixture was incubated at 37°C for 15 minutes and digestion product was run on 2% agarose gel to further analyze the pattern of digestion fragments.

Annealed PCR Product	19.5 µl
T7EI (10,000U/ml) (NEB)	0.5 µl

Cell Lysis, SDS Gel, Transfer and Western-Blot: For LRBA protein western-blot, Jurkat cells were collected, centrifuged, and washed with 1X PBS. 100 µl lysis buffer per $5x10^6$ cells was added and cells were completely resuspended in lysis buffer. After 30 minutes incubation on ice cell lysate was centrifuge at 4°C, 15000 RPM for 10 minutes. The supernatant was collected and divided into 20 µl aliquots to be kept at -80 °C or immediately used. The cell lysate was mixed with appropriate laemmli buffer and boiled

at 95°C for 10 minutes. For better separation of proteins larger than 100 kDa, 3-8% Tris-Acetate gradient gel was used. To make the gel, 1 ml of 8% tris-acetate gel was poured on the bottom of a 1.5mm glass spacer. Then, with a 10ml pipet 4ml of 3% and 4ml 8% gel was sucked respectively, and two of them were mixed gently by sucking an air bubble. After that it was poured in spacer on top of 1ml 8% with constant speed. For stacking make 3% gel was used. Running step was performed in tricine 1X buffer, at 120 V constant voltage for 1.5-2 hours.

After running, the gel was transferred to a 0.45 μm PVDF membranes in 1X transfer buffer at 100 V constant voltage for 3 hours. Membranes were then blocked in 10 mL PBST - milk for 1 hour at room temperature with constant shaking. The primary antibodies were incubated overnight at 4°C, and the secondary antibodies were incubated for 1 hour at room temperature. Following incubation, membranes were washed three times with PBST for ten minutes each.

Sequencing targeted genomic DNA: Sequencing verified the mutations on CRISPR/Cas9 edited single cells. The targeted region was PCR amplify from gDNA isolated from single clonal cell by primers binding intron on 5' and 3' ends of targeted exon. The PCR product was cloned into pCR-Blunt II-TOPO (Zero Blunt TOPO PCR Coloning Kit) following the protocol provided by the kit and transformed into DH5α competent cell. The plasmid DNA was isolated from at least 10 colonies and sequenced.

3.2.4. Biotinylation assay

The biotinylation of cell surface proteins was performed with ThermoScientific “Cell surface Protein Biotinylation and Isolation” kit (A44390). The cell surface proteins of Jurkat cells were biotinylated following the protocol provided by the kit for cell surface biotinylation of suspension cells. Briefly, the cells were grown to $1.6x10^6$ cell/ml in RPMI medium, 15 ml of cell (24x106 cells in total) were transferred in a 50 ml conical falcon tube. After centrifuge and discarding the medium the cells were washed with ambient PBS 1X once. The content of one vial of Sulfo-NHS-SS-Biotin was dissolved in 24 ml of ambient PBS 1X. The cells were resuspended in 10 ml of biotin solution and incubated at room temperature for 10 minutes. Centrifuge the cells 300 g for 3 minutes and remove

label. Wash cells with 15 ml ice-cold TBS 1X for two times. Then the cells were lysed in the lysis buffer provided in the kit after adding protease inhibitor. The cells were incubated on ice for 30 minutes and they were vortexed 5 seconds at the beginning and end of the incubation. The cell lysate was centrifuged at 15000 g for 5 minutes and clarified supernatant was transferred to a new 1.5 ml tube. 250 µl NeutrAvidin Agarose slurry was added to small columns provided in the kit and centrifuged to at 1000 g for 1 minute to remove the storage solution. To isolate labeled proteins, cell lysate was added to resin and after tightly closing column from cap and bottom, the columns were incubated for 30 minutes at room temperature with end-over-end mixing on a rotator. Lastly, the resin was washed three times with wash buffer and biotinylated proteins on washed resin was send to Koç University Proteomic Facility (KUPAM) for Mass Spectrometry (MS) analysis.

3.2.5. Reduction, Alkylation, and Enzymatic digestion prior to MS analysis

All these steps were performed in KUPAM for MS analysis sample preparation.

Streptavidin agarose beads were thoroughly washed with 8 M urea in 0.1 M Tris/HCl pH 8.5 before being reduced and alkylated in a sealed system. Then beads were incubated with trypsin overnight at 37 °C in 50 mM ammonium bicarbonate. The peptides were collected by centrifugation at 1000g for 5 minutes. After that, the beads were rinsed with 50 mM ammonium bicarbonate, and the second tryptic fraction was combined with the first. After acidification, tryptic peptides were desalted with stage tips and fractionated using the strong anion exchange (SAX) method.

Peptides were analyzed using Thermo Scientific Q Exactive Quadrupole-Orbitrap Mass Spectrometer with nano Liquid Chromatography,UltiMate 3000 NCS-3500RS (n-LC MS/MS). Over 120 minutes with 300 nL/min flow. MaxQuant version 1.5.2.8.30 was used to process the raw files. Cysteine carbamidomethylation was used as a fixed modification, while acetylation (protein N-termini) and methionine oxidation were used as variable modifications. The tryptic peptides were allowed a maximum of two missed cleavages. The tolerance for precursor mass was set to 20 ppm, and both the peptide and protein false discovery rates (FDRs) were set to 0.01.

3.2.6. Flow cytometry

Cell surface staining: for cell surface staining $1x10^6$ cells were washed with PBS 1X and they were incubated with appropriate amount of diluted antibody based on titration result or the amount recommended by manufacturer's protocol. The cells were incubated with conjugated antibodies, FITC-anti-hCD3, FITC-anti-hCD4, FITC-anti-hCD1d, PE-anti-hNOTCH3, PE-anti-hPVRIG, FITC-anti-hCD53, PE-anti-hCD134, AF488-anti-hCD154, FITC-anti-hCD25, or FITC-anti-hCD69 for 30 minutes on ice at dark and after being washed with PBS 1X they were ready for flow cytometry analysis and as control unstained cells or proper isotype control was used. For unconjugated antibodies, the cells were first incubated with primary antibody, anti-hA33, anti-hCD70, or anti-hCD148 for 30 minutes on ice and after being washed with PBS 1X, then they were incubated with proper conjugated secondary antibody for 30 minutes on ice at dark. finally, they were washed with PBS 1X and analysed with flow cytometry, as control the cells were stained with only secondary antibody or the proper isotype control.

Intracellular staining: For intracellular staining $1x10^6$ cells were washed with PBS 1X. The cells were firstly fixed by 20 minutes incubation in 4% PFA solution. Then cells were washed with 1X permeabilization buffer. The antibodies were diluted in 1X permeabilization buffer based on titration result or manufacturer's recommendation. For unconjugated antibodies, anti-hLRBA, anti-hCTLA-4 the cells were first incubated with proper amount of diluted antibody for 30 minutes on ice. Then they were washed three times with 1X permeabilization buffer and incubated with conjugated seccondary antibody 30 minutes on ice at dark. The last wash was also with 1X permeabilization buffer and cells were resuspended in PBS 1X for flocytometry analysis. As control the cells were stained with only secondary antibody.

Data was collected with BD accuri C6 instrument and analyzed with FlowJo software.

4. RESULTS

4.1. Generation of LRBA KO Jurkat cell line

4.1.1. Lentiviral CRISPR/Cas9 editing of the LRBA gene

4.1.1.1. Targeted exons and gRNA design

LRBA is a large protein translated from 58 exons of a gene that is 750839 bp long, making gRNA design more challenging compared to smaller genes. We designed more than one gRNA targeting different exons, encoding N-terminal and C-terminal parts of the protein to maximize the chances of generating a nonfunctional allele (Fig.4-1A). Exon 2 and exon 6, encoding the N-terminal parts of the protein, were targeted with gRNA-1 and gRNA-6. Also, exon 42 was explicitly targeted as one of the exons encoding the PH-BEACH domain, which is the critical domain in the protein vesicular trafficking function (Fig.4-1B). Two gRNAs were designed to target exon 42 on both the 5' and 3' ends to ensure the total removal of this exon from the genome. The gRNAs were cloned into the lentiCRISPRv2 plasmid to express gRNAs and cas9 the Cas9 enzyme in targeted cells. Following the standard protocol of virus production and transductions, Jurkat cells were infected with lentivirus-containing supernatants.

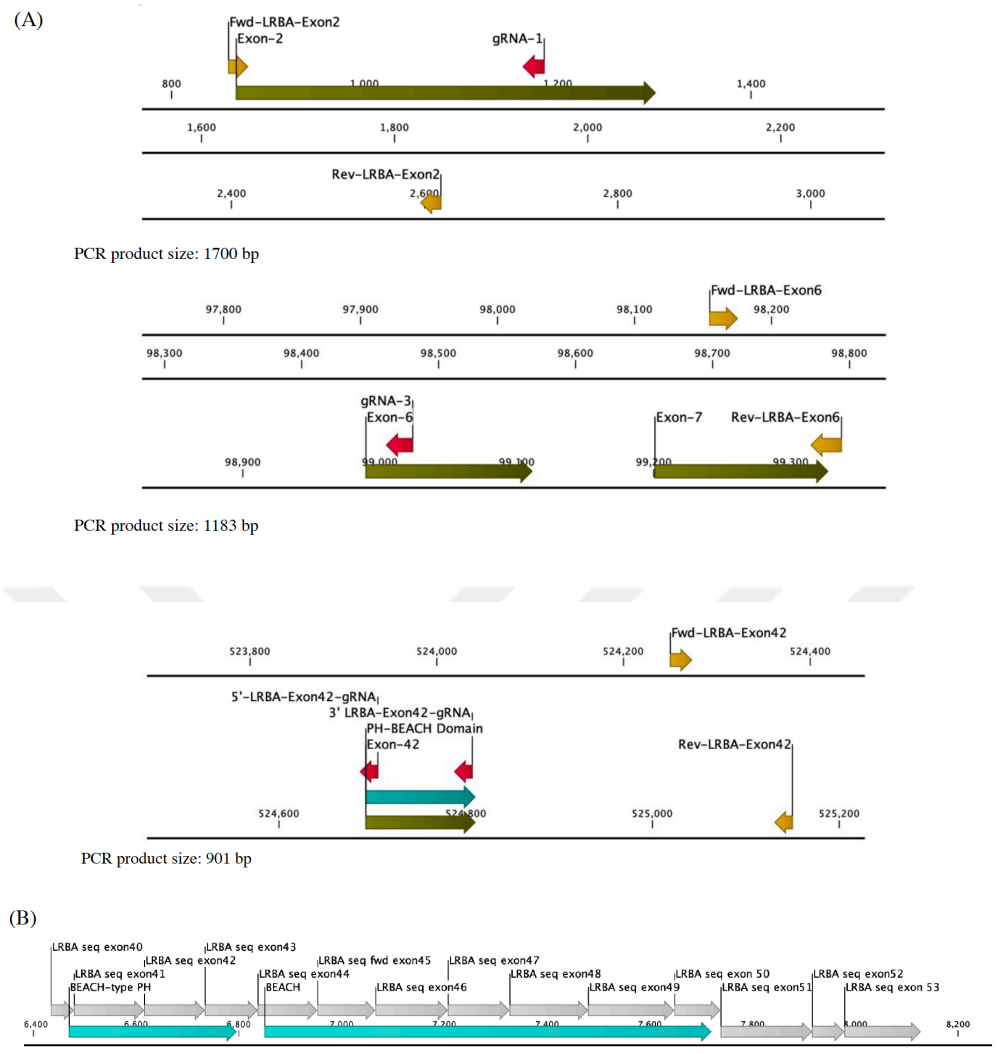

Figure 4-1 A) Map of the LRBA gene locus that shows the location of the three targeted exons, gRNAs, and the primers used to amplify the targeted regions. B) The map of the LRBA cDNA regions encoding the PH-BEACH domain and the exons that encode this gene region.

4.1.1.2. Confirmation and validation of generated KO cell line

Three different targeted Jurkat cells (exon 2, exon 6, exon 42) and WT Jurkat cells were intracellularly stained with anti-LRBA antibodies and analyzed by flow cytometry (Fig.4-2). The mean fluorescence intensity (MFI) has an apparent decrease in exon2 and exon42 targeted cells (green histograms) when compared to the MFI of WT Jurkat cells (orange histograms). On the other hand, exon6 targeted cells (green histograms) express similar

levels of intracellular LRBA when compared to WT Jurkat cells. Thus, we conclude that genome editing efficiency was higher for exon 2 and exon 42 targeted cells compared to exon 6 targeted cells. In all three cases, the MFI is higher than unstained controls, which could be due to the presence of truncated proteins that retain the anti-LRBA antibody epitopes, encoded by the targeted gene loci. Another possibility is the possibility of limited transduction and targeting efficiency.

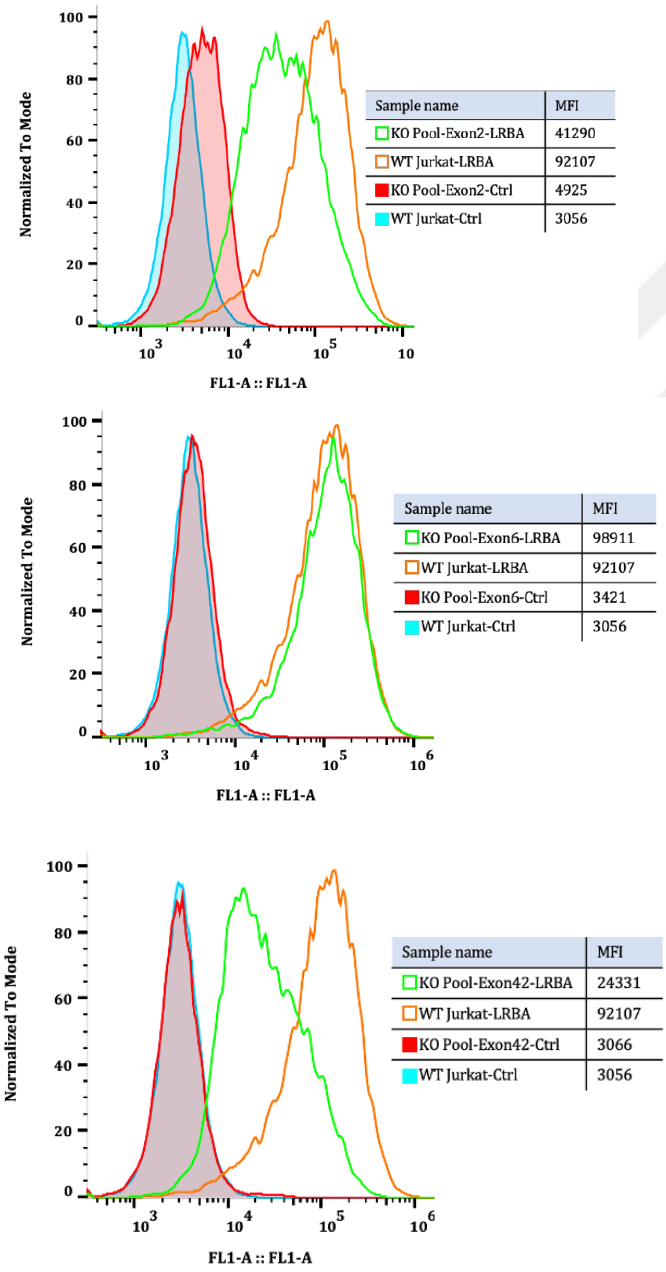

Figure 4-2. Intracellular LRBA staining of targeted and WT Jurkat cells. The cells were stained with primary rabbit anti-LRBA antibody followed by secondary anti-rabbit

dylight-488 conjugated antibody, and as a control, the cells were only stained with secondary antibodies.

The three different pools of cells were also analyzed for possible mutations by the T7 endonuclease1 (T7E1) assay. T7 endonuclease1 recognizes and cleaves mismatches in DNA heteroduplexes due to the CRISPR/Cas9 induced mutations in genomic DNA. The principle of the T7E1 assay is to identify mismatches arising from CRISPR/Cas9 introduced mutations, as a result of random non-homologous end-joining (NHEJ) repair events. Genomic DNA amplified from targeted cells provides both targeted and non-targeted (WT) alleles, which when amplified in a mixed reaction followed by denaturation and annealing results in heteroduplexes DNA containing mismatches. In the case of targeted cells, as shown in the gel images, digested smaller bands appear after digestion by T7E1 enzyme (Fig.4-3). The extra bands indicate the presence of mutations in the genome of the targeted cell population in the targeted region. Similar to our findings by flow cytometry, in this T7E1 assay, the efficiency of CRISPR KO appears to be better in exon 2 and exon 42 targeted cells compared to exon 6 targeted cells, as the intensity of T7 digested bands appear to be higher and more apparent when compared to WT.

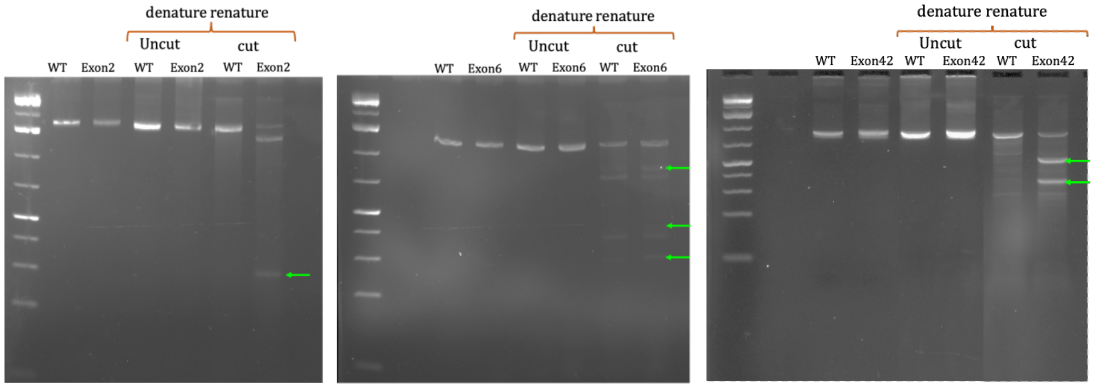

Figure 4-3. T7 endonuclease1 assay for three different targeted pools of cells. In each gel, the first two lanes are PCR amplified targeted regions using primers shown in Fig4-1A. The second two lanes are denatured and renatured PCR products before being digested with the T7 endonuclease enzyme, and the third two lanes contain digested DNA.

As a confirmation of the flow cytometry experiments, we assessed LRBA protein levels in targeted cells also by western blotting. Similar to the other methods, LRBA protein levels were decreased in exon 42, and exon 2 targeted cells compared to exon 6 targeted and WT Jurkat cells (Fig4-4).

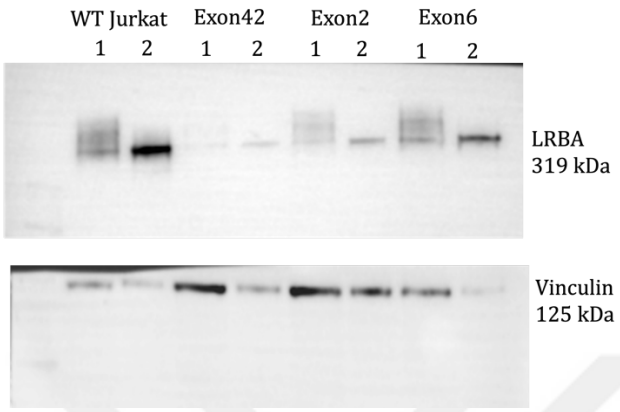

Figure 4-4. Western blot analysis of LRBA protein expression in WT and targeted pools of cells. For each cell line, two different amounts of lysate was loaded where lanes marked by 1 contained 20 µl and lanes marked by 2 contained 40 µl of lysate. Vinculin staining of the same blot served as a loading control.

4.1.1.3. Single clonal cell line generation

As all three experiments with pools of targeted cells showed, targeting worked better for exon 42 and exon 2 targeted cells; therefore, we continued our analysis with these two cell lines and generated single-cell clones. The single cells were first intracellularly stained for LRBA, and the expression level was confirmed by flow cytometry (Fig. 4-5).

Single-cell clones were stained on two different days in groups of six or twelve, and WT Jurkat cells were stained as controls each time. In all graphs, the orange histograms represent WT, and green histograms represent LRBA targeted single cell clones stained with anti-LRBA antibodies. While some clones have mean fluorescence intensity (MFI) levels similar to WT cells; some, like clone C.12, show increased MFI compared to WT. While it is not clear if this is due to an increase in LRBA expression levels passing cells through a single cell cloning procedure inadvertently results in selective events that may result in changes of phenotypes, perhaps due to epigenetic changes. Thus, we think that

this apparent increase in LRBA expression levels is due to the characteristics of this specific clone. In this analysis, we identified multiple single cell clones that showed decreased LRBA staining levels compared to WT cells (clones C7, C8, C10, C13, C14, and C17). To confirm the absence of LRBA protein expression, we performed western blotting for these cells.

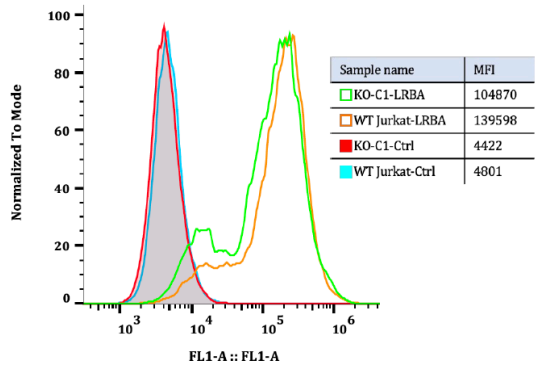

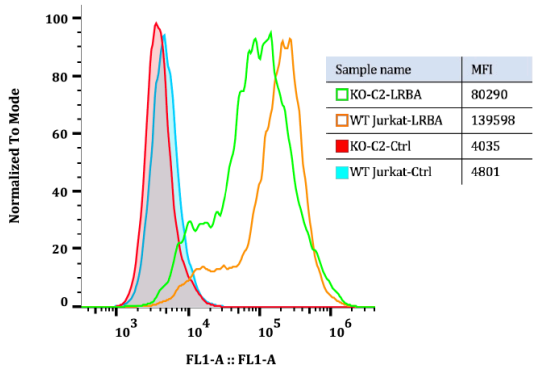

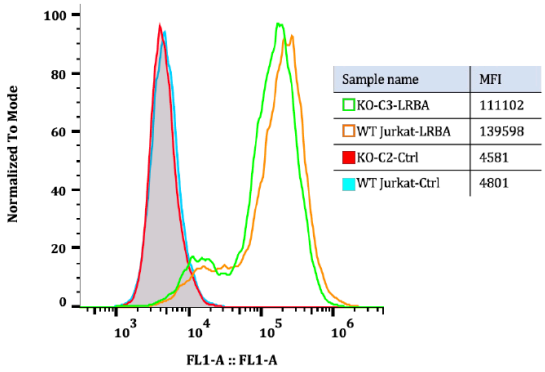

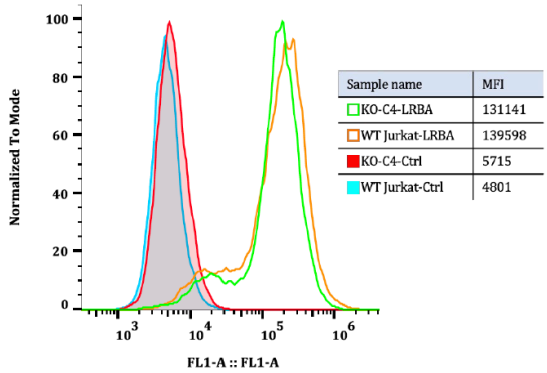

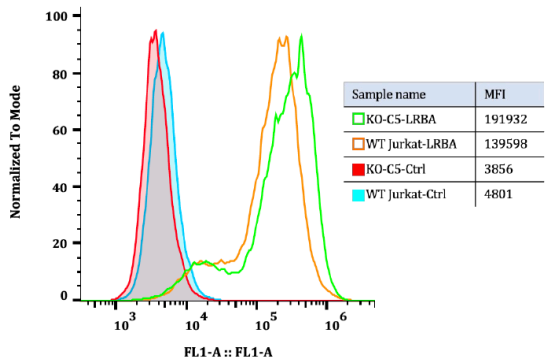

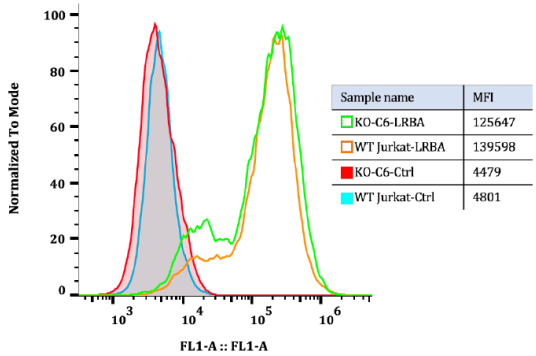

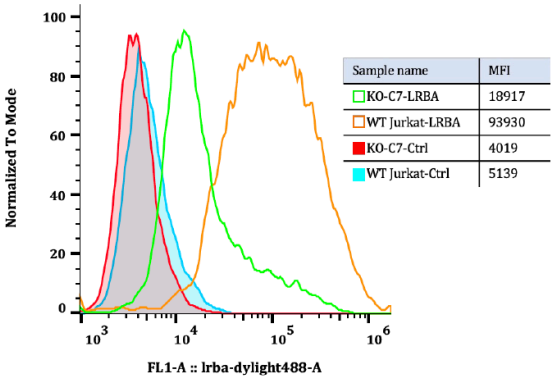
Normalized To Mode
FL1-A :: lrba-dylight488-A
Sample name | MFI
KO-C7-LRBA | 18917
WT Jurkat-LRBA | 93930
KO-C7-Ctrl | 4019
WT Jurkat-Ctrl | 5139

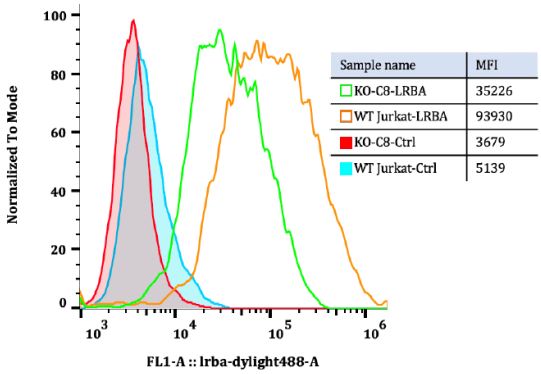
Normalized To Mode
FL1-A :: lrba-dylight488-A
Sample name | MFI
KO-C8-LRBA | 35226
WT Jurkat-LRBA | 93930
KO-C8-Ctrl | 3679
WT Jurkat-Ctrl | 5139

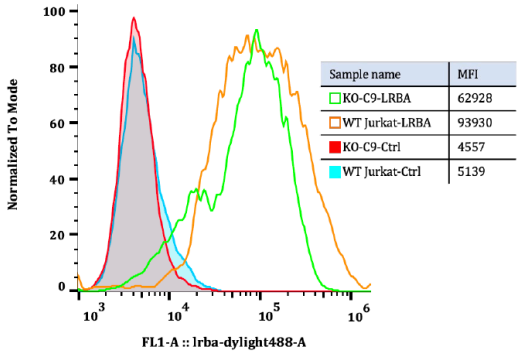
Normalized To Mode
FL1-A :: lrba-dylight488-A
Sample name | MFI
KO-C9-LRBA | 62928
WT Jurkat-LRBA | 93930
KO-C9-Ctrl | 4557
WT Jurkat-Ctrl | 5139

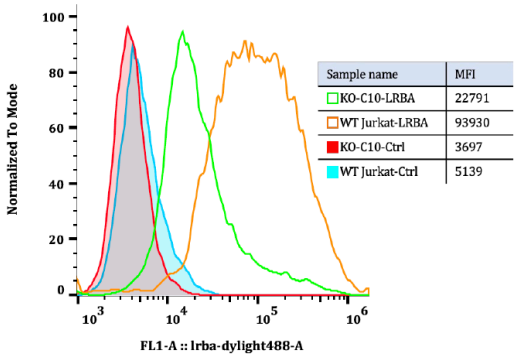
Normalized To Mode
FL1-A :: lrba-dylight488-A
Sample name | MFI
KO-C10-LRBA | 22791
WT Jurkat-LRBA | 93930
KO-C10-Ctrl | 3697
WT Jurkat-Ctrl | 5139

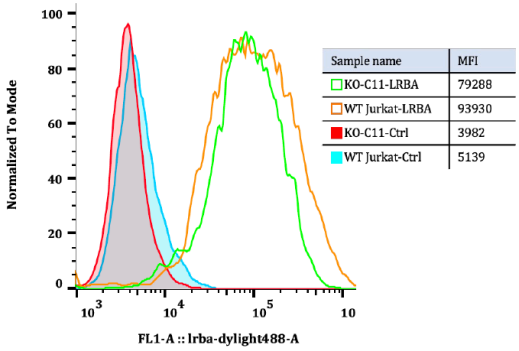
Normalized To Mode
FL1-A :: lrba-dylight488-A
Sample name | MFI
KO-C11-LRBA | 79288
WT Jurkat-LRBA | 93930
KO-C11-Ctrl | 3982
WT Jurkat-Ctrl | 5139

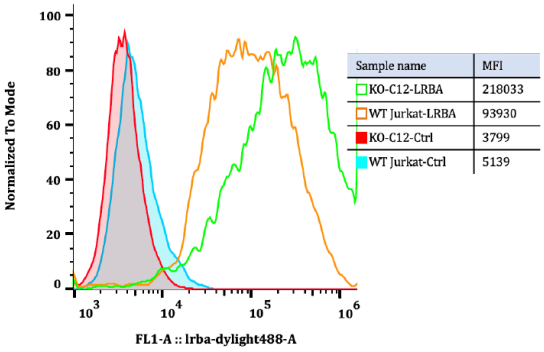
Normalized To Mode
FL1-A :: lrba-dylight488-A
Sample name | MFI
KO-C12-LRBA | 218033
WT Jurkat-LRBA | 93930
KO-C12-Ctrl | 3799
WT Jurkat-Ctrl | 5139

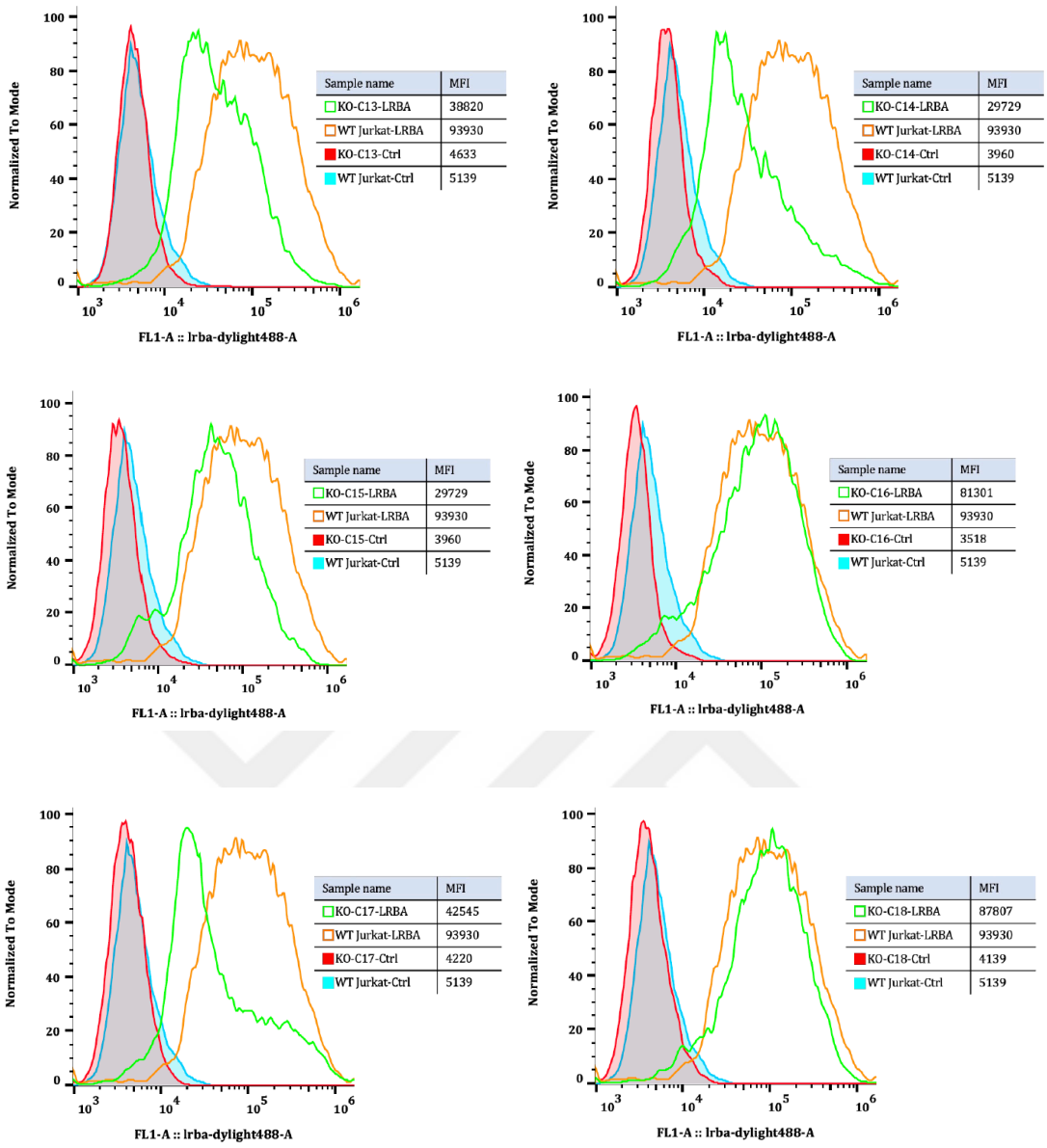

Figure 4-5. Flow cytometry analysis of LRBA targeted single-cell clones. The cells were stained with primary rabbit anti-LRBA antibodies followed by secondary anti-rabbit dylight-488 conjugated antibodies, and as a control cells were only stained with secondary antibodies. Blue highlighted histogram: WT Jurkat control staining, Red highlighted histogram: LRBA-KO single clonal cells control staining, Orange line histogram: WT Jurkat LRBA staining, Green line histogram: LRBA-KO single clonal cells LRBA staining.

When single-cell clones with a decreased LRBA levels by intracellular staining were analyzed by western blotting, not all clones demonstrated a lack of protein expression. Clones C10, C13, and C17 were observed to still express the full-length LRBA protein, while in clones C7, C8, and C14, the full-length LRBA protein was undetectable. Clone C8 showed a lower size band that can be indicative of a truncated protein. Of the three clones lacking LRBA expression, C7 had the thickest lysate control band (Vinculin staining) indicating a large amount of lysate wihtout any detectable LRBA protein, thus it was chosen as the best candidate LRBA knockout cell line for the surface biotinylation assay. To identify any possible truncated proteins in these targeted single cell clones we repeated the Western-blot experiment with lysates from clones C7, C8, and C14 and compared LRBA expression levels to WT and pooled targeted cells (Fig. 4-7). While pools of targeted cells contained reduced levels of LRBA bands, indicative of many alleles in the pool to contain mutant out of frame mutations, some expression persisted, indicating that in pools targeting was not complete. In contrast in the seleceted single cell clones there was no detectable LRBA reactivity except for a truncated band in lysates from clone C8. This indicated that in clone C7 and C14, there were bi-allelic out of frame mutations which resulted in the absence of LRBA reactivity.

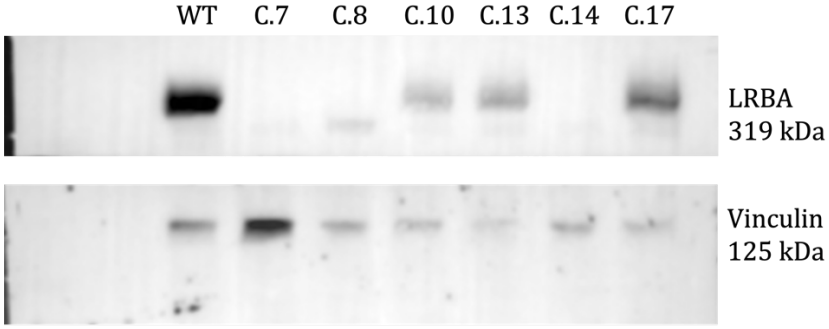

Figure 4-6. Western-blot analysis for selected single-cell clones. For each cell line the loaded sample contained 20 µl of cell lysate and vinculin staining of the same blot served as a loading control.

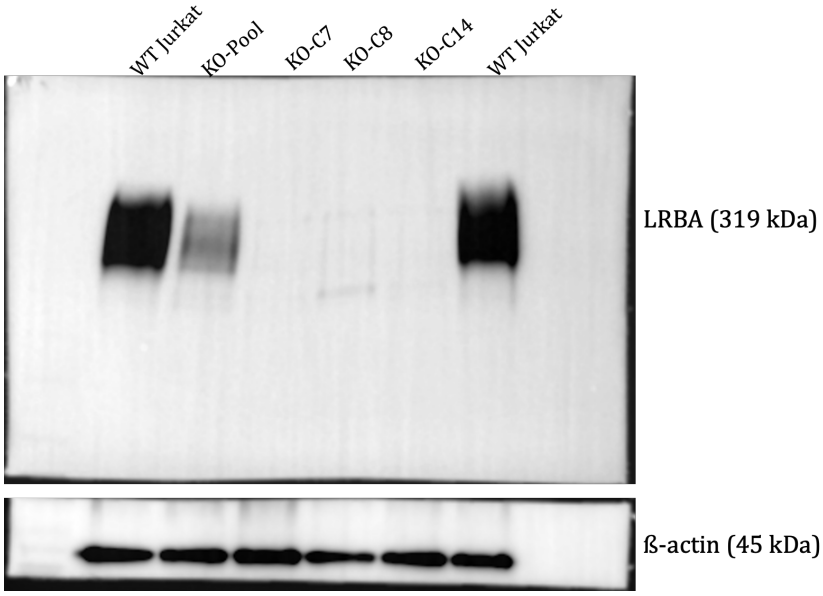

Figure 4-7. Western blot analysis was repeated for C7, C8, and C14. For each cell line the loaded sample contained 20 µl of cell lysate and ß-actin staining of the same blot served as a loading control.

We repeated the T7E1 assay for all three single cell clones and found that the genomic DNA in fact contained mismatches compared to WT (Fig. 4-8). In this assay if both alleles of a single cell clone contain the same mutation, it is expected to be indistinguishable than clones that contain only WT alleles. Interestingly, for clone C8, we obtained very thick bands around 1.5 kbp indicating the presence of a large insertion. Digested bands in the T7E1 assay that are indicative of small deletions were present in amplified genomic DNA from pooled targeted cells, and clones C14 and C7.

To determine the identity of the specific mutations generated in each cell line, we amplified a 900 bp fragment containing the targeted sites from the gDNA of the single clonal cells. After cloning the PCR product into the pCR-Blunt II-TOPO plasmid, the vector was transformed into DH5alpha competent *E.coli*, and plasmid DNA was isolated from several colonies and analyzed by Sanger DNA sequencing (Fig. 4-9). The sequencing results shows that only one of the gRNA has made mutations, and there are two different mutations in every single clonal cell. The C7 cell line contains two alleles, that have a single and five base pair insertions. Clone C14 has a two base pair deletion and a two base pair insertion in its two alleles, and clone C8 has a two base pair deletion

and a 405 base pair insertion in its two alleles. We conclude that the 1.5kbp bands in the T7E1 assay for clone C8 were due to this large insertion. As CRISPR/Cas9 induced double stranded breaks are mainly repaired by NHEJ, they result in random INDELs. In the case of clone C8 the insertion seems to be a result of homologous recombination of this 405bp DNA fragment. To identify the source of the homology we analyzed this sequence by Blast analysis and found that the insertion resulted from a DNA molecule in reversed strand of Zinc finger CCHC domain-containing protein 10 (ZCCHC10, a member of the human CCDS family) gene that is located on the human chromosome 5.

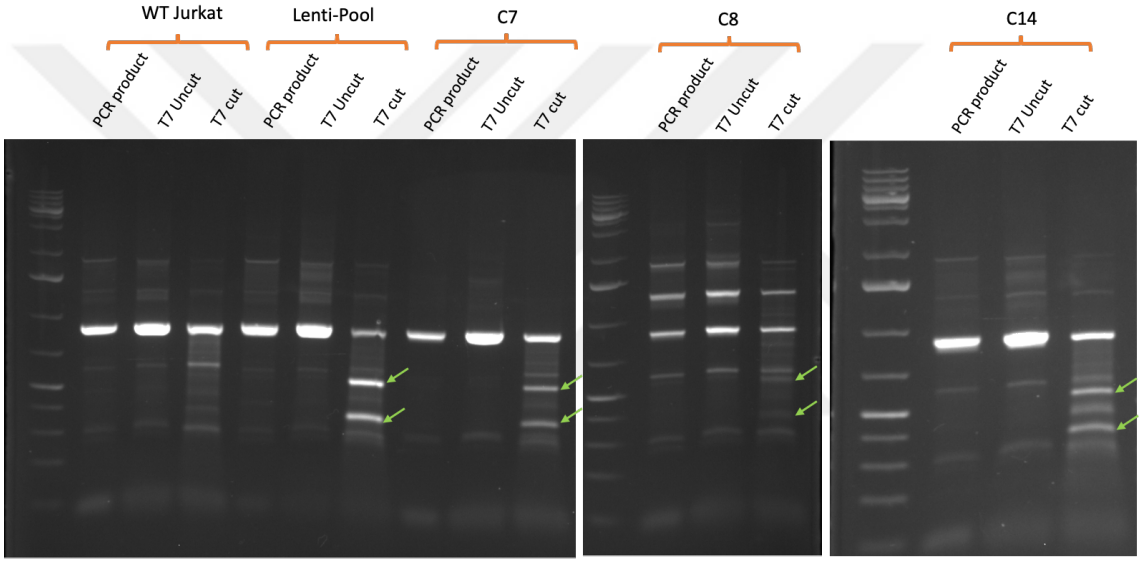

Figure 4-8. T7 E1 assay for single clonal cells. Genomic DNA from each cell type was amplified and PCR products were analyzed by agarose gel electrophoresis without any modification (PCR product lanes), by being exposed to T7 restriction enzyme reactions without the enzyme (T7 uncut), same conditions with the T7 enzyme (T7 cut). Bands in the first two lanes for each sample indicate presence of large INDELs while bands in the last lanes (T7 cut) for each sample indicate the mismatches detected by the T7E1 assay.

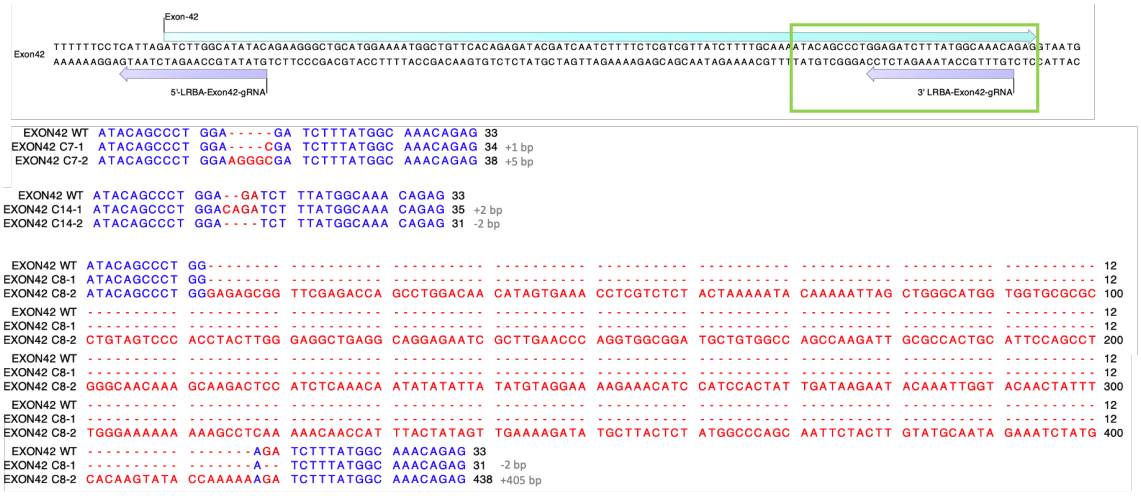

Figure 4-9. Sequencing result for CRISPR/Cas9 induced mutations in PCR amplified genomic DNA from single clonal cells. The gRNA binding sites are indicated. In each case, the WT genomic DNA sequence is aligned with the genomic DNA sequence from the indicated single cell clones (C7, C8,C14). When two alleles were detected in multiple DNA sequences they were annotated as follows: clone name-1 or clone name-2. Thus, the single cell clone C7 contained two detectable alleles C7-1 and C7-2, the single cell clone C8 contained two detectable alleles C8-1 and C8-2 and the single cell clone C14 contained two detectable alleles C14-1 and C14-2. Note that allele C8-2 contained a 405bp DNA insert.

4.1.1.4. Biotinylation assay and Mass Spectrometry analysis

After confirming the absence of LRBA protein in the C7 single clonal cell, we aimed to find differentially expressed proteins on the surface of WT and C7 cells. For this purpose, we performed a biotinylation assay on both WT Jurkat and C7 KO cells to label all cell surface proteins. Biotinylated proteins were enriched on neutravidin agarose beads and following tryptic digestion the generated peptides were analyzed by mass spectrometry (MS). Figure 4-10 is a schematic representation of the general steps included in this experiment, starting from biotinylation until MS analysis. We performed two biological replicates for each WT and C7 samples and identified proteins were reported in three technical replicates. The high confidence proteins were reported based on their Mascot and Sequest analysis scores. The Peptide spectrum match (PSM) number for each protein was considered to be relevant to the abundance of the protein in the sample. As

represented in the heat map plot, the expression levels of surface proteins found in WT and C7 samples clustered in two different categories. In this experiment, biological and technical replicates were closely related (Fig. 4-11).

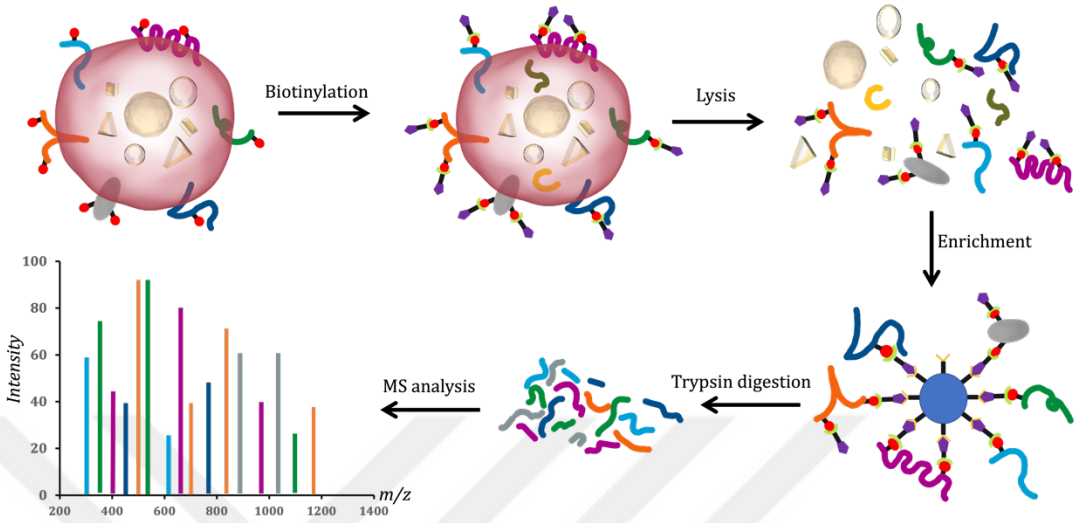

Figure 4-10. Schematic representation of the workflow of the surface biotinylation assay and MS analysis. The cell surface proteins are labeled with a thiol-cleavable amine-reactive biotinylation reagent. Labeled cells were lysed and biotinylated proteins enriched on NeutrAvidin agarose beads. Subsequently, on bead digestion was performed, and generated peptides were analyzed by MS.

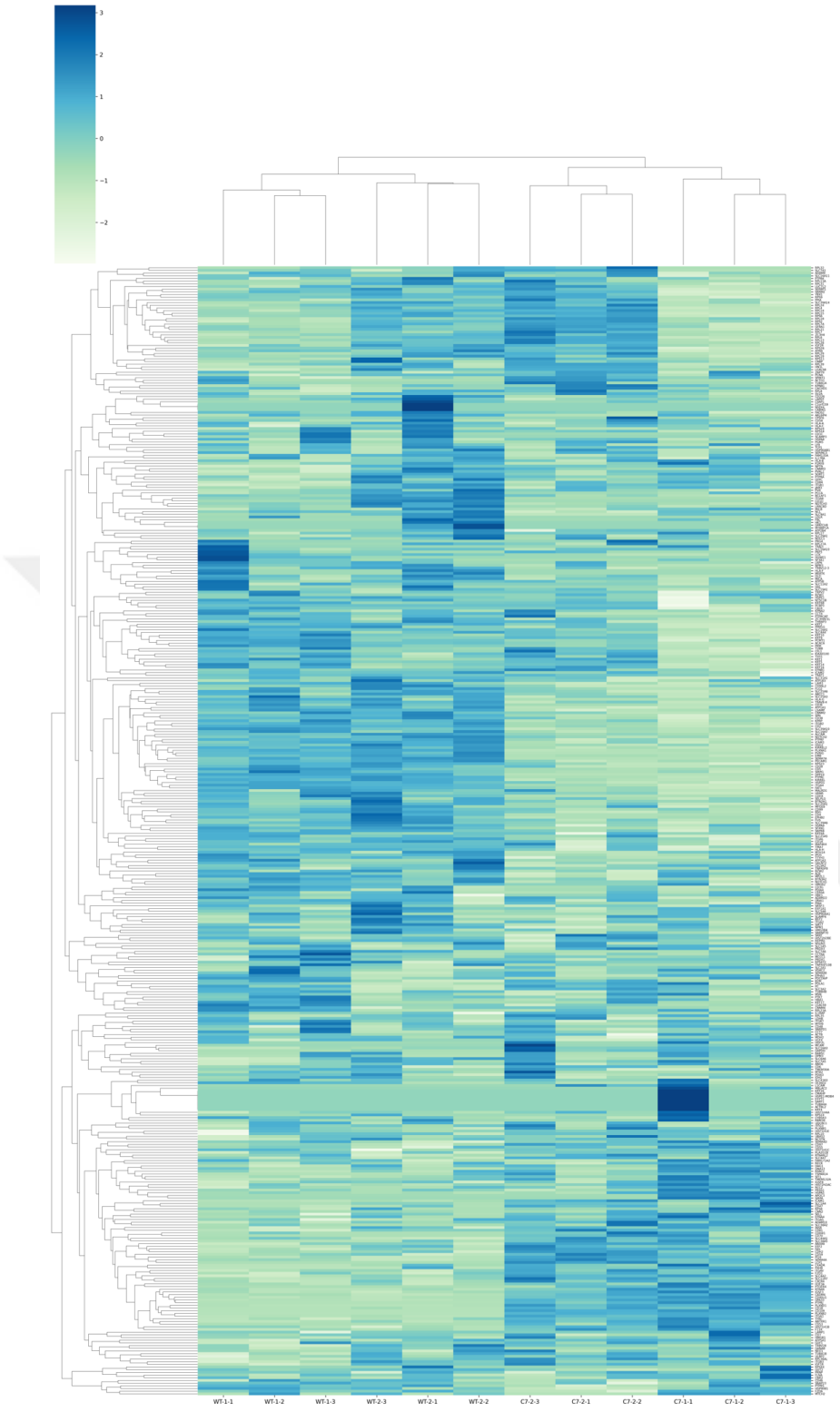

Figure 4-11. Heat map plot representing identified proteins in all biological and technical replicates of WT and clone C7 samples in MS analysis. Hierarchical clustering was performed using the seaborn clustering algorithm. Legend indicates the expression levels

(blue to green= high-expression to low-expression) normalized in rows by Z-score scaling ((sample value- the mean)/ the standard deviation).

4.1.1.5. Gene Ontology analysis (g: Profiler analysis)

Gene Ontology (GO) is a directed acyclic graph structure that defines biological functions and their interrelationships. The GO annotations, accompanied by evidence-based statements, describe the relationship between a specific gene product and a specific ontology term (physical function). The GO has three major sub ontologies: Molecular Functions (MF), which describe the functions of a gene product; Biological Process (BP), which defines which biological process the gene product participates in; and Cellular Component (CC), which describes which part of the cell the particular gene product is physically located.

The analysis was performed for the list of all proteins detected in both WT and KO single clonal cell Jurkat using g: Profiler, a web-based tool to find various biological categories enriched in a given list of genes or proteins. G: GOSt (Gene Ontology Statistics) is one of the g: profiler tools used in this study to identify the statistically significantly enriched biological pathways and processes in the provided list of proteins [70]. Figure 4-12 represents part of the cellular components for all proteins found in both WT and C7 samples. The analysis result confirms that most detected proteins have a membrane, cell surface, and extracellular organs related localization, which is determined as a cellular compartment term. The cellular components for proteins found in each of the WT and C7 samples have also been shown in more detail in figure 4-13. Of course, each protein could belong to more than one cellular component, and as we know, based on protein trafficking, each protein may physically be presented in the cytoplasm before being sorted to the cell surface, which might be the reason for also having a high number for proteins in the cytoplasm.

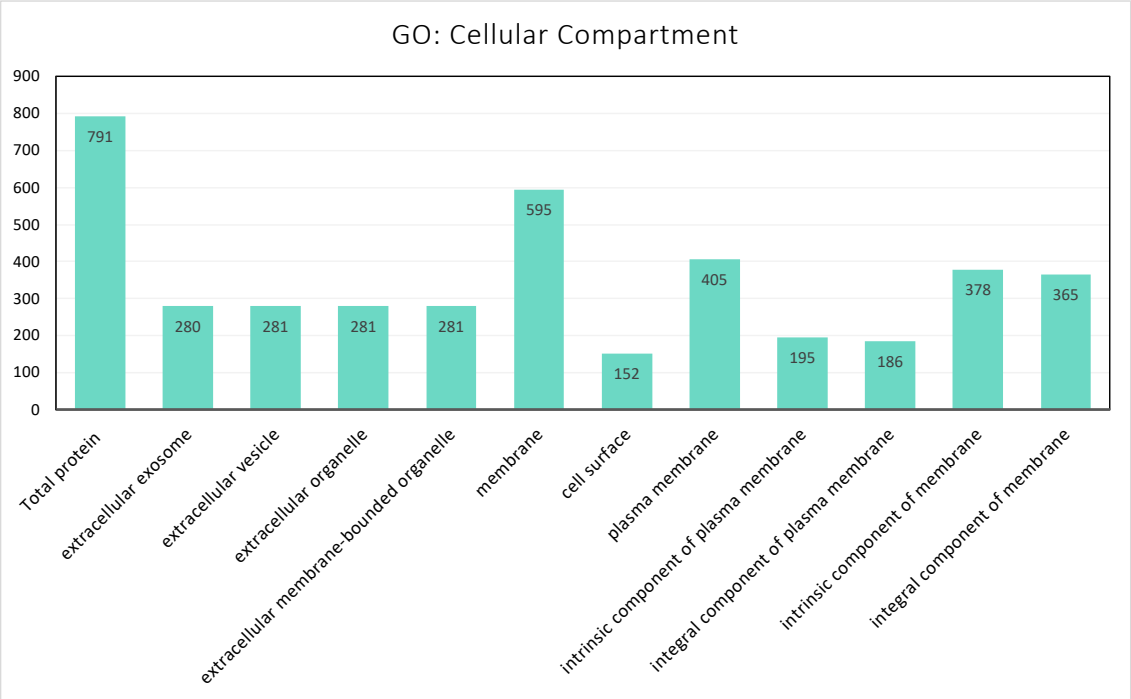

Figure 4-12. g: Profiler analysis. Selected cellular components for all proteins found in WT and C7 samples in MS analysis.

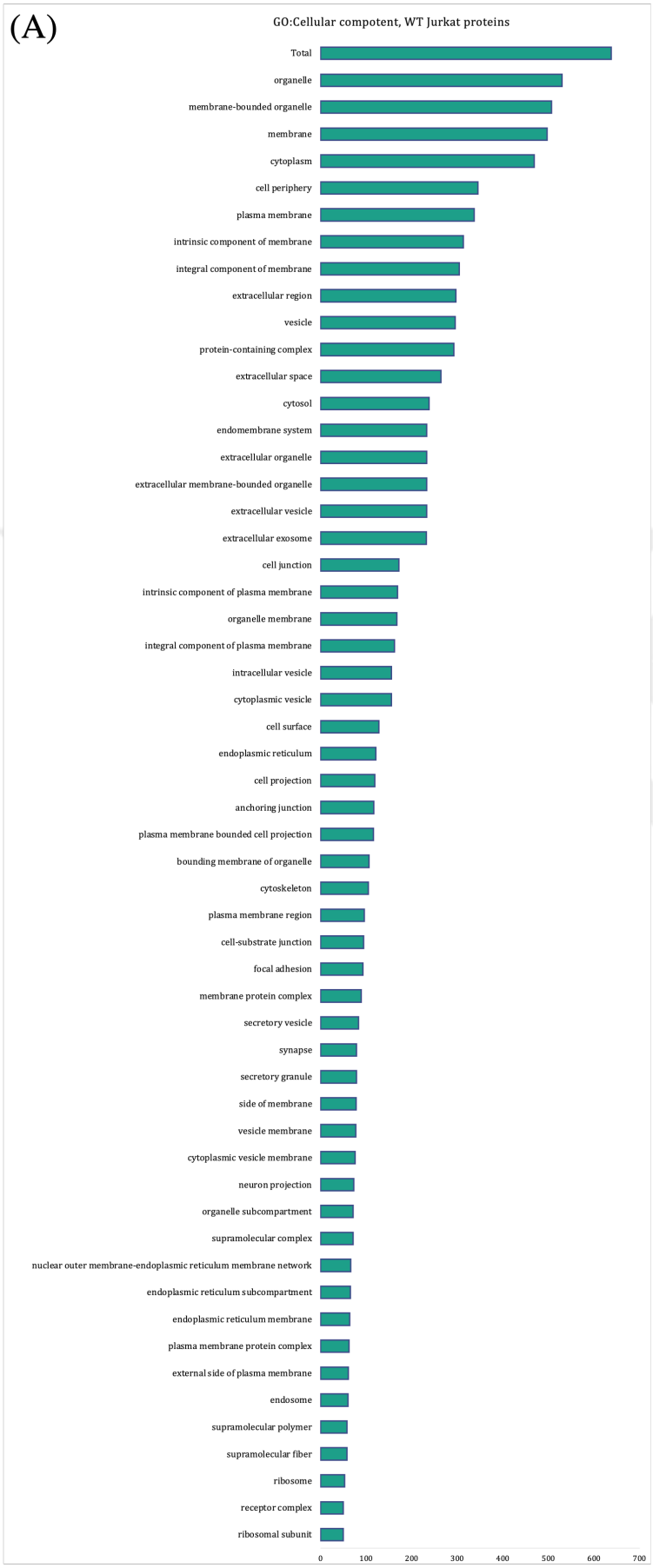
(A)
GO:Cellular compotent, WT Jurkat proteins
Total
organelle
membrane-bounded organelle
membrane
cytoplasm
cell periphery
plasma membrane
intrinsic component of membrane
integral component of membrane
extracellular region
vesicle
protein-containing complex
extracellular space
cytosol
endomembrane system
extracellular organelle
extracellular membrane-bounded organelle
extracellular vesicle
extracellular exosome
cell junction
intrinsic component of plasma membrane
organelle membrane
integral component of plasma membrane
intracellular vesicle
cytoplasmic vesicle
cell surface
endoplasmic reticulum
cell projection
anchoring junction
plasma membrane bounded cell projection
bounding membrane of organelle
cytoskeleton
plasma membrane region
cell-substrate junction
focal adhesion
membrane protein complex
secretory vesicle
synapse
secretory granule
side of membrane
vesicle membrane
cytoplasmic vesicle membrane
neuron projection
organelle subcompartment
supramolecular complex
nuclear outer membrane-endoplasmic reticulum membrane network
endoplasmic reticulum subcompartment
endoplasmic reticulum membrane
plasma membrane protein complex
external side of plasma membrane
endosome
supramolecular polymer
supramolecular fiber
ribosome
receptor complex
ribosomal subunit
0
100
200
300
400
500
600
700

(B)

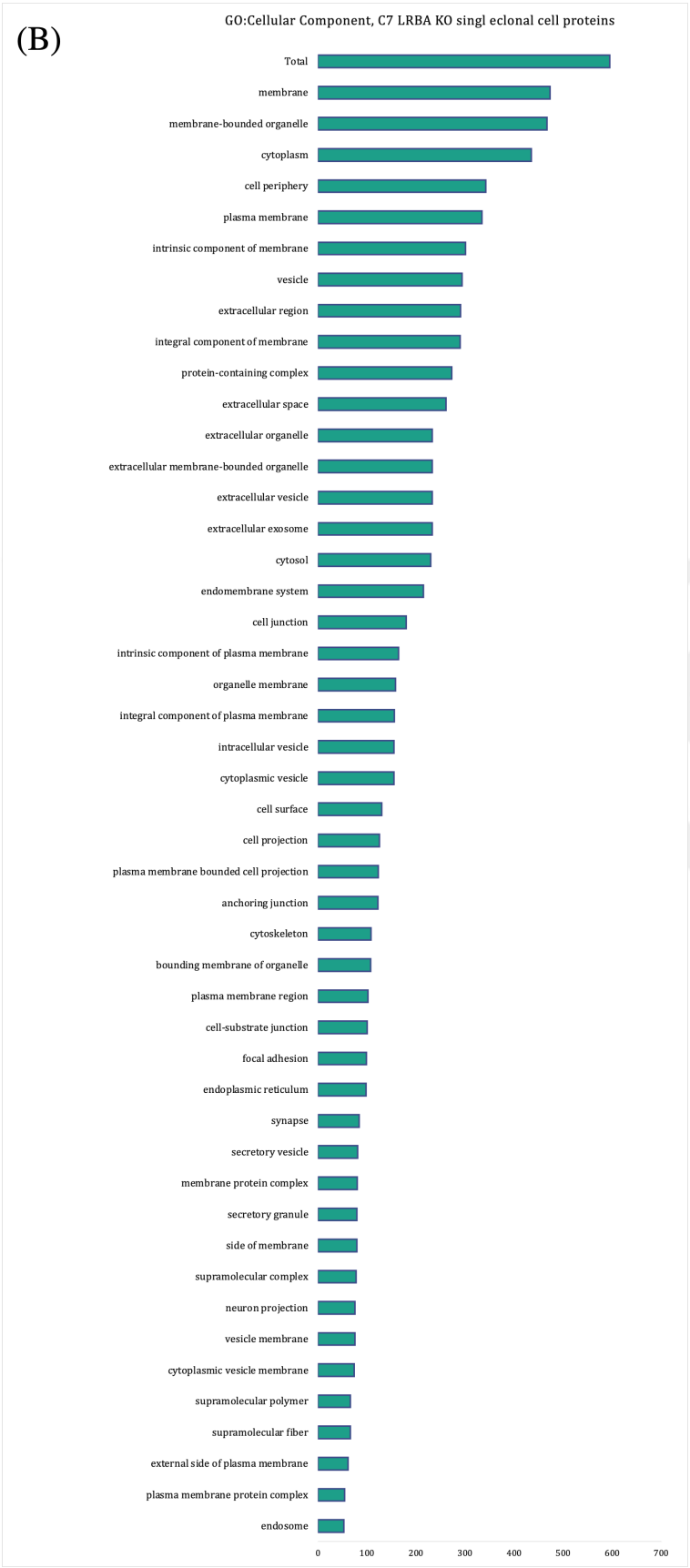
GO:Cellular Component, C7 LRBA KO singl eclonal cell proteins
Total
membrane
membrane-bounded organelle
cytoplasm
cell periphery
plasma membrane
intrinsic component of membrane
vesicle
extracellular region
integral component of membrane
protein-containing complex
extracellular space
extracellular organelle
extracellular membrane-bounded organelle
extracellular vesicle
extracellular exosome
cytosol
endomembrane system
cell junction
intrinsic component of plasma membrane
organelle membrane
integral component of plasma membrane
intracellular vesicle
cytoplasmic vesicle
cell surface
cell projection
plasma membrane bounded cell projection
anchoring junction
cytoskeleton
bounding membrane of organelle
plasma membrane region
cell-substrate junction
focal adhesion
endoplasmic reticulum
synapse
secretory vesicle
membrane protein complex
secretory granule
side of membrane
supramolecular complex
neuron projection
vesicle membrane
cytoplasmic vesicle membrane
supramolecular polymer
supramolecular fiber
external side of plasma membrane
plasma membrane protein complex
endosome
0
100
200
300
400
500
600
700

Figure 4-13. G: Profiler analysis. Cellular Component of proteins found in A) WT Jurkat cells. B) C7 single clonal cell in MS analysis.

4.1.1.6. Statistical analysis of MS data with SAINT software

The Significance Analysis of INTeractome (SAINT) software package is used to score protein-protein interactions in affinity purification – mass spectrometry (AP-MS) experiments using label-free quantitative proteomics data (e.g., spectral count or intensity). Here we used this software to compare the list of proteins expressed on the surface of the WT and KO Jurkat cells. Two biological replicates were prepared from wild type Jurkat and clone C.7. Three technical replicates (mass spectrometry analysis) were conducted for each [71].

SAINT uses the quantitative information from a mass spectrometry analysis, including peptide counts (e.g., spectral counts or number of unique peptides) or MS1 intensity-based values, and measures the confidence score for the presence of a protein or its interaction with a bait. The input files of SAINT encompass the gene name or accession number and length of the protein together with the quantitative factor of each protein coming from mass spectrometry analysis which in our case was the peptide spectrum count (PSM) of each protein. All files were prepared according to the instructions of the software, and the analysis was conducted twice, first considering WT Jurkat as a “test” sample and C7 KO cell as a “control”, second C7 KO cells as a “test” sample and wild type Jurkat as a “control”. In the first case, the software will look for proteins found or expressed more in WT than in the KO sample. In other words, it will give the list of downregulated proteins in KO cells. The second analysis will have a list of proteins upregulated in KO cells. In the final output of SAINT, the most significant upregulated or down-regulate proteins are those with AvgP (main probability score) higher than or equal to 0.5 and those with FDR (false discovery rate) less than or equal to 0.05. The report also includes fold change, the average spectral count in the test sample divided by the average in controls [72,73].

Table 4-1 shows the list of proteins found or upregulated in WT samples or the ones downregulated in KO cells. Table 4-2 shows the list of proteins found or upregulated in

KO samples. The highlighted proteins are found in both biological replicates and are significantly different from control samples. On the other hand, proteins that are not highlighted are present just in one replicate.

Bait	Prey	PreyGene	Description	Spec	SpecSum	AvgSpec	NumReplicates	ctrlCounts	AvgP	MaxP	TopoAvgP	TopoMaxP	SaintScore	logOddsScore	FoldChange	BFDR
WT1	O75326	SEMA7A	Semaphorin-7A OS=Homo sapiens GN=SEMA7A PE=1 SV=1	10|22|13	45	15	3	0|0|0|0|0|0	1	1	1	1	1	15.78	150	0
WT2	O75326	SEMA7A	Semaphorin-7A OS=Homo sapiens GN=SEMA7A PE=1 SV=1	26|26|22	74	24.67	3	0|0|0|0|0|0	1	1	1	1	1	33.72	246.67	0
WT1	P01730	CD4	T-cell surface glycoprotein CD4 OS=Homo sapiens GN=CD4 PE=1 SV=1	10|12|10	32	10.67	3	0|0|0|0|0|0	1	1	1	1	1	15.78	106.67	0
WT2	P01730	CD4	T-cell surface glycoprotein CD4 OS=Homo sapiens GN=CD4 PE=1 SV=1	16|12|30	58	19.33	3	0|0|0|0|0|0	1	1	1	1	1	18.83	193.33	0
WT2	P07766	CD3E	T-cell surface glycoprotein CD3 epsilon chain OS=Homo sapiens GN=CD3E PE=1 SV=2	6|10|12	28	9.33	3	0|0|0|2|2|2	0.98	1	0.98	1	0.98	2.85	9.33	0
WT1	P07766	CD3E	T-cell surface glycoprotein CD3 epsilon chain OS=Homo sapiens GN=CD3E PE=1 SV=2	8|12|4	24	8	3	0|0|0|2|2|2	0.87	1	0.87	1	0.87	0.43	8	0.02
WT2	P23229	ITGA6	Integrin alpha-6 OS=Homo sapiens GN=ITGA6 PE=1 SV=5	14|18|14	46	15.33	3	0|0|0|0|0|0	1	1	1	1	1	2.185	153.33	0
WT1	P23229	ITGA6	Integrin alpha-6 OS=Homo sapiens GN=ITGA6 PE=1 SV=5	3|2|4	9	3	3	0|0|0|0|0|0	0.97	1	0.97	1	0.97	2.58	30	0
WT1	P50747	HLCS	Biotin--protein ligase OS=Homo sapiens GN=HLCS PE=1 SV=1	6|6|4	16	5.33	3	0|0|0|0|0|0	1	1	1	1	1	6.17	53.33	0
WT2	P50747	HLCS	Biotin--protein ligase OS=Homo sapiens GN=HLCS PE=1 SV=1	2|2|4	8	2.67	3	0|0|0|0|0|0	0.95	1	0.95	1	0.95	2.58	26.67	0.01
WT2	P55283	CDH4	Cadherin-4 OS=Homo sapiens GN=CDH4 PE=2 SV=2	4|4|8	16	5.33	3	0|0|0|0|0|0	1	1	1	1	1	6.17	53.33	0
WT1	P55283	CDH4	Cadherin-4 OS=Homo sapiens GN=CDH4 PE=2 SV=2	6|2|10	18	6	3	0|0|0|0|0|0	0.98	1	0.98	1	0.98	2.58	60	0
WT1	Q6DKI7	PVRIG	Transmembrane protein PVRIG OS=Homo sapiens GN=PVRIG PE=2 SV=1	8|9|9	26	8.67	3	0|0|0|0|0|0	1	1	1	1	1	12.67	86.67	0
WT2	Q6DKI7	PVRIG	Transmembrane protein PVRIG OS=Homo sapiens GN=PVRIG PE=2 SV=1	7|14|11	32	10.67	3	0|0|0|0|0|0	1	1	1	1	1	11.09	106.67	0
WT1	Q6PCB8	EMB	Embigin OS=Homo sapiens GN=EMB PE=1 SV=1	24|22|26	72	24	3	8|4|14|10|10|8	1	1	1	1	1	4.74	3.27	0
WT2	Q6PCB8	EMB	Embigin OS=Homo sapiens GN=EMB PE=1 SV=1	26|36|32	94	31.33	3	8|4|14|10|10|8	1	1	1	1	1	10.75	4.27	0
WT1	Q8N608	DPP10	Inactive dipeptidyl peptidase 10 OS=Homo sapiens GN=DPP10 PE=1 SV=2	4|4|4	12	4	3	0|0|0|0|0|0	1	1	1	1	1	6.17	40	0
WT2	Q8N608	DPP10	Inactive dipeptidyl peptidase 10 OS=Homo sapiens GN=DPP10 PE=1 SV=2	4|2|4	10	3.33	3	0|0|0|0|0|0	0.98	1	0.98	1	0.98	2.58	33.33	0
WT1	Q96J84	KIRREL	Kin of IRRE-like protein 1 OS=Homo sapiens GN=KIRREL PE=1 SV=2	34|32|26	92	30.67	3	6|6|8|12|8|4	1	1	1	1	1	10.75	4.18	0
WT2	Q96J84	KIRREL	Kin of IRRE-like protein 1 OS=Homo sapiens GN=KIRREL PE=1 SV=2	34|30|40	104	34.67	3	6|6|8|12|8|4	1	1	1	1	1	1.68	4.73	0
WT1	Q9UIW2	PLXNA1	Plexin-A1 OS=Homo sapiens GN=PLXNA1 PE=1 SV=3	113|130|108	351	117	3	47|33|44|38|42|34	1	1	1	1	1	7.42	2.95	0
WT2	Q9UIW2	PLXNA1	Plexin-A1 OS=Homo sapiens GN=PLXNA1 PE=1 SV=3	129|148|136	413	137.67	3	47|33|44|38|42|34	1	1	1	1	1	32.66	3.47	0
WT1	O60831	PRAP2	PRA1 family protein 2 OS=Homo sapiens GN=PRAP2 PE=1 SV=1	4|4|4	12	4	3	0|0|0|0|0|0	1	1	1	1	1	6.17	40	0
WT2	P01737	TRAV8-4	T-cell receptor alpha chain V region PY14 OS=Homo sapiens PE=1 SV=1	9|13|12	34	11.33	3	0|0|0|6|7|0	0.77	0.85	0.77	0.85	0.77	5.23	0.04	
WT1	P06239	LCK	Tyrosine-protein kinase Lck OS=Homo sapiens GN=LCK PE=1 SV=6	14|6|4	24	8	3	0|2|2|2|0|2	0.73	1	0.73	1	0.73	0.63	6	0.05
WT1	P0CG43	FAM157C	Putative protein FAM157C OS=Homo sapiens GN=FAM157C PE=3 SV=1	5|6|6	17	5.67	3	0|0|0|0|0|0	1	1	1	1	1	7.85	56.67	0
WT2	P12236	SLC25A6	ADP/ATP translocase 3 OS=Homo sapiens GN=SLC25A6 PE=1 SV=4	1|4|11|11	36	12	3	0|3|10|6|10|7	0.75	0.86	0.75	0.86	0.75	0.86	4.5	0.05
WT2	P15260	IFNGR1	Interferon gamma receptor 1 OS=Homo sapiens GN=IFNGR1 PE=1 SV=1	4|2|6	12	4	3	0|0|0|0|0|0	0.98	1	0.98	1	0.98	2.58	40	0
WT2	P15813	CD1D	Antigen-presenting glycoprotein CD1d OS=Homo sapiens GN=CD1D PE=1 SV=1	1|3|12|12	37	12.33	3	0|0|0|0|0|0	1	1	1	1	1	1.883	123.33	0
WT1	P16473	TSHR	Thyrotropin receptor OS=Homo sapiens GN=TSHR PE=1 SV=2	2|2|2	6	2	3	0|0|0|0|0|0	0.93	0.93	0.93	0.93	0.93	2.58	20	0.01
WT2	P17181	IFNAR1	Interferon alpha/beta receptor 1 OS=Homo sapiens GN=IFNAR1 PE=1 SV=3	2|4|4	10	3.33	3	0|0|2|0|0|0	0.8	0.9	0.8	0.9	0.8	0.36	10	0.04
WT1	P17693	HLA-G	HLA class I histocompatibility antigen, alpha chain G OS=Homo sapiens GN=HLA-G PE=1 SV=1	1|2|19|13	44	14.67	3	0|0|0|0|0|0	1	1	1	1	1	1.883	146.67	0
WT1	P37268	FDFT1	Squalene synthase OS=Homo sapiens GN=FDFT1 PE=1 SV=1	4|6|4	14	4.67	3	0|0|2|0|0|0	0.93	0.98	0.93	0.98	0.93	2.21	14	0.01
WT1	Q00610	CLTC	Clathrin heavy chain 1 OS=Homo sapiens GN=CLTC PE=1 SV=5	4|4|8	16	5.33	3	2|2|0|0|0|0	0.82	0.99	0.82	0.99	0.82	1.04	8	0.03
WT2	Q01844	EWSR1	RNA-binding protein EWS OS=Homo sapiens GN=EWSR1 PE=1 SV=1	2|2|4	8	2.67	3	0|0|0|0|0|0	0.95	1	0.95	1	0.95	2.58	26.67	0.01
WT1	Q04695	KRT17	Keratin, type I cytoskeletal 17 OS=Homo sapiens GN=KRT17 PE=1 SV=2	48|40|57	145	48.33	3	0|0|0|0|4|0	0.91	0.94	0.91	0.94	0.91	2.01	6.04	0.02
WT1	Q14318	FKBP8	Peptidyl-prolyl cis-trans isomerase FKBP8 OS=Homo sapiens GN=FKBP8 PE=1 SV=2	2|2|2	6	2	3	0|0|0|0|0|0	0.93	0.93	0.93	0.93	0.93	2.58	20	0.01
WT2	Q5D862	FLG2	Filaggrin-2 OS=Homo sapiens GN=FLG2 PE=1 SV=1	8|10|12	30	10	3	0|0|0|2|0|4	0.94	0.98	0.94	0.98	0.94	2.11	10	0.01
WT2	Q66PJ3	ARL6IP4	ADP-ribosylation factor-like protein 6-interacting protein 4 OS=Homo sapiens GN=ARL6IP4 PE=1 SV=2	6|4|4	14	4.67	3	4|0|0|0|0|0	0.75	0.86	0.75	0.86	0.75	0.86	7	0.04
WT1	Q7Z6Z7	HUWE1	E3 ubiquitin-protein ligase HUWE1 OS=Homo sapiens GN=HUWE1 PE=1 SV=3	6|2|2	10	3.33	3	0|0|0|0|0|0	0.95	1	0.95	1	0.95	2.58	33.33	0.01
WT1	Q8TEX9	IPO4	Importin-4 OS=Homo sapiens GN=IPO4 PE=1 SV=2	6|12|6	24	8	3	0|0|0|0|0|4	0.9	0.98	0.9	0.98	0.9	1.79	12	0.02
WT2	Q9H8M5	CNNM2	Metal transporter CNNM2 OS=Homo sapiens GN=CNNM2 PE=1 SV=2	12|6|8	26	8.67	3	0|0|0|4|0|4	0.8	0.95	0.8	0.95	0.8	0.61	6.5	0.03
WT1	Q9P1W8	SIRPG	Signal-regulatory protein gamma OS=Homo sapiens GN=SIRPG PE=1 SV=3	24|44|32	100	33.33	3	14|21|4|8|8|10	0.84	1	0.84	1	0.84	0.12	4.35	0.02
WT1	Q9ULE5	SLC39A10	Zinc transporter ZIP10 OS=Homo sapiens GN=SLC39A10 PE=1 SV=2	53|54|50	157	52.33	3	16|22|21|4|18|24|12		1		1	1	5.17	2.96	0
WT2	Q9UM47	NOTCH3	Neurogenic locus notch homolog protein 3 OS=Homo sapiens GN=NOTCH3 PE=1 SV=2	12|16|17	45	15	3	2|0|4|2|4|0		1		1	1	4.33	7.5	0

Table 4-1. SAINT output for WT as the test sample. Proteins that are significantly expressed higher in the WT sample (e.g., Proteins downregulated in KO sample)

Bait	Prey	PreyGene	Description	Spec	SpecSum	AvgSpec	NumReplicates	ctrlCounts	AvgP	MaxP	TopoAvgP	TopoMaxP	SaintScore	logOddsScore	FoldChange	BFDR
C7-1	Q6YHK3	CD109	CD109 antigen OS=Homo sapiens GN=CD109 PE=1 SV=2	28|24|14	66	22	3	0|0|0|0|0|0	1	1	1	1	1	21.66	220	0
C7-2	Q6YHK3	CD109	CD109 antigen OS=Homo sapiens GN=CD109 PE=1 SV=2	22|22|26	70	23.33	3	0|0|0|0|0|0	1	1	1	1	1	33.52	233.33	0
C7-1	P29016	CD1B	T-cell surface glycoprotein CD1b OS=Homo sapiens GN=CD1B PE=1 SV=1	8|18|10	36	12	3	0|0|0|0|0|2	1	1	1	1	1	5.01	36	0
C7-2	P29016	CD1B	T-cell surface glycoprotein CD1b OS=Homo sapiens GN=CD1B PE=1 SV=1	8|14|12	34	11.33	3	0|0|0|0|0|2	1	1	1	1	1	5.01	34	0
C7-1	P29965	CD40LG	CD40 ligand OS=Homo sapiens GN=CD40LG PE=1 SV=1	40|42|32	114	38	3	4|0|4|4|4|0	1	1	1	1	1	18.06	14.25	0
C7-2	P29965	CD40LG	CD40 ligand OS=Homo sapiens GN=CD40LG PE=1 SV=1	25|30|22	77	25.67	3	4|0|4|4|4|0	1	1	1	1	1	10.34	9.63	0
C7-1	Q9Y624	F11R	Junctional adhesion molecule A OS=Homo sapiens GN=F11R PE=1 SV=1	26|24|16	66	22	3	2|2|8|8|4|4	0.96	1	0.96	1	0.96	1.88	4.71	0.01
C7-2	Q9Y624	F11R	Junctional adhesion molecule A OS=Homo sapiens GN=F11R PE=1 SV=1	26|16|14	56	18.67	3	2|2|8|8|4|4	0.79	1	0.79	1	0.79	0.01	4	0.03
C7-1	Q99795	GPA33	Cell surface A33 antigen OS=Homo sapiens GN=GPA33 PE=1 SV=1	46|48|42	136	45.33	3	8|10|10|8|10|6	1	1	1	1	1	21.13	5.23	0
C7-2	Q99795	GPA33	Cell surface A33 antigen OS=Homo sapiens GN=GPA33 PE=1 SV=1	30|46|40	116	38.67	3	8|10|10|8|10|6	1	1	1	1	1	8	4.46	0
C7-1	P56199	ITGA1	Integrin alpha-1 OS=Homo sapiens GN=ITGA1 PE=1 SV=2	85|78|103	266	88.67	3	4|10|8|4|6|15	1	1	1	1	1	24.6	11.32	0
C7-2	P56199	ITGA1	Integrin alpha-1 OS=Homo sapiens GN=ITGA1 PE=1 SV=2	69|60|90	219	73	3	4|10|8|4|6|15	1	1	1	1	1	16.93	9.32	0
C7-1	O15031	PLXNB2	Plexin-B2 OS=Homo sapiens GN=PLXNB2 PE=1 SV=3	112|112|11	343	114.33	3	0|0|0|0|0|2	1	1	1	1	1	63	343	0
C7-2	O15031	PLXNB2	Plexin-B2 OS=Homo sapiens GN=PLXNB2 PE=1 SV=3	108|100|97	305	101.67	3	0|0|0|0|0|2	1	1	1	1	1	54.97	305	0
C7-1	Q9Y4D7	PLXND1	Plexin-D1 OS=Homo sapiens GN=PLXND1 PE=1 SV=3	32|42|32	106	35.33	3	2|0|0|0|2|0	1	1	1	1	1	24.71	53	0
C7-2	Q9Y4D7	PLXND1	Plexin-D1 OS=Homo sapiens GN=PLXND1 PE=1 SV=3	26|40|45	111	37	3	2|0|0|0|2|0	1	1	1	1	1	19.8	55.5	0
C7-1	Q12913	PTPRJ	Receptor-type tyrosine-protein phosphatase eta OS=Homo sapiens GN=PTPRJ PE=1 SV=3	6|6|4	16	5.33	3	0|0|0|0|0|0	1	1	1	1	1	5.97	53.33	0
C7-2	Q12913	PTPRJ	Receptor-type tyrosine-protein phosphatase eta OS=Homo sapiens GN=PTPRJ PE=1 SV=3	2|4|4	10	3.33	3	0|0|0|0|0|0	0.97	1	0.97	1	0.97	2.38	33.33	0
C7-1	Q9BZR6	RTN4R	Reticulon-4 receptor OS=Homo sapiens GN=RTN4R PE=1 SV=1	8|10|10	28	9.33	3	2|0|0|2|0|0	1	1	1	1	1	4.52	14	0
C7-2	Q9BZR6	RTN4R	Reticulon-4 receptor OS=Homo sapiens GN=RTN4R PE=1 SV=1	4|10|4	18	6	3	2|0|0|2|0|0	0.8	1	0.8	1	0.8	0.85	9	0.02
C7-2	P43489	TNFRSF4	Tumor necrosis factor receptor superfamily member 4 OS=Homo sapiens GN=TNFRSF4 PE=1 SV=1	4|4|6	14	4.67	3	0|0|0|0|0|0	1	1	1	1	1	5.97	46.67	0
C7-1	P43489	TNFRSF4	Tumor necrosis factor receptor superfamily member 4 OS=Homo sapiens GN=TNFRSF4 PE=1 SV=1	2|6|6	14	4.67	3	0|0|0|0|0|0	0.97	1	0.97	1	0.97	2.38	46.67	0
C7-2	P63261	ACTG1	Actin, cytoplasmic 2 OS=Homo sapiens GN=ACTG1 PE=1 SV=1	129|116|13	380	126.67	3	127|0|0|0|0|0	0.94	0.94	0.94	0.94	0.94	2.52	5.98	0.01
C7-1	P02656	APOC3	Apolipoprotein C-III OS=Homo sapiens GN=APOC3 PE=1 SV=1	6|6|6	18	6	3	0|0|0|0|0|0	1	1	1	1	1	9.29	60	0
C7-1	Q8NFZ8	CADM4	Cell adhesion molecule 4 OS=Homo sapiens GN=CADM4 PE=1 SV=1	24|32|24	80	26.67	3	8|10|10|6|8|6	0.97	1	0.97	1	0.97	2.9	3.33	0.01
C7-1	P19397	CD53	Leukocyte surface antigen CD53 OS=Homo sapiens GN=CD53 PE=1 SV=1	6|4|6	16	5.33	3	0|0|0|0|0|0	1	1	1	1	1	5.97	53.33	0
C7-2	P32970	CD70	CD70 antigen OS=Homo sapiens GN=CD70 PE=1 SV=2	2|4|2	8	2.67	3	0|0|0|0|0|0	0.94	1	0.94	1	0.94	2.38	26.67	0.01
C7-1	Q99439	CNN2	Calponin-2 OS=Homo sapiens GN=CNN2 PE=1 SV=4	2|8|10	20	6.67	3	0|2|0|1|0|2	0.71	1	0.71	1	0.71	-1.79	8	0.04
C7-2	P20023	CR2	Complement receptor type 2 OS=Homo sapiens GN=CR2 PE=1 SV=2	2|2|2	6	2	3	0|0|0|0|0|0	0.92	0.92	0.92	0.92	0.92	2.38	20	0.01
C7-1	Q14344	GNA13	Guanine nucleotide-binding protein subunit alpha-13 OS=Homo sapiens GN=GNA13 PE=1 SV=2	4|4|4	12	4	3	2|0|0|0|0|2	0.7	0.7	0.7	0.7	0.7	0.85	6	0.05
C7-2	P05362	ICAM1	Intercellular adhesion molecule 1 OS=Homo sapiens GN=ICAM1 PE=1 SV=2	19|24|16	59	19.67	3	4|4|3|4|6|6	0.99	1	0.99	1	0.99	3.9	4.37	0
C7-2	P13164	IFITM1	Interferon-induced transmembrane protein 1 OS=Homo sapiens GN=IFITM1 PE=1 SV=3	2|9|2	13	4.33	3	0|0|0|0|0|0	0.94	1	0.94	1	0.94	2.38	43.33	0.01
C7-2	P13796	LCP1	Plastin-2 OS=Homo sapiens GN=LCP1 PE=1 SV=6	8|10|10	28	9.33	3	0|0|0|0|0|0	1	1	1	1	1	12.47	93.33	0
C7-2	O95232	LUC7L3	Luc7-like protein 3 OS=Homo sapiens GN=LUC7L3 PE=1 SV=2	8|2|6	16	5.33	3	0|0|0|0|0|0	0.97	1	0.97	1	0.97	2.38	53.33	0
C7-1	P43121	MCAM	Cell surface glycoprotein MUC18 OS=Homo sapiens GN=MCAM PE=1 SV=2	4|2|2	8	2.67	3	0|0|0|0|0|0	0.94	1	0.94	1	0.94	2.38	26.67	0.01
C7-2	Q96RD7	PANX1	Pannexin-1 OS=Homo sapiens GN=PANX1 PE=1 SV=4	10|6|7	23	7.67	3	1|0|2|0|0|4	0.82	0.96	0.82	0.96	0.82	0.84	6.57	0.02
C7-1	P35408	PTGER4	Prostaglandin E2 receptor EP4 subtype OS=Homo sapiens GN=PTGER4 PE=1 SV=1	8|4|8	20	6.67	3	0|0|0|0|0|0	1	1	1	1	1	5.97	66.67	0
C7-2	Q92692	PVRL2	Nectin-2 OS=Homo sapiens GN=PVRL2 PE=1 SV=1	4|6|6	16	5.33	3	0|0|0|0|0|0	1	1	1	1	1	5.97	53.33	0
C7-2	P18124	RPL7	60S ribosomal protein L7 OS=Homo sapiens GN=RPL7 PE=1 SV=1	18|12|24	54	18	3	0|2|0|2|10|8	0.71	0.94	0.71	0.94	0.71	-0.55	4.91	0.05
C7-2	P62277	RPS13	40S ribosomal protein S13 OS=Homo sapiens GN=RPS13 PE=1 SV=2	4|10|6	20	6.67	3	0|2|0|0|4|0	0.72	0.94	0.72	0.94	0.72	-0.08	6.67	0.04
C7-1	P78324	SIRPA	Tyrosine-protein phosphatase non-receptor type substrate 1 OS=Homo sapiens GN=SIRPA PE=1 SV	4|4|2	10	3.33	3	0|0|0|0|0|0	0.97	1	0.97	1	0.97	2.38	33.33	0
C7-2	P43007	SLC1A4	Neutral amino acid transporter A OS=Homo sapiens GN=SLC1A4 PE=1 SV=1	4|4|4	12	4	3	0|0|0|2|0|2	0.7	0.7	0.7	0.7	0.7	0.85	6	0.05
C7-1	Q8NG11	TSPAN14	Tetraspanin-14 OS=Homo sapiens GN=TSPAN14 PE=1 SV=1	4|6|6	16	5.33	3	0|0|0|0|4|0	0.77	0.83	0.77	0.83	0.77	0.67	8	0.03
C7-2	P31946	YWHAB	14-3-3 protein beta/alpha OS=Homo sapiens GN=YWHAB PE=1 SV=3	2|6|2	10	3.33	3	0|0|0|0|0|0	0.94	1	0.94	1	0.94	2.38	33.33	0.01

Table 4-2. SAINT output for KO as the test sample. Proteins that are significantly expressed higher in the KO sample (e.g., Proteins upregulated in the KO sample)

According to the heat map graph, there are groups of proteins that are expressed cell-type-specific manner showing that WT and C7 have distinct cell surface protein expression profiles for a group of proteins (Fig.4-14).

Of all 791 cell surface proteins found in both WT and C7 samples, 34 were significantly downregulated, and 33 were significantly upregulated in C7 cells. The log2 (fold change) approximately ranges from 1.5 to 9 for these proteins Fig.4-15.

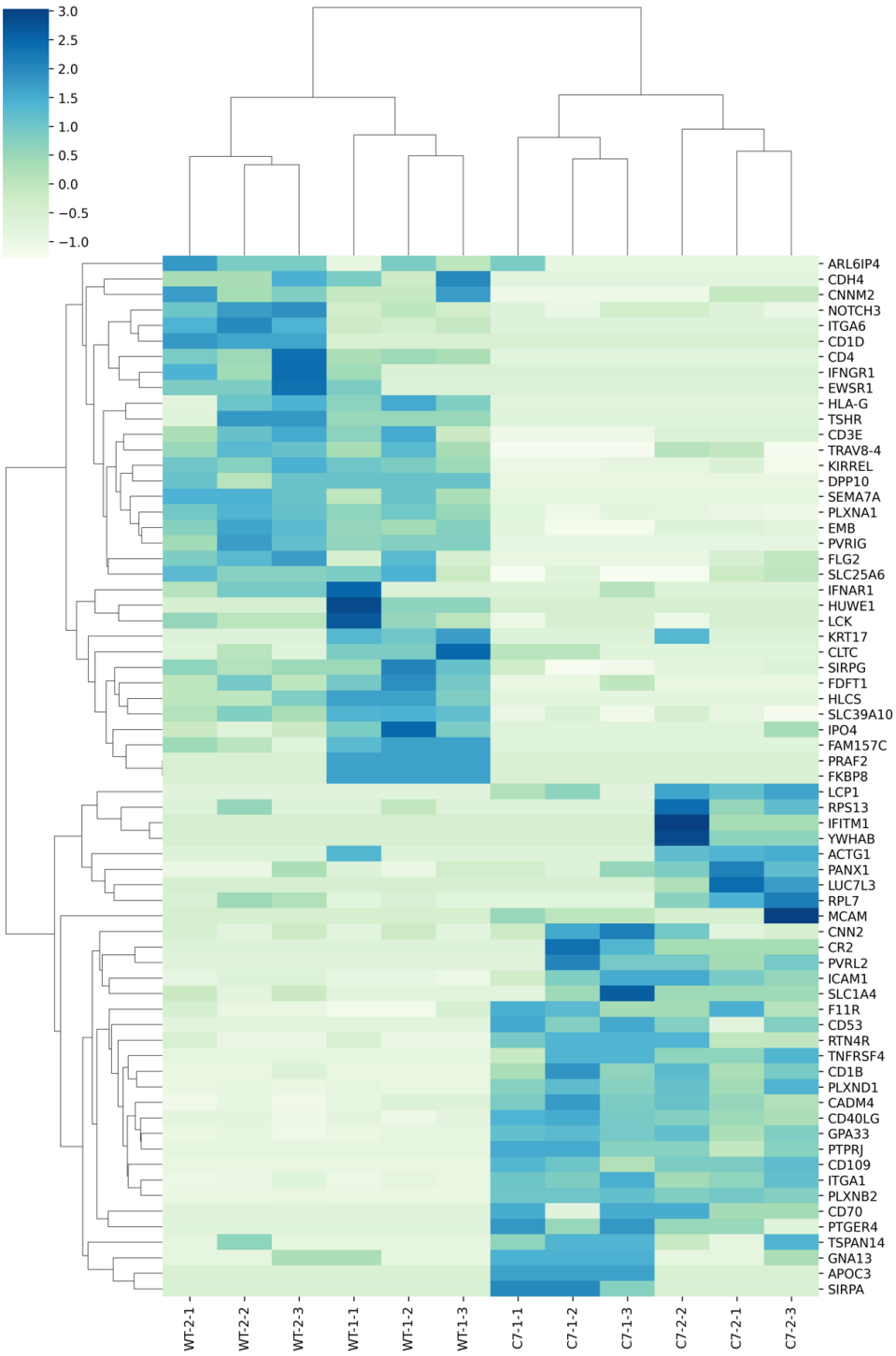

Figure 4-14. Heat map plot representing Peptide Spectrum Match (PSM) of differentially expressed cell surface protein in all biological replicates in both WT and C7 samples. Hierarchical clustering was performed using the seaborn clustering algorithm. Legend indicates the expression levels (blue to green= high-expression to low-expression) normalized in rows by Z-score scaling ((sample value- the mean)/ the standard deviation).

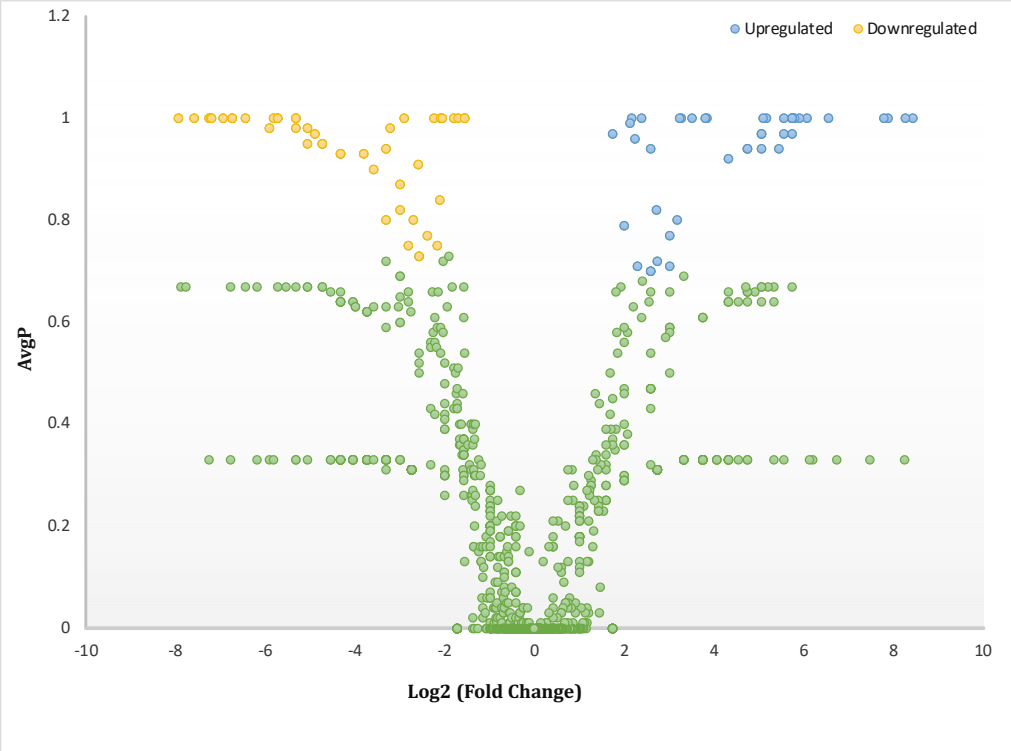

Figure 4-15. Volcano plot representing proteins significantly upregulated (blue) or downregulated (yellow) in LRBA KO single clonal cell C7.

The Gene Ontology analysis was performed for both lists of proteins, upregulated and downregulated. Gene ontology for biological process terms shows that most of the covered proteins in both lists are involved in the immune system process, cell adhesion, and positive or negative regulation of the immune system table 4-3 and table 4-4.

source	term_name	term_size	query_size	intersection_size	intersections
GO:MF	CD8 receptor binding	3	32	2	LCK,HLA-G
GO:MF	interferon receptor activity	6	32	2	IFNGR1,IFNAR1
GO:MF	T cell receptor binding	10	32	2	CD3E,LCK
GO:BP	positive regulation of T cell activation	221	32	6	CD4,CD3E,LCK,CD1D,HLA-G,SIRPG
GO:BP	positive regulation of lymphocyte activation	368	32	7	CD4,CD3E,LCK,CD1D,HLA-G,SIRPG,SLC39A10
GO:BP	positive regulation of leukocyte cell-cell adhesion	242	32	6	CD4,CD3E,LCK,CD1D,HLA-G,SIRPG
GO:BP	positive regulation of leukocyte activation	415	32	7	CD4,CD3E,LCK,CD1D,HLA-G,SIRPG,SLC39A10
GO:BP	positive regulation of cell activation	430	32	7	CD4,CD3E,LCK,CD1D,HLA-G,SIRPG,SLC39A10
GO:BP	positive regulation of cell-cell adhesion	288	32	6	CD4,CD3E,LCK,CD1D,HLA-G,SIRPG
GO:BP	cell-cell adhesion	913	32	9	CD4,CD3E,ITGA6,CDH4,EMB,LCK,CD1D,HLA-G,SIRPG
GO:BP	cell adhesion	1489	32	11	CD4,CD3E,ITGA6,CDH4,EMB,PLXNA1,LCK,CD1D,HLA-G,FLG2,SIRPG
GO:BP	positive regulation of immune system process	936	32	9	SEMA7A,CD4,CD3E,PVRIG,LCK,CD1D,HLA-G,SIRPG,SLC39A10
GO:BP	leukocyte activation	953	32	9	CD4,CD3E,LCK,IFNGR1,CD1D,TSHR,HLA-G,SIRPG,SLC39A10
GO:BP	regulation of leukocyte cell-cell adhesion	334	32	6	CD4,CD3E,LCK,CD1D,HLA-G,SIRPG
GO:BP	regulation of T cell activation	342	32	6	CD4,CD3E,LCK,CD1D,HLA-G,SIRPG
GO:BP	regulation of lymphocyte activation	529	32	7	CD4,CD3E,LCK,CD1D,HLA-G,SIRPG,SLC39A10
GO:BP	leukocyte cell-cell adhesion	373	32	6	CD4,CD3E,LCK,CD1D,HLA-G,SIRPG
GO:BP	lymphocyte activation	794	32	8	CD4,CD3E,LCK,CD1D,TSHR,HLA-G,SIRPG,SLC39A10
GO:BP	immune system process	2781	32	14	SEMA7A,CD4,CD3E,ITGA6,PVRIG,TRAV8-4,LCK,IFNGR1,CD1D,TSHR,IFNAR1,HLA-G,SIRPG,SLC39A10
GO:BP	lymphocyte differentiation	391	32	6	CD4,CD3E,LCK,CD1D,TSHR,HLA-G
GO:BP	cell surface receptor signaling pathway	2811	32	14	SEMA7A,CD4,CD3E,ITGA6,PVRIG,PLXNA1,LCK,IFNGR1,TSHR,IFNAR1,HLA-G,FKBP8,SLC39A10,NOTCH3
GO:BP	cell activation	1094	32	9	CD4,CD3E,LCK,IFNGR1,CD1D,TSHR,HLA-G,SIRPG,SLC39A10
GO:BP	positive regulation of immune response	600	32	7	CD4,CD3E,PVRIG,LCK,CD1D,HLA-G,SLC39A10
GO:BP	cell differentiation	4160	32	17	SEMA7A,CD4,CD3E,ITGA6,CDH4,EMB,PLXNA1,LCK,IFNGR1,CD1D,TSHR,HLA-G,CLTC,KRT17,FKBP8,HUWE1,NOTCH3
GO:BP	axon guidance	237	32	5	SEMA7A,CDH4,EMB,PLXNA1,NOTCH3
GO:BP	neuron projection guidance	238	32	5	SEMA7A,CDH4,EMB,PLXNA1,NOTCH3
KEGG	Th1 and Th2 cell differentiation	86	22	5	CD4,CD3E,LCK,IFNGR1,NOTCH3
KEGG	PD-L1 expression and PD-1 checkpoint pathway in cancer	88	22	4	CD4,CD3E,LCK,IFNGR1
KEGG	Hematopoietic cell lineage	91	22	4	CD4,CD3E,ITGA6,CD1D
KEGG	Primary immunodeficiency	37	22	3	CD4,CD3E,LCK
KEGG	Th17 cell differentiation	104	22	4	CD4,CD3E,LCK,IFNGR1
KEGG	Human T-cell leukemia virus 1 infection	211	22	5	CD4,CD3E,LCK,SLC25A6,HLA-G
KEGG	Natural killer cell mediated cytotoxicity	117	22	4	LCK,IFNGR1,IFNAR1,HLA-G
KEGG	Osteoclast differentiation	124	22	4	LCK,IFNGR1,IFNAR1,SIRPG
KEGG	Cell adhesion molecules	143	22	4	CD4,ITGA6,CDH4,HLA-G
REAC	Translocation of ZAP-70 to Immunological synapse	20	25	4	CD4,CD3E,TRAV8-4,LCK
REAC	Phosphorylation of CD3 and TCR zeta chains	23	25	4	CD4,CD3E,TRAV8-4,LCK
REAC	PD-1 signaling	24	25	4	CD4,CD3E,TRAV8-4,LCK
REAC	Generation of second messenger molecules	35	25	4	CD4,CD3E,TRAV8-4,LCK
REAC	Costimulation by the CD28 family	67	25	4	CD4,CD3E,TRAV8-4,LCK
REAC	Downstream TCR signaling	98	25	4	CD4,CD3E,TRAV8-4,LCK
REAC	TCR signaling	120	25	4	CD4,CD3E,TRAV8-4,LCK

Table 4-3. Gene ontology terms for proteins downregulated in clone C7. MF: Molecular function, BP: Biological process, KEGG: Kyoto Encyclopedia of Genes and Genomes, REAC: Reactome pathways.

source	term_name	term_size	query_size	intersection_size	intersections
GO:MF	cell adhesion molecule binding	560	31	9	CD40LG,F11R,ITGA1,PTPRJ,CNN2,JCAM1,LCP1,SIRPA,YWHAB
GO:MF	integrin binding	158	31	5	CD40LG,F11R,ITGA1,JCAM1,LCP1
GO:MF	virus receptor activity	76	31	4	F11R,TNFRSF4,CR2,JCAM1
GO:MF	exogenous protein binding	77	31	4	F11R,TNFRSF4,CR2,JCAM1
GO:MF	signaling receptor binding	1556	31	11	CD40LG,F11R,ITGA1,PTPRJ,APOC3,CADM4,CD70,GNA13,JCAM1,LCP1,PANX1
GO:BP	localization of cell	1655	31	15	F11R,ITGA1,PLXNB2,PLXND1,PTPRJ,ACTG1,CADM4,CNN2,GNA13,JCAM1,IFITM1,LCP1,MCAM,PTGER4,SIRPA
GO:BP	cell motility	1655	31	15	F11R,ITGA1,PLXNB2,PLXND1,PTPRJ,ACTG1,CADM4,CNN2,GNA13,JCAM1,IFITM1,LCP1,MCAM,PTGER4,SIRPA
GO:BP	cell migration	1461	31	14	F11R,ITGA1,PLXNB2,PLXND1,PTPRJ,ACTG1,CNN2,GNA13,JCAM1,IFITM1,LCP1,MCAM,PTGER4,SIRPA
GO:BP	locomotion	1833	31	15	F11R,ITGA1,PLXNB2,PLXND1,PTPRJ,ACTG1,CADM4,CNN2,GNA13,JCAM1,IFITM1,LCP1,MCAM,PTGER4,SIRPA
GO:BP	cell activation	1094	31	12	CD40LG,F11R,PTPRJ,TNFRSF4,ACTG1,CD70,CR2,GNA13,JCAM1,LCP1,PTGER4,SIRPA
GO:BP	movement of cell or subcellular component	2085	31	15	F11R,ITGA1,PLXNB2,PLXND1,PTPRJ,ACTG1,CADM4,CNN2,GNA13,JCAM1,IFITM1,LCP1,MCAM,PTGER4,SIRPA
GO:BP	regulation of cell motility	952	31	11	PLXNB2,PLXND1,PTPRJ,ACTG1,CADM4,CNN2,GNA13,JCAM1,IFITM1,MCAM,PTGER4
GO:BP	cellular extravasation	72	31	5	F11R,ITGA1,JCAM1,PTGER4,SIRPA
GO:BP	response to wounding	558	31	9	CD109,CD40LG,F11R,RTN4R,ACTG1,CADM4,CNN2,GNA13,MCAM
GO:BP	regulation of locomotion	997	31	11	PLXNB2,PLXND1,PTPRJ,ACTG1,CADM4,CNN2,GNA13,JCAM1,IFITM1,MCAM,PTGER4
GO:BP	signaling	6451	31	24	CD109,CD40LG,F11R,ITGA1,PLXNB2,PLXND1,PTPRJ,RTN4R,TNFRSF4,APOC3,CADM4,CD53,CD70,CR2,GNA13,JCAM1,IFITM1,LCP1,PANX1,PTGER4,SIRPA,SLC1A4,TSPAN14,YWHAB
GO:BP	regulation of cellular component movement	1028	31	11	PLXNB2,PLXND1,PTPRJ,ACTG1,CADM4,CNN2,GNA13,JCAM1,IFITM1,MCAM,PTGER4
GO:BP	cell communication	6508	31	24	CD109,CD40LG,F11R,ITGA1,PLXNB2,PLXND1,PTPRJ,RTN4R,TNFRSF4,APOC3,CADM4,CD53,CD70,CR2,GNA13,JCAM1,IFITM1,LCP1,PANX1,PTGER4,SIRPA,SLC1A4,TSPAN14,YWHAB
GO:BP	wound healing	429	31	8	CD109,CD40LG,F11R,ACTG1,CADM4,CNN2,GNA13,MCAM
GO:BP	response to stimulus	8885	31	27	CD109,CD1B,CD40LG,F11R,ITGA1,PLXNB2,PLXND1,PTPRJ,RTN4R,TNFRSF4,ACTG1,APOC3,CADM4,CD53,CD70,CNN2,CR2,GNA13,JCAM1,IFITM1,LCP1,MCAM,PANX1,PTGER4,SIRPA
GO:BP	immune effector process	661	31	9	CD1B,CD40LG,PTPRJ,TNFRSF4,CD70,CR2,JCAM1,LCP1,PTGER4
GO:BP	immune system process	2781	31	16	CD109,CD1B,CD40LG,F11R,ITGA1,PTPRJ,TNFRSF4,ACTG1,CD70,CNN2,CR2,JCAM1,IFITM1,LCP1,PTGER4,SIRPA
GO:BP	regulation of cell migration	893	31	10	PLXNB2,PLXND1,PTPRJ,ACTG1,CNN2,GNA13,JCAM1,IFITM1,MCAM,PTGER4
GO:BP	positive regulation of biological process	6224	31	23	CD1B,CD40LG,F11R,ITGA1,PLXNB2,PLXND1,PTPRJ,RTN4R,TNFRSF4,ACTG1,CD53,CD70,CNN2,CR2,JCAM1,IFITM1,LCP1,MCAM,PANX1,PTGER4,SIRPA,TSPAN14,YWHAB
GO:BP	cell adhesion	1489	31	12	CD40LG,F11R,ITGA1,PLXNB2,PLXND1,PTPRJ,ACTG1,CADM4,CD70,JCAM1,MCAM,SIRPA
GO:BP	signal transduction	5957	31	22	CD109,CD40LG,F11R,ITGA1,PLXNB2,PLXND1,PTPRJ,RTN4R,TNFRSF4,APOC3,CADM4,CD53,CD70,CR2,GNA13,JCAM1,IFITM1,LCP1,PTGER4,SIRPA,TSPAN14,YWHAB
GO:BP	lymphocyte activation	794	31	9	CD40LG,PTPRJ,TNFRSF4,CD70,CR2,JCAM1,LCP1,PTGER4,SIRPA
GO:BP	regulation of localization	2725	31	15	PLXNB2,PLXND1,PTPRJ,ACTG1,APOC3,CADM4,CNN2,GNA13,JCAM1,IFITM1,LCP1,MCAM,PTGER4,SIRPA,YWHAB
GO:BP	cellular response to stimulus	7399	31	24	CD109,CD40LG,F11R,ITGA1,PLXNB2,PLXND1,PTPRJ,RTN4R,TNFRSF4,ACTG1,APOC3,CADM4,CD53,CD70,CNN2,CR2,GNA13,JCAM1,IFITM1,LCP1,PTGER4,SIRPA,TSPAN14,YWHAB
GO:BP	viral entry into host cell	147	31	5	F11R,TNFRSF4,CR2,JCAM1,IFITM1
GO:BP	entry into host	154	31	5	F11R,TNFRSF4,CR2,JCAM1,IFITM1
GO:BP	negative regulation of cellular process	4856	31	19	CD109,CD40LG,F11R,ITGA1,PLXNB2,PLXND1,PTPRJ,RTN4R,TNFRSF4,APOC3,CADM4,CNN2,GNA13,JCAM1,IFITM1,PTGER4,RPS13,SIRPA,YWHAB
GO:BP	movement in host environment	179	31	5	F11R,TNFRSF4,CR2,JCAM1,IFITM1
GO:BP	leukocyte activation	953	31	9	CD40LG,PTPRJ,TNFRSF4,CD70,CR2,JCAM1,LCP1,PTGER4,SIRPA
GO:BP	T cell activation	504	31	7	CD40LG,TNFRSF4,CD70,JCAM1,LCP1,PTGER4,SIRPA
GO:BP	immune response	1906	31	12	CD1B,CD40LG,PTPRJ,TNFRSF4,ACTG1,CD70,CR2,JCAM1,IFITM1,LCP1,PTGER4,SIRPA
GO:BP	regulation of cell adhesion	740	31	8	CD40LG,F11R,PLXNB2,PLXND1,PTPRJ,ACTG1,CD70,SIRPA
GO:BP	biological process involved in interaction with host	194	31	5	F11R,TNFRSF4,CR2,JCAM1,IFITM1
GO:BP	regulation of immune effector process	349	31	6	CD1B,CD40LG,PTPRJ,TNFRSF4,CR2,JCAM1
GO:BP	cell population proliferation	1958	31	12	CD109,CD40LG,ITGA1,PLXNB2,PTPRJ,TNFRSF4,CADM4,CD70,CNN2,CR2,GNA13,IFITM1
GO:BP	protein localization to bicellular tight junction	4	31	2	F11R,ACTG1
GO:BP	B cell proliferation	101	31	4	CD40LG,TNFRSF4,CD70,CR2
GO:BP	cell surface receptor signaling pathway	2811	31	14	CD109,CD40LG,ITGA1,PLXNB2,PLXND1,PTPRJ,RTN4R,TNFRSF4,CADM4,CD70,CR2,JCAM1,IFITM1,TSPAN14
GO:BP	negative regulation of biological process	5876	31	20	CD109,CD40LG,F11R,ITGA1,PLXNB2,PLXND1,PTPRJ,RTN4R,TNFRSF4,APOC3,CADM4,CNN2,CR2,GNA13,JCAM1,IFITM1,PTGER4,RPS13,SIRPA,YWHAB
GO:BP	regulation of response to stimulus	3895	31	16	CD109,CD1B,F11R,ITGA1,PTPRJ,RTN4R,ACTG1,APOC3,CADM4,CR2,GNA13,JCAM1,PTGER4,SIRPA,TSPAN14,YWHAB
KEGG	Viral myocarditis	55	19	3	CD40LG,ACTG1,JCAM1
REAC	Immune System	2041	28	16	CD1B,CD40LG,PTPRJ,TNFRSF4,ACTG1,CD53,CD70,CNN2,CR2,JCAM1,IFITM1,LCP1,PANX1,SIRPA,TSPAN14,YWHAB

Table 4-4. Gene ontology terms for proteins upregulated in clone C7. MF: Molecular function, BP: Biological process, KEGG: Kyoto Encyclopedia of Genes and Genomes, REAC: Reactome pathways.

4.1.2. Electroporation induced CRISPR/Cas9 editing of the LRBA gene in Jurkat T cells

Since all the up and downregulated proteins resulting from mass spectrometry analysis were just confirmed in the C7 single clonal cell, we decided to look at the expression of these proteins in the pool of cells in order not to be biased by the individual expression properties of single cell derived clones. Moreover the lentiviral CRISPR/Cas9 infection strategy we used for generating our single cell clones integrates into the genome and stably expresses the gRNA and Cas9 cassette in the cells, increasing the possiblity of off target digestion and mutagenesis. For this purpose, we used the Neon electroporation mediated transfection method to transiently transfect Jurkat cells. We used the same gRNA/Cas9 construct as it has a U6 promoter that drives the expression of these genes in transfected cells. Due to the presence of a puromycin resistance casette, transfected cells can be selected, increasing transfection and mutation efficiency.

Two batches of Jurkat cells were transfected with two plasmids, one including sgRNA targeting the 3' end and the other one targeting the 5' end of exon 42 of the LRBA gene. For one batch, a week after transfection, puromycin selection was started, while the other kept growing without any selection. Knock-out efficiency was controlled by western-blotting and the T7E1 assay. In the T7E1 assay, the Neon transfected cells without puromycin selection have the same pattern as WT cells. At the same time, there are different bands in Neon transfected cells with puromycin selection after being cut with the T7E1 enzyme (Fig. 4-16).

Moreover, western blot analysis showed a total absence of LRBA protein in Neon transfected cells with puromycin selection. In contrast, Neon transfected cells without selection have the same protein expression as WT (Fig.4-17). Therefore, for the rest of the analysis of these cells, Neon transfected cells without selection were used as controls.

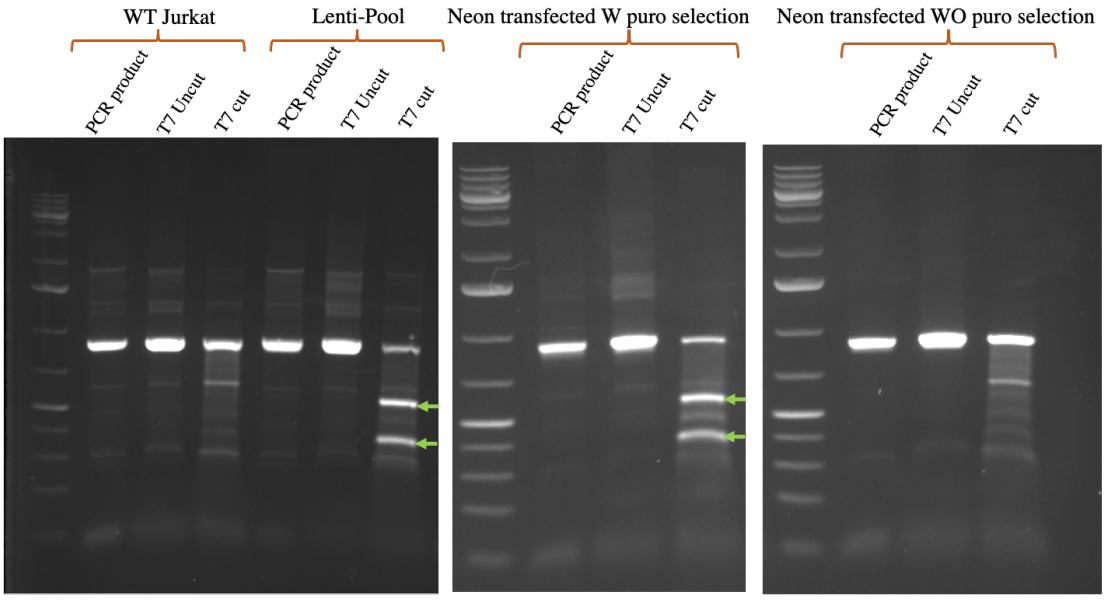

Figure 4-16. T7E1 assay for mutations in the LRBA gene locus of transfected Jurkat cells. The targeted region was PCR amplified with the primers showed in Figure 4-1.A and in each category the first lane is the PCR product, second is the same product denatured and renatured without the addition of T7 E1 enzyme and third group is the same denatured and renatured PCR product that has been digested with the T7E1 enzyme.

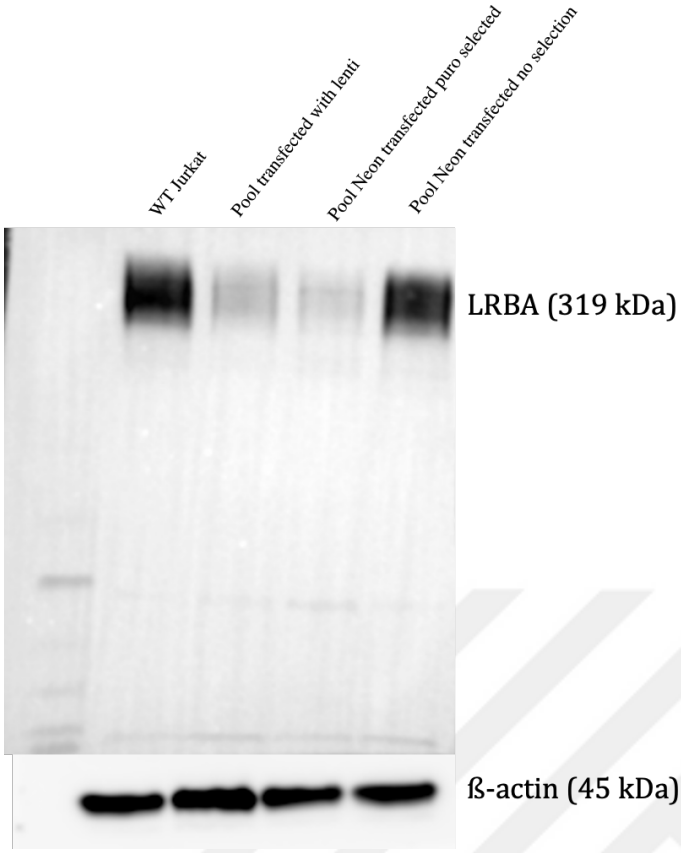

Figure 4-17. Western blot analysis of Neon transfected cells. Anti- Beta actin staining was used as a loading control.

4.2. Downregulated receptors in LRBA KO cell line

To verify the effect of downregulated receptors in LRBA KO cells, further analysis was done by flow cytometry on WT and C7 cells to confirm the MS result. Moreover, other LRBA KO single clonal cells and pools were included in the analysis to validate that observed result is due to LRBA absence.

4.2.1. CD3 epsilon

The TCR-CD3 complex plays an important role in adaptive immune responses. When antigen-presenting cells (APCs) activate the T-cell receptor (TCR), CD3D, CD3E, CD3G, and CD3Z send signals to the cells through the cell membrane that are mediated

by the TCR. During their cytoplasmic domain, all CD3 chains contain immunoreceptor activation motifs (ITAMs). On engagement of a TCR, these motifs are phosphorylated by the protein tyrosine kinases LCK and FYN, which results in the activation of downstream signaling pathways [74]. It is not only important for T-cell activation to be present, but also for T-cell development to be present. As a result of the endocytosis sequences found in CD3E's cytosolic region, it forms the two heterodimers CD3D/CD3E and CD3G/CD3E, which are responsible for assembling the TCR-CD3 complexes and internalizing and down-regulating them on the surface of the cell [75]. Despite the fact that CD3E-related signal is not necessary for T cell maturation, it does contribute to T cell survival; this effect is quantitatively correlated with the TCR signaling pathway [76].

Our mass spectrometry results showed that CD3E was decreased in C7 single clonal cell compared to WT Jurkat. To validate this result, we did cell surface staining of CD3E in other single clonal cells (C8 and C14) and pool of cells. The CD3 MFI was low in C7, and it shows a negative population. However, the other two single clonal cell lines were CD3 positive, and pool KO had an MFI close to WT Jurkat (Fig.4-18). The repeat of staining resulted in the same conclusion besides the same decrease was seen in new generated KO pool Fig. 4-25.A.

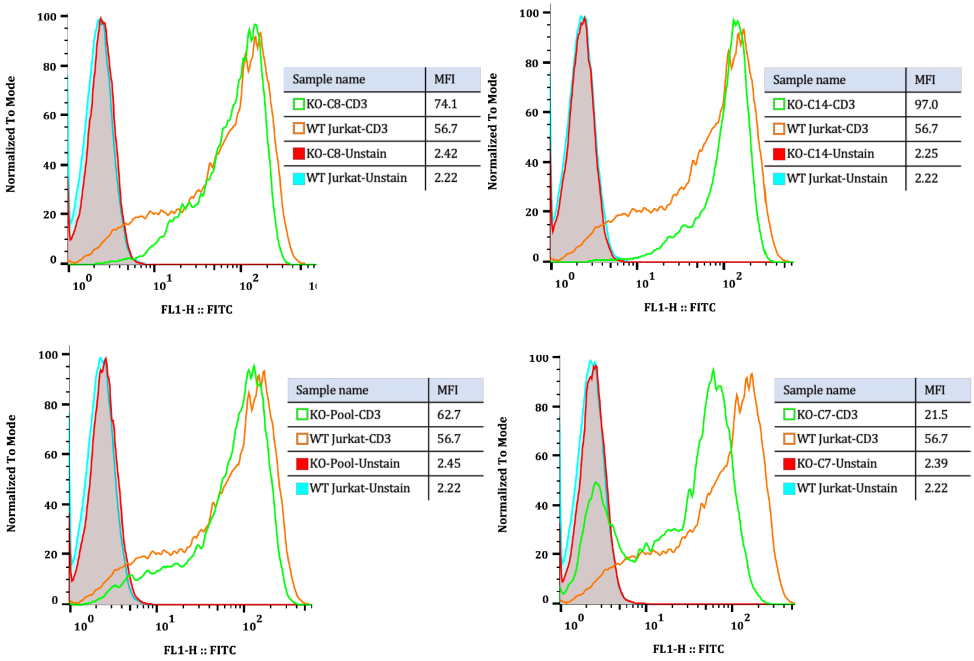

Figure 4-18. CD3 cell surface staining of LRBA KO cell lines. WT and KO samples were stained with FITC-anti- hCD3 antibody and as controle unstained cells were used.

4.2.2. CD4

As a transmembrane glycoprotein, CD4 plays an important role in the immune response and performs multiple functions in response to external and internal threats. It mainly functions as a coreceptor in T cells for MHC class II molecules: peptides. A class II peptide contains antigens that are derived from extracellular proteins, while a class I peptide contains antigens derived from cytosolic proteins. CD4 interacts with the TCR and MHC class II present in antigen-presenting cells in order to recruit LCK to the vicinity of the TCR-CD3 complex. The LCK signaling pathway initiates a number of intracellular signaling pathways that are responsible for producing lymphokines, motility, adhesion, and activating T-helper cells. By phosphorylating multiple substrates, LCK initiates a number of intracellular signaling pathways [77,78].

CD4 cell surface staining of WT Jurkat and C7 single clonal cell confirmed the results from MS, but in the pool, C8 and C14, the expression was even higher or so close to WT expression (Fig. 4-19). The repeated staining confirmed these results; plus, the new generated KO pool had lower CD4 MIF than the control (Fig. 4-25.B).

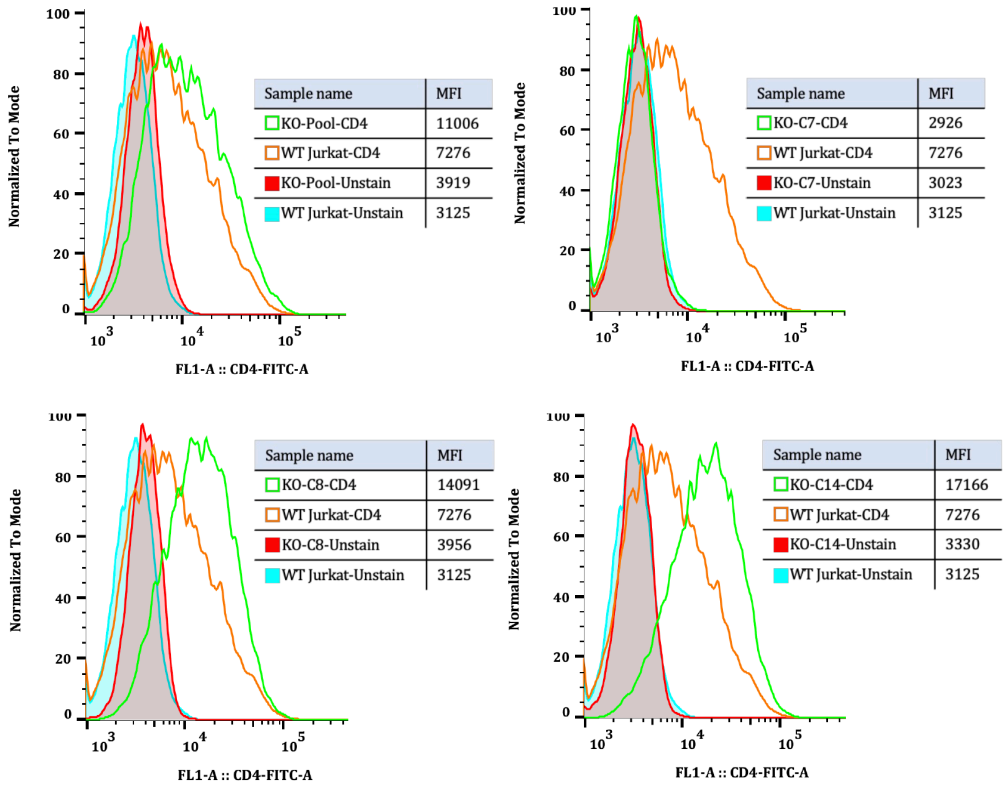

Figure 4-19. CD4 cell surface staining of LRBA KO cell lines. WT and KO cells were stained with FITC-anti-hCD4 antibody and as control unstained.

4.2.3. CD1d

CD1d molecules bind lipids and glycolipids and present them to CD1d-restricted NKT cells on the cell surface. Unlike antigenic peptides derived from intracellular and extracellular proteins, which are divided into separate MHC class I or class II presentation pathways, CD1d molecules present lipids derived from both intracellular and extracellular sources [79,80].

There is a possibility that CD1-restricted T cells may be activated simultaneously with the innate immune response. As a means of amplifying the innate immune response and influencing the adaptive immune response, CD1-reactive T cells can stimulate DC differentiation and lead DC maturation into IL-12-producing inflammatory DCs, activating NK cells, other T cells, and B cells, as well as activating NK cells. However, CD1-restricted T cells are tolerogenic since they secrete TH2 cytokines and have a CD1-dependent effect on other regulatory cells [79].

Though being an exciting candidate receptor to be affected by LRBA absence, CD1d cell surface expression was just lower in C7 when compared to WT and higher in C8 and C14 single clonal cells. The CD1d cell surface staining in the pool of knock-out cells was almost like WT (Fig.4-20). To confirm this result, the staining was repeated, and still, CD1d was decreased only in C7 and not in other KO cell lines. Besides, the new KO pool (Neon transfected with puromycin selection) had almost similar CD1d expression to control (Fig. 4-25.C).

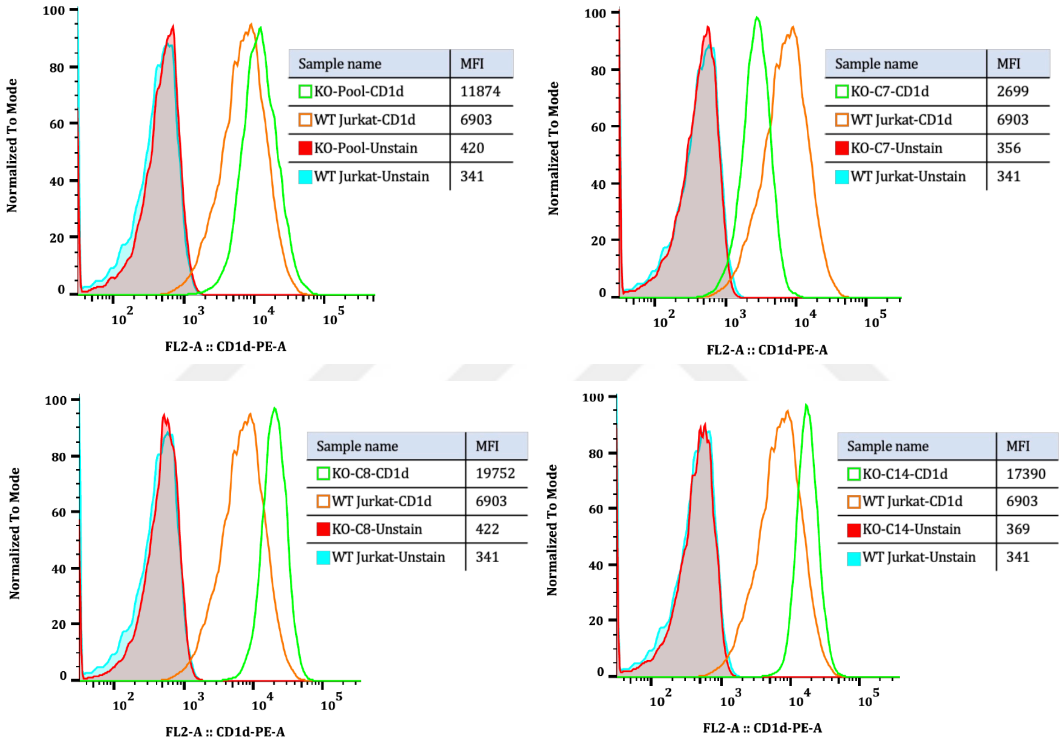

Figure 4-20. CD1d cell surface staining of LRBA KO cell lines. WT and KO cells were stained with PE-anti-hCD1d antibody and as controle unstain cells were used.

4.2.4. NOTCH3

The NOTCH receptors are type I transmembrane heterodimers composed of a single chain precursor and get cleaved by Furin in the trans-Golgi network of the cell. In addition to cleaving NOTCH receptors, Furin activates several NOTCH signaling proteases like ADAM10 and ADAM17 [81]. Stem cells and their lineages, as well as other cellular

processes, are regulated by Notch receptors in adult tissue maintenance and repair [82]. In macrophages, NOTCH3 plays an important role in regulating the expression of proinflammatory genes by increasing p38-dependent NF-B activation [81].

In the case of NOTCH3, cell surface staining showed that while its expression in C7 was the same as in WT cells, it was higher in the pool, C8 and C14 single cells (Fig.4-21). This result was not consistence with the MS result that showed NOTCH3 is downregulated in C7 cells. In the repeated staining, C7 had lower MFI compared to WT, and other cells had relatively similar MFI to WT. The NOTCH3 expression was decreased in the KO pool with puromycin selection, but it was not so significant (Fig. 4-25.D).

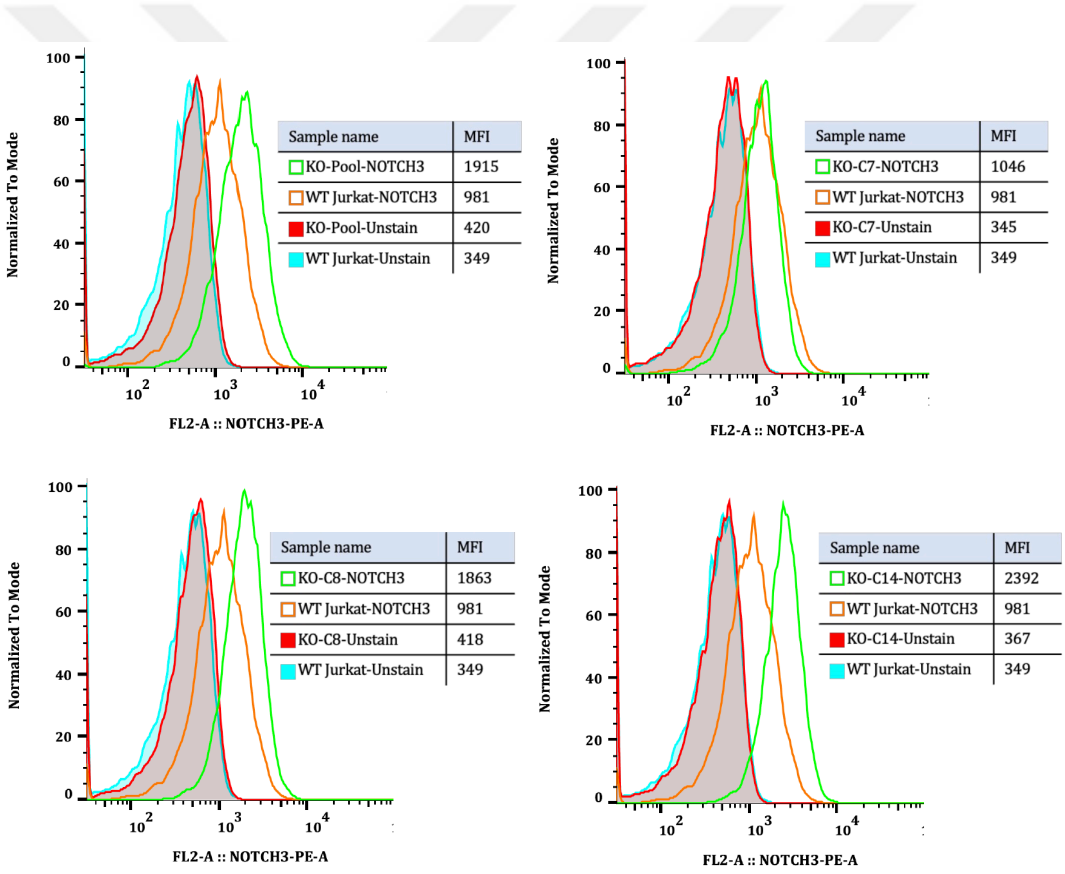

Figure 4-21. NOTCH3 cell surface staining of LRBA KO cell lines. WT and KO cells were stained with PE-anti-hNOTCH3 antibody and as control unstained cells were used.

4.2.5. PVRIG

T and NK cells express a variety of receptors that interact with ligands belonging to the Nectin/Nectin-like (Necl) family, such as DNAM-1 (DNAX-associated molecule 1), TIGIT (a protein with an ITIM domain that binds to T cells), TACTILE (a protein that activates T cells and expresses them late), and PVRIG (a protein related to PVR). As a result of the engagement of TIGIT and PVRIG, NK cell function is inhibited, while DNAM-1 is an activating/costimulatory receptor. Unlike CTLA-4 receptor, which does not regulate NK cells, PVRIG receptor, also known as CD112R, binds to its ligand CD112 on target cells with great affinity, inhibiting lymphocyte cytotoxicity. It was found that this receptor was downregulated in C7 single clonal LRBA KO cells and had a similar inhibitory function to CTLA-4 [83,84].

The cell surface staining confirmed lower expression of this receptor in C7 than in WT, while C8 and C14 had almost similar or slightly decreased expression (Fig. 4-22.A). If PVRIG was being recycled from cell surface so frequently, like CTLA-4, the intracellular staining could give a better description of its expression in the absence or presence of LRBA. The total expression level of PVRIG was decreased in all KO single clonal cells and pool compared to WT Fig. 4-22.B. Since PVRIG was known to have inhibitory effects on NK cells, the same cell surface and intracellular staining were performed on NK cells (Fig. 4-22.C). Interestingly, cell surface expression of PVRIG on NK cells was higher than that on WT Jurkat, whereas the total expression of PVRIG was higher in Jurkat cells. This can be due to the inhibitory role of PVRIG that is primarily being defined for NK cells. PVRIG cell surface staining was repeated for all LRBA KO cells, and the decrease was just seen in C7 and not in other KO cells (Fig.4-25.E).

(A)

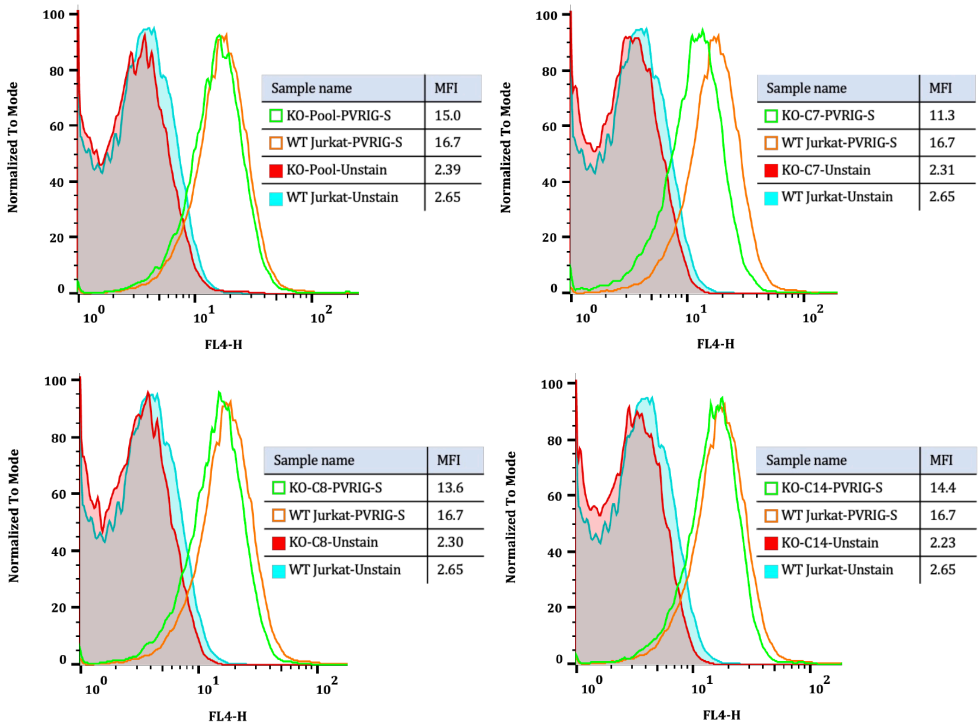
Normalized To Mode
FL4-H
Sample name | MFI
KO-Pool-PVRIG-S | 15.0
WT Jurkat-PVRIG-S | 16.7
KO-Pool-Unstain | 2.39
WT Jurkat-Unstain | 2.65
Sample name | MFI
KO-C7-PVRIG-S | 11.3
WT Jurkat-PVRIG-S | 16.7
KO-C7-Unstain | 2.31
WT Jurkat-Unstain | 2.65
Sample name | MFI
KO-C8-PVRIG-S | 13.6
WT Jurkat-PVRIG-S | 16.7
KO-C8-Unstain | 2.30
WT Jurkat-Unstain | 2.65
Sample name | MFI
KO-C14-PVRIG-S | 14.4
WT Jurkat-PVRIG-S | 16.7
KO-C14-Unstain | 2.23
WT Jurkat-Unstain | 2.65

(B)

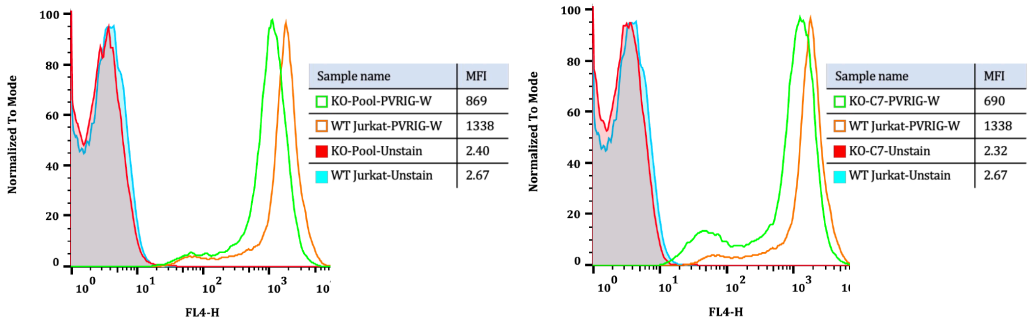
Normalized To Mode
FL4-H
Sample name | MFI
KO-Pool-PVRIG-W | 869
WT Jurkat-PVRIG-W | 1338
KO-Pool-Unstain | 2.40
WT Jurkat-Unstain | 2.67
Sample name | MFI
KO-C7-PVRIG-W | 690
WT Jurkat-PVRIG-W | 1338
KO-C7-Unstain | 2.32
WT Jurkat-Unstain | 2.67

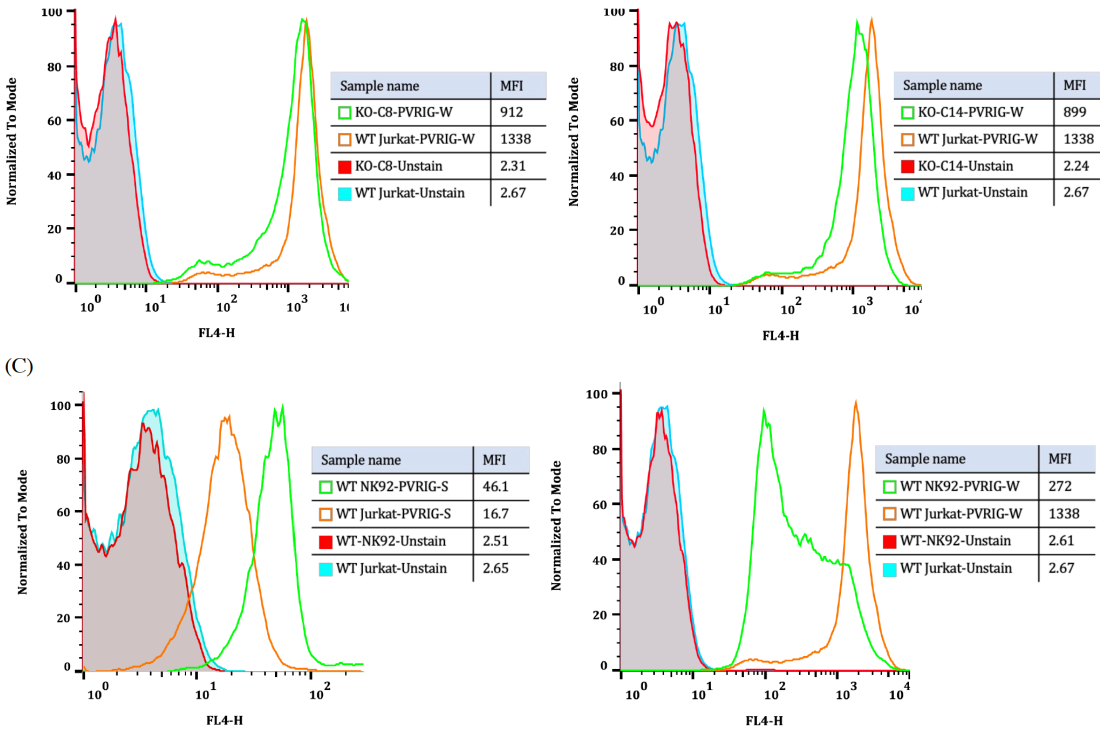

Figure 4-22. PVRIG staining. A) Cell surface staining of LRBA KO cells, B) Intracellular staining of LRBA KO cells, and C) Cell surface and intracellular staining of NK cells. WT and KO cells were stained with AF647-anti-hPVRIG antibody. PVRIG-S: cell surface staining. PVRIG-W: intracellular staining. As control unstained cells were used.

4.2.6. Sema7A

This protein consists of a conserved amino-terminal domain called 'Sema' and is associated with the membrane. In vitro, semaphorin 7A, one of the cell-bound isoforms of viral semaphorins encoded by vaccinia and herpesvirus, is able to bind to Plexin C, the only GPI-linked protein within the semaphorin family. In addition to causing monocyte chemotaxis and cytokine production, Sema7A can also be expressed in activated lymphocytes and thymocytes, which implies that it plays a role in the immune system. Furthermore, Sema7A is expressed by most of the human T lymphocytes and natural killer cells. The expression of Sema7A on activated T cells induces macrophages to produce proinflammatory cytokines that cause inflammation in the body [85]. Several studies have shown that Sema7A may inhibit T cell proliferation by regulating T cell response when Sema7A isn't present in T cells when Sema7A isn't present in T cells [86].

Based on cell surface staining, Sema7A was relatively low in C7 and high in the pool, C8, and C14 cells compared to WT (Fig.4-23). Still, based on its known functions, it can be an excellent candidate to be studied in patient samples.

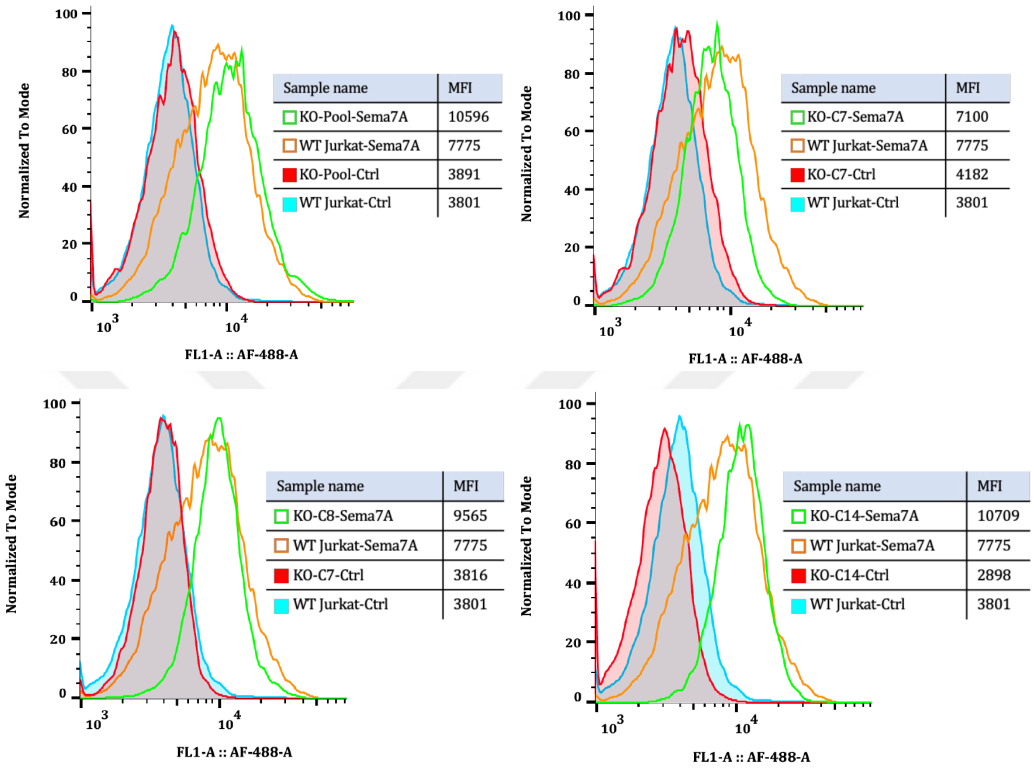

Figure 4-23. Sema7A cell surface staining of LRBA KO cells. WT and KO cells were stained with primary anti-hSema7A antibody followed by secondary AF488-anti-rabbit antibody. As control cells were stained only with secondary antibody.

4.2.7. Screening Neon transfected cells for downregulated receptors in LRBA KO cell

CD3 and CD4 cell surface staining represented a decreased MFI value for the KO pool with puromycin selection (green line) compared to its control sample (orange line) (Fig 4-24), which is consistence with our expectation. The MFI of CD1d in the KO pool is slightly lower than control, but NOTCH and PVRIG cell surface staining have almost

similar MFI for the KO pool and control. The total staining of PVRIG in the KO pool showed an MFI of nearly 800 units lower than control.

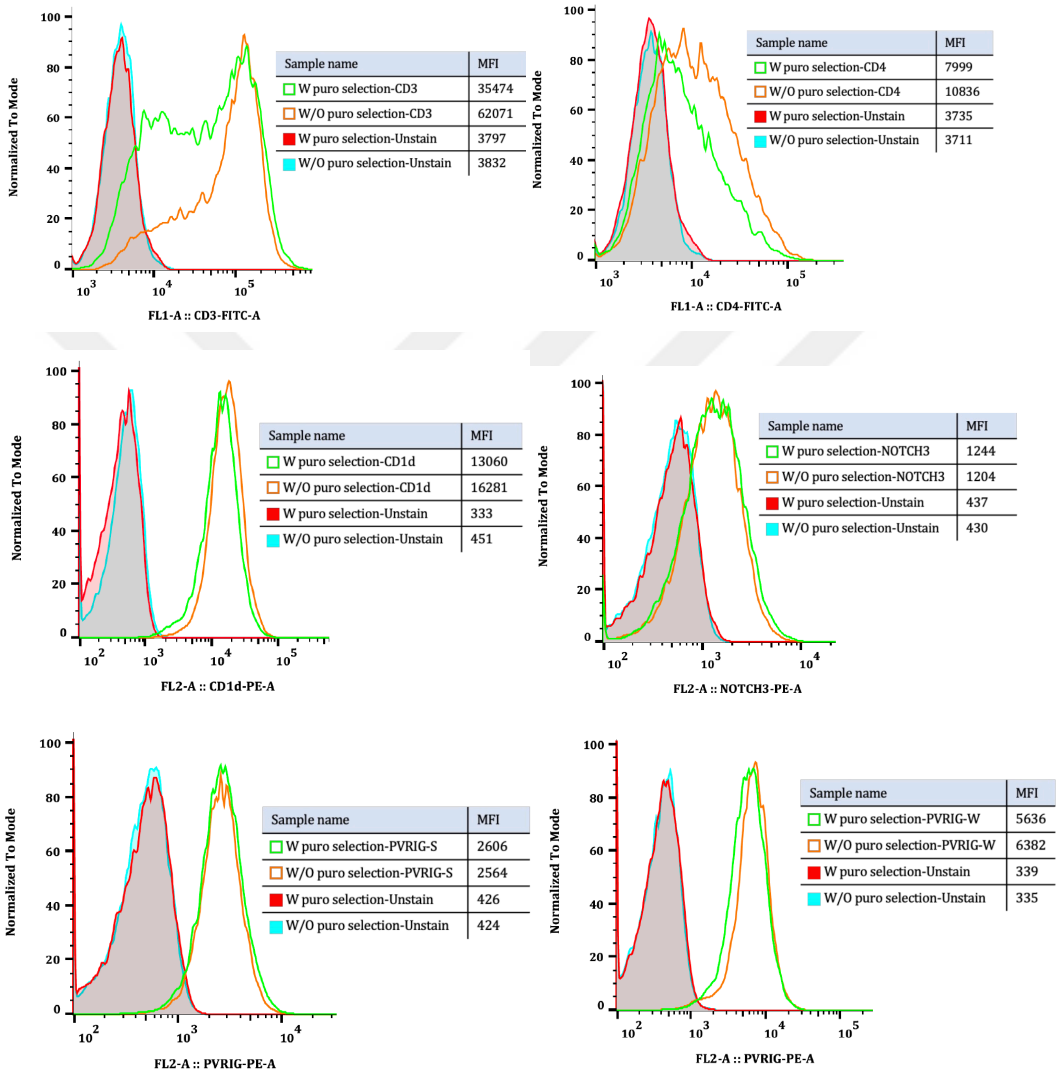

Figure 4-24. Downregulated receptors staining of Neon transfected cells.

(A)

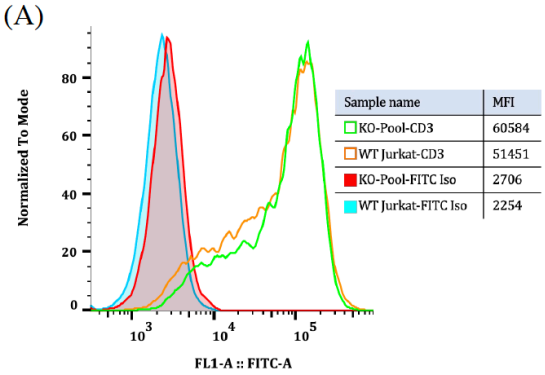

Sample name	MFI
KO-Pool-CD3	60584
WT Jurkat-CD3	51451
KO-Pool-FITC Iso	2706
WT Jurkat-FITC Iso	2254

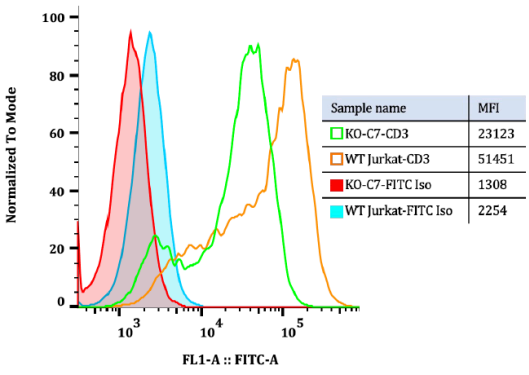

Sample name	MFI
KO-C7-CD3	23123
WT Jurkat-CD3	51451
KO-C7-FITC Iso	1308
WT Jurkat-FITC Iso	2254

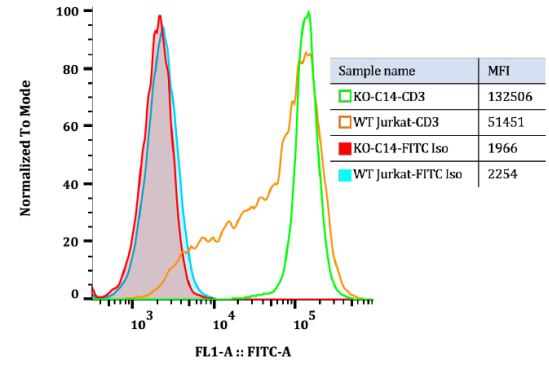

Sample name	MFI
KO-C14-CD3	132506
WT Jurkat-CD3	51451
KO-C14-FITC Iso	1966
WT Jurkat-FITC Iso	2254

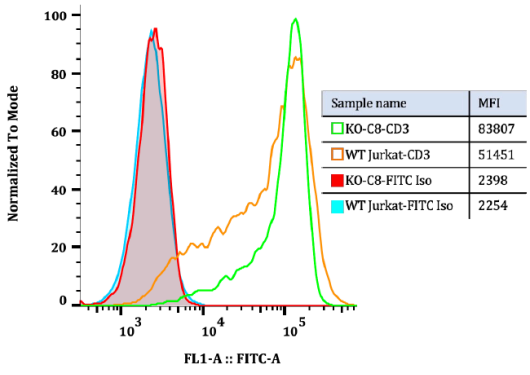

Sample name	MFI
KO-C8-CD3	83807
WT Jurkat-CD3	51451
KO-C8-FITC Iso	2398
WT Jurkat-FITC Iso	2254

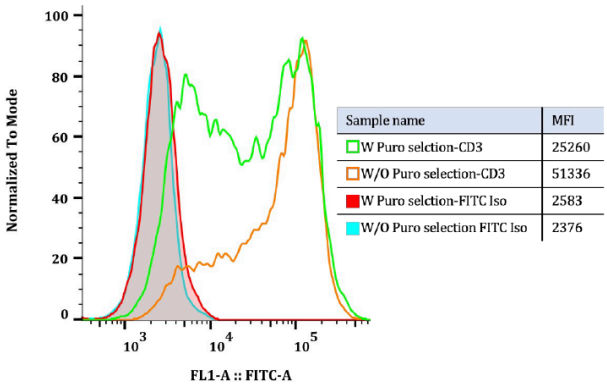

Sample name	MFI
W Puro selction-CD3	25260
W/O Puro selection-CD3	51336
W Puro selction-FITC Iso	2583
W/O Puro selection FITC Iso	2376

(B)

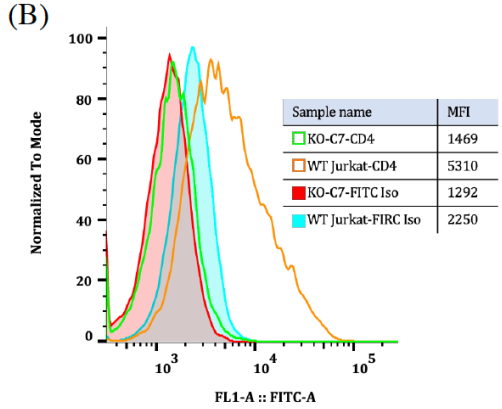
Normalized To Mode
FL1-A :: FITC-A
Sample name | MFI
KO-C7-CD4 | 1469
WT Jurkat-CD4 | 5310
KO-C7-FITC Iso | 1292
WT Jurkat-FIRC Iso | 2250

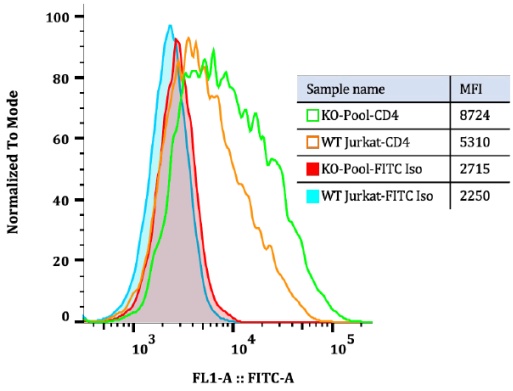
Normalized To Mode
FL1-A :: FITC-A
Sample name | MFI
KO-Pool-CD4 | 8724
WT Jurkat-CD4 | 5310
KO-Pool-FITC Iso | 2715
WT Jurkat-FITC Iso | 2250

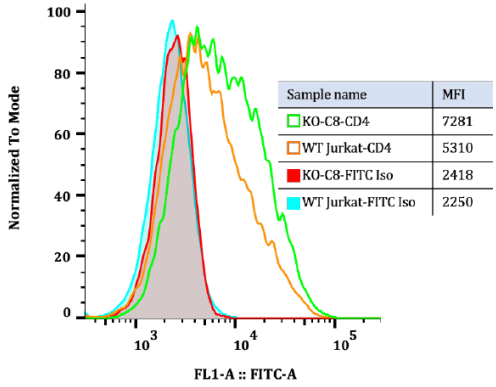
Normalized To Mode
FL1-A :: FITC-A
Sample name | MFI
KO-C8-CD4 | 7281
WT Jurkat-CD4 | 5310
KO-C8-FITC Iso | 2418
WT Jurkat-FITC Iso | 2250

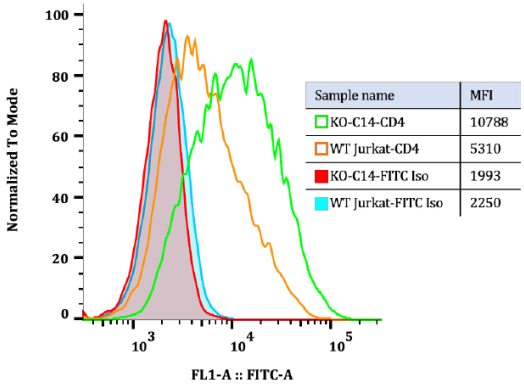
Normalized To Mode
FL1-A :: FITC-A
Sample name | MFI
KO-C14-CD4 | 10788
WT Jurkat-CD4 | 5310
KO-C14-FITC Iso | 1993
WT Jurkat-FITC Iso | 2250

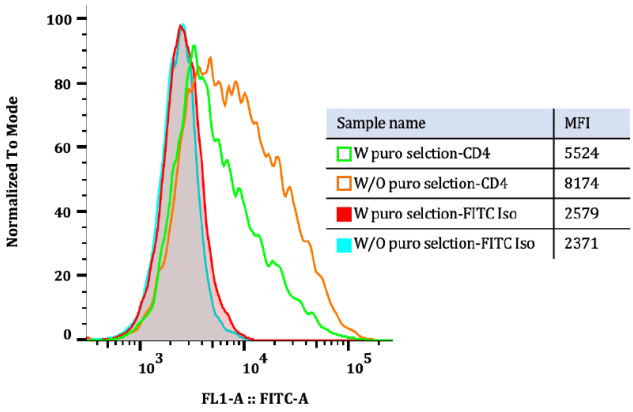
Normalized To Mode
FL1-A :: FITC-A
Sample name | MFI
W puro selction-CD4 | 5524
W/O puro selction-CD4 | 8174
W puro selction-FITC Iso | 2579
W/O puro selction-FITC Iso | 2371

(C)

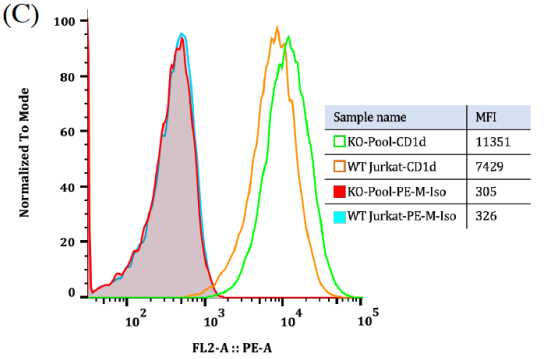

Sample name	MFI
KO-Pool-CD1d	11351
WT Jurkat-CD1d	7429
KO-Pool-PE-M-Iso	305
WT Jurkat-PE-M-Iso	326

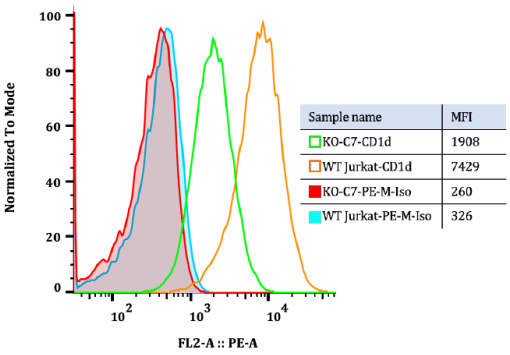

Sample name	MFI
KO-C7-CD1d	1908
WT Jurkat-CD1d	7429
KO-C7-PE-M-Iso	260
WT Jurkat-PE-M-Iso	326

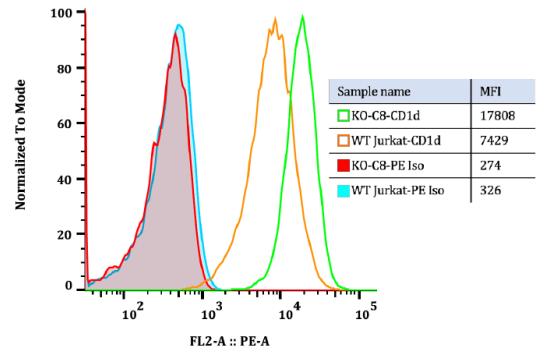

Sample name	MFI
KO-C8-CD1d	17808
WT Jurkat-CD1d	7429
KO-C8-PE Iso	274
WT Jurkat-PE Iso	326

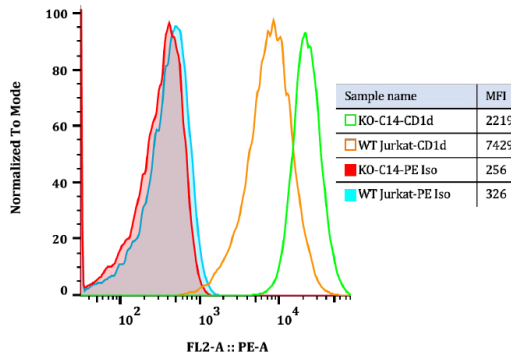

Sample name	MFI
KO-C14-CD1d	22195
WT Jurkat-CD1d	7429
KO-C14-PE Iso	256
WT Jurkat-PE Iso	326

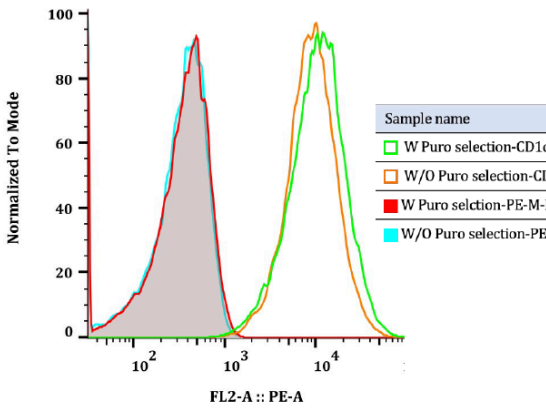

Sample name	MFI
W Puro selection-CD1d	10158
W/O Puro selection-CD1d	8945
W Puro selction-PE-M-Iso	298
W/O Puro selection-PE-M-Iso	279

(D)

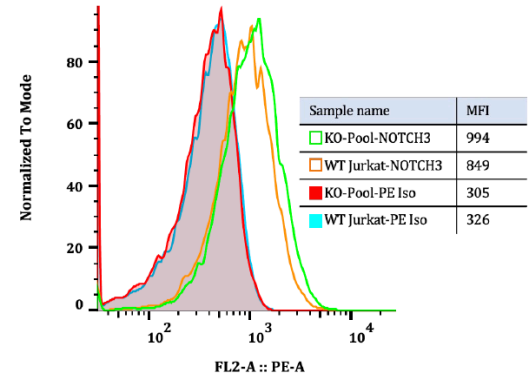
Normalized To Mode
FL2-A :: PE-A
Sample name | MFI
KO-Pool-NOTCH3 | 994
WT Jurkat-NOTCH3 | 849
KO-Pool-PE Iso | 305
WT Jurkat-PE Iso | 326

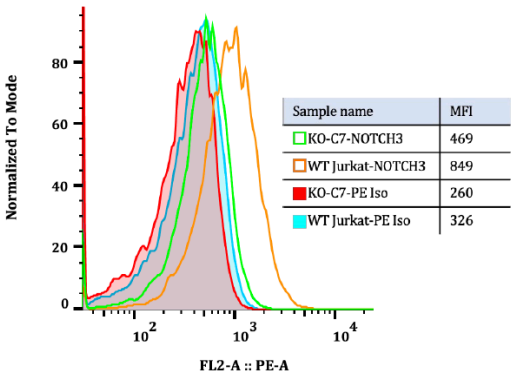
Normalized To Mode
FL2-A :: PE-A
Sample name | MFI
KO-C7-NOTCH3 | 469
WT Jurkat-NOTCH3 | 849
KO-C7-PE Iso | 260
WT Jurkat-PE Iso | 326

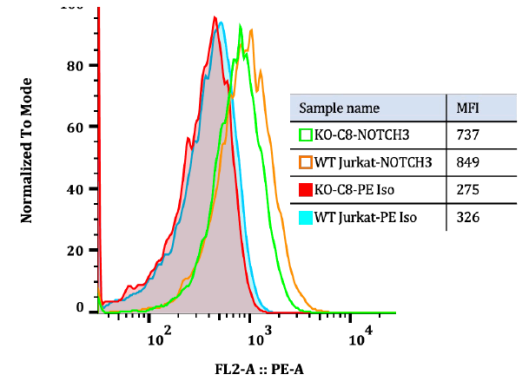
Normalized To Mode
FL2-A :: PE-A
Sample name | MFI
KO-C8-NOTCH3 | 737
WT Jurkat-NOTCH3 | 849
KO-C8-PE Iso | 275
WT Jurkat-PE Iso | 326

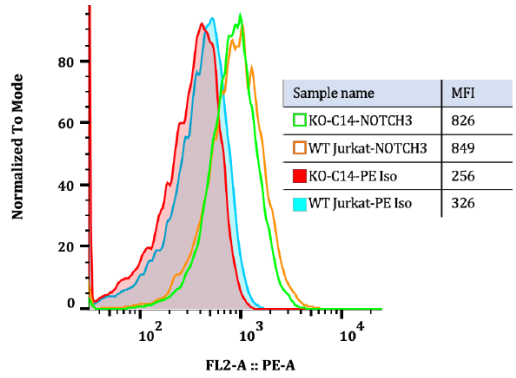
Normalized To Mode
FL2-A :: PE-A
Sample name | MFI
KO-C14-NOTCH3 | 826
WT Jurkat-NOTCH3 | 849
KO-C14-PE Iso | 256
WT Jurkat-PE Iso | 326

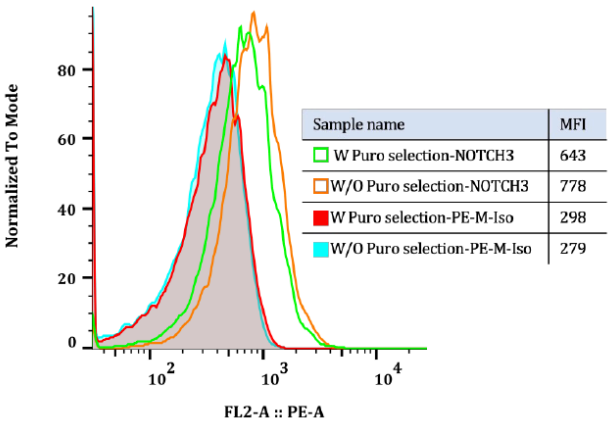
Normalized To Mode
FL2-A :: PE-A
Sample name | MFI
W Puro selection-NOTCH3 | 643
W/O Puro selection-NOTCH3 | 778
W Puro selection-PE-M-Iso | 298
W/O Puro selection-PE-M-Iso | 279

(E)

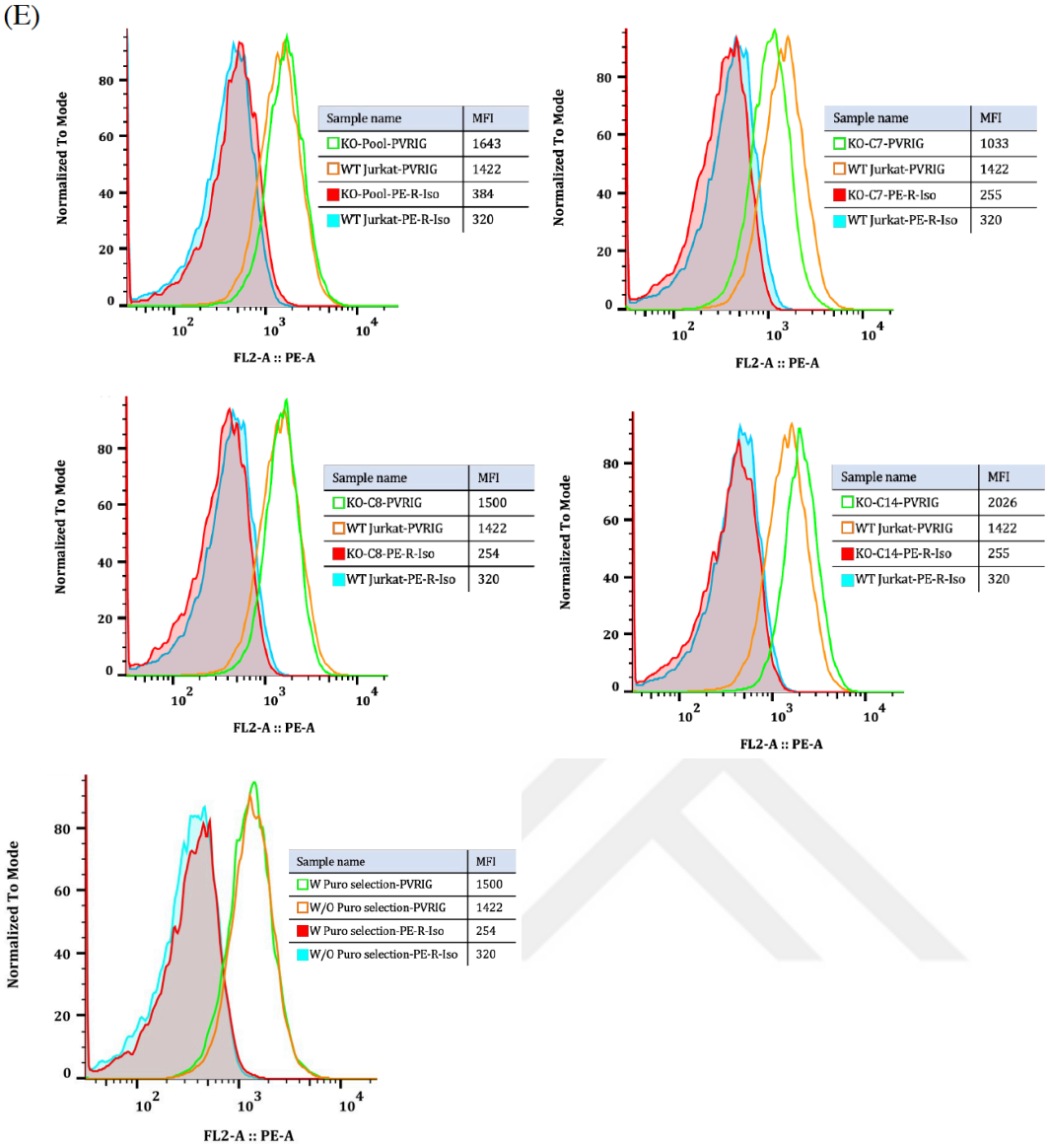

Figure 4-25. Downregulated receptors staining for all LRBA KO cells. A) CD3, B) CD4, C) CD1d, D) NOTCH3, E) PVRIG cell surface staining. As control the the cells were stained with proper conjugated isotype antibody.

4.3. Upregulated receptors in the LRBA KO cells

To verify the effect of upregulated receptors in LRBA KO cells, further analysis was done by flow cytometry on WT and C7 cells to confirm the MS result. Moreover, other LRBA KO single clonal cells and pools were included in the analysis to validate that observed result is due to LRBA absence.

4.3.1. CD53

CD53 is a member of the tetraspanin family, only found in immune compartments and is known to have a critical role in organizing cellular processes like signaling, adhesion, migration, and cell fusion. Direct interaction of CD53 with potential partners like LFA-1, CD2, and IL-7R may result in functional consequences of adhesion, signaling and cell activation, survival, and differentiation, respectively [87]. Overexpression of this receptor on the cell surface may reinforce its effects and dysregulation of its functions. According to MS results, CD53 was upregulated in C7, but flow cytometry results showed no significant increase in C7 compared to WT. However, its expression was slightly higher in the KO pool with puromycin selection compared to its control (Fig.4-26.A). Thus, the staining was repeated, and this time other single cells, C8 and C14, were also included in the staining. The second staining confirmed the expression increase in both C7 and KO pools with puromycin selection. However, C8 and C14 showed a lower expression level than WT (Fig.4-26.B). Still, CD53 could be a potential candidate for further study in patient samples.

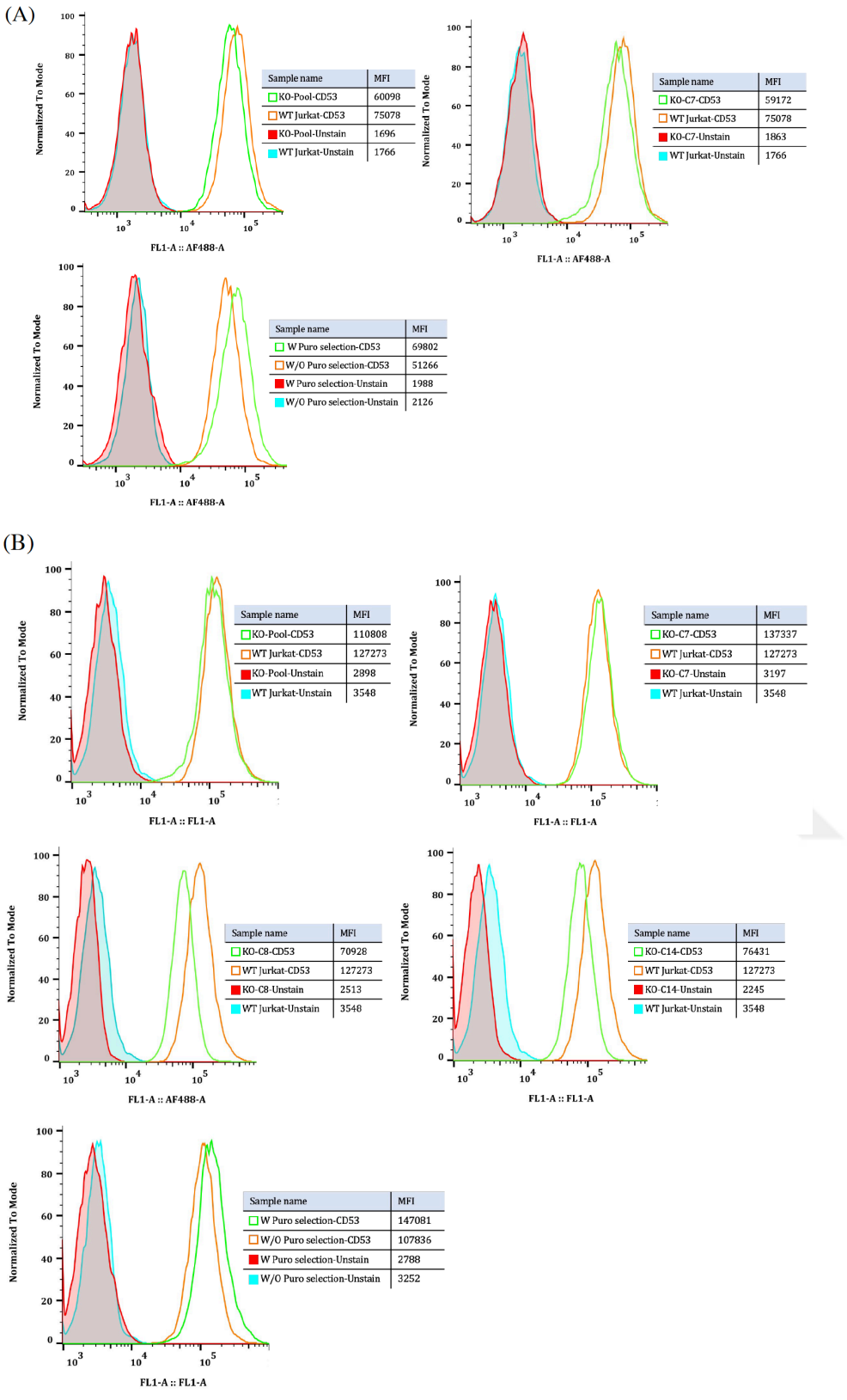

Figure 4-26. CD53 staining of all KO cells. A) First trial. B) the Second trial. WT and KO cells were stained with FITC-anti-hCD53 antibody and as control unstained cells were used.

4.3.2. CD148

In order to maintain immune balance, inhibitory signals like CTLA-4 must be delivered in order to control these stimulatory signals. T cells are activated by signals from TCR and other molecules such as CD28, LFA-1, CD2, CD27, and CD40. Human T cells inactivated in a negative environment express CD148 as a receptor-type PTP (R-PTP) that regulates the interaction between positive and negative signals. The protein tyrosine kinases (PTK4) and the protein tyrosine phosphatases (PTP) are crucial for the interaction between positive and negative signals. CD148 binding to a specific mAb increased the proliferation of T cells activated by anti-CD3 mAbs [88,89]. It has been shown in some studies that Jurkat cells do not contain CD148 [88], our cell surface staining shows that although low, it expresses CD148 on cell surface.

Moreover, the expression of this molecule was higher in C7 cells. KO pool with puromycin selection was slightly higher than its control (Fig.4-27.A). The second time staining confirmed the results, and the cell surface expression of CD148 was more elevated in KO C7 single clonal cell and KO pool of cell (Fig.4-27.B). Functioning as a

negative regulator of T cells, this over expression could be related to the absence of LRBA protein, and it could be a potential target in monitoring patients with LRBA deficiency.

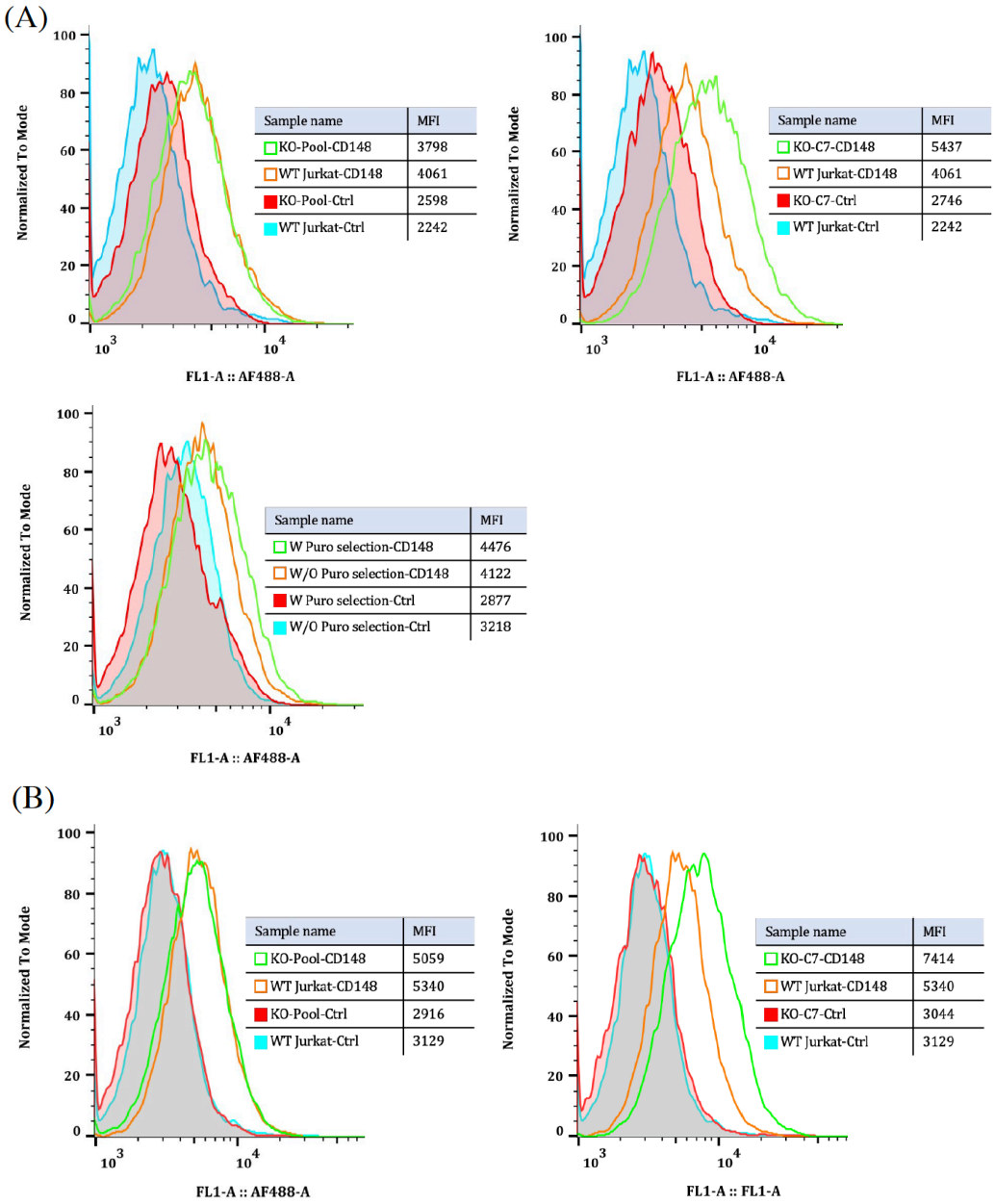

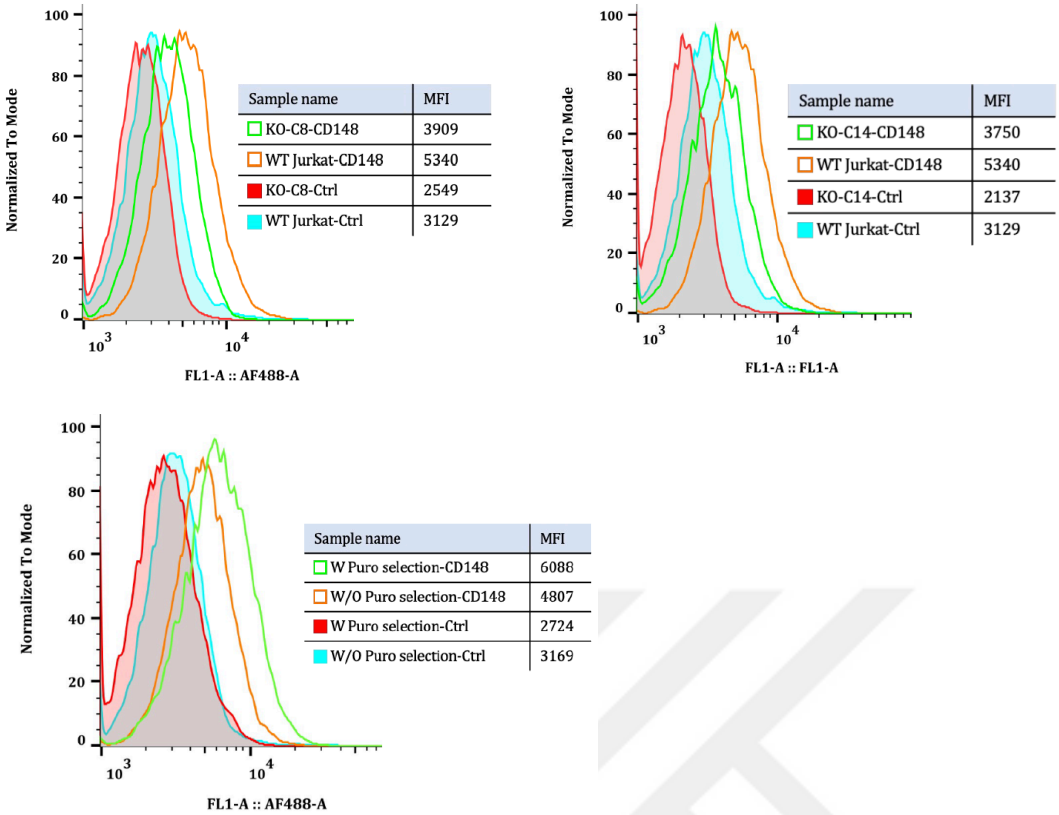

Figure 4-27. CD148 staining of all LRBA KO cells. A) First trial. B) the Second trial. WT and KO cells were stained with primary anti-hCD148 followed by secondary AF488-anti-mouse IgG antibody. As control the cells were only stained with secondary antibody.

4.3.3. CD154 (CD40L)

T-helper cell and B cell cognate interactions are required for T-cell-dependent (TD) humoral immune responses. CD40L, a member of the tumor necrosis factor (TNF) gene family, is a key component of this interaction [90]. In an antigen presenting cell-independent model and in the presence of TCR/CD3 and CD28 ligation, it was shown that IL-4 production in $CD4^+$ cells is mainly governed by CD40L upregulation on T cells [91]. Another study demonstrated that CD40/CD40L interaction is required for switching from IgM to other Ig isotypes, and patients lacking CD40L, though having a normal level of circulating IgM and IgD, lack the expression of IgA or IgE [92]. Since LRBA deficient patients also have an unbalanced distribution of Ig isotypes, CD40L level could correlate

with LRBA protein. As flow cytometry results demonstrate, WT Jurkat has two separate populations (negative and positive) regarding cell surface expression of CD40L, and the same pattern applies to the KO pool of cells. C7 cells, which are totally positive, seem to be selected from the positive population of WT Jurkat, and this feature is independent of the absence of LRBA protein (Fig.4-28).

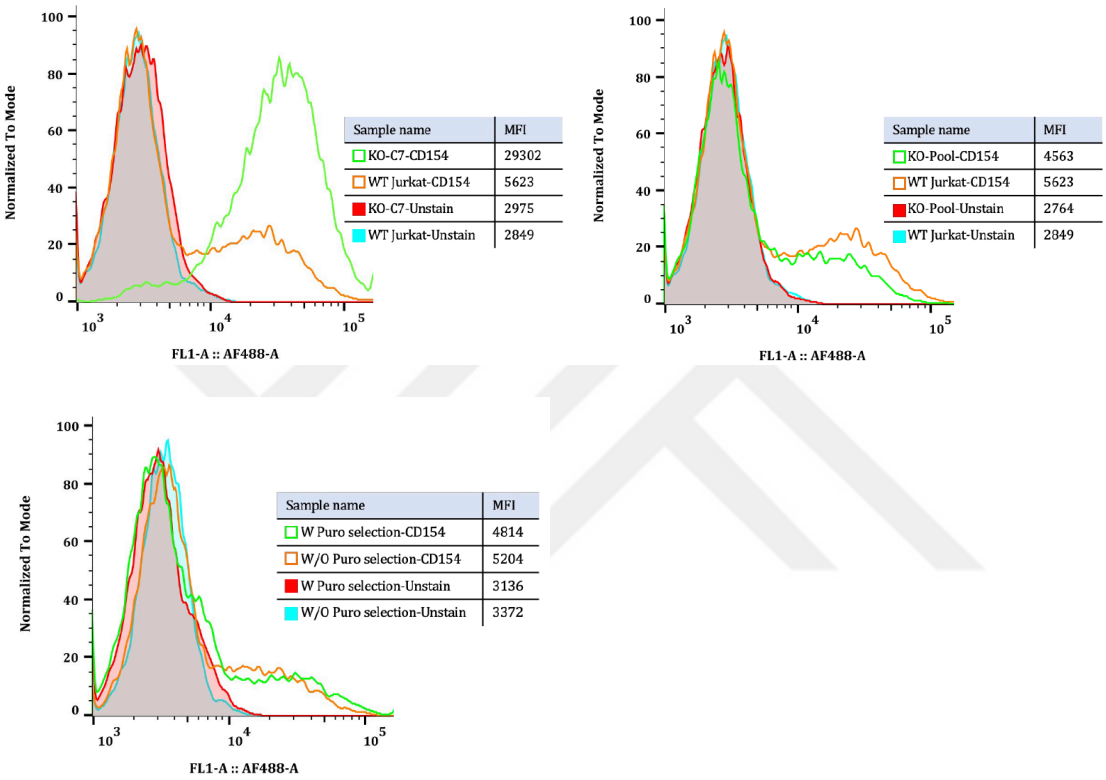

Figure 4-28. CD154 staining of all LRBA KO cells. WT and KO cells were stained with AF488-anti-hCD154 antibody and as control unstained cells were used.

4.3.4. CD134

It has been established that OX40 (CD134), a member of the tumor necrosis factor receptor superfamily (TNFR) superfamily, is a costimulatory molecule that promotes differentiation, proliferation, and long-term survival of effector T cells following activation.

Furthermore, it inhibits the suppressive activity of regulatory T cells, which contributes to tumor cell resistance to T cell immunity [93]. According to the function of CD134, its upregulation could have a role in suppressing regulatory T cells in LRBA deficient patients. However, flow cytometry results revealed that this protein's expression was upregulated in C7 cells while WT and KO pools were CD134 negative (Fig.4-29).

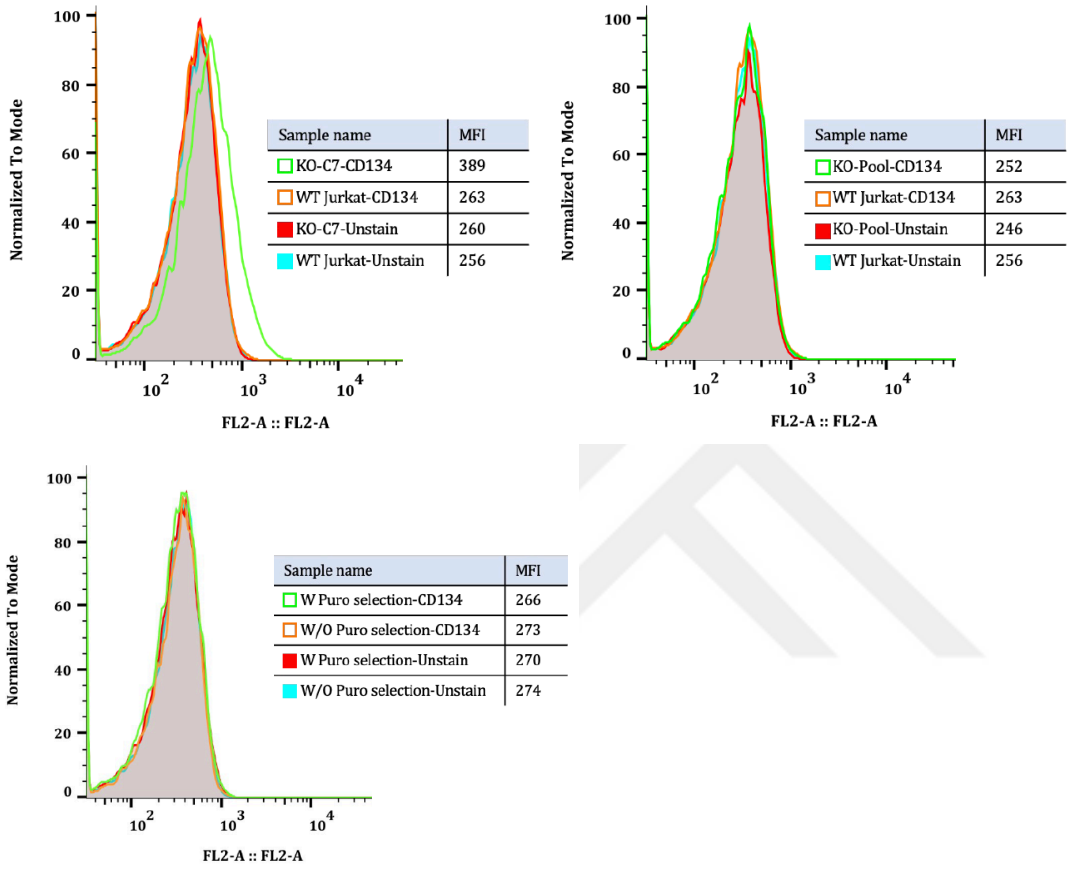

Figure 4-29. CD134 cell surface staining of all LRBA KO cells. WT and KO cells were stained with PE-anti-hCD134 antibody and as control unstained cells were used.

4.3.5. A33

A33 is a single-pass transmembrane glycoprotein in the immunoglobulin superfamily, which may function in cell-cell adhesion and signaling [94]. The upregulation in C7 cells seen in MS results was confirmed in flow cytometry, but in the KO pool, the increase was not as significant as in C7 cells (Fig.4-30).

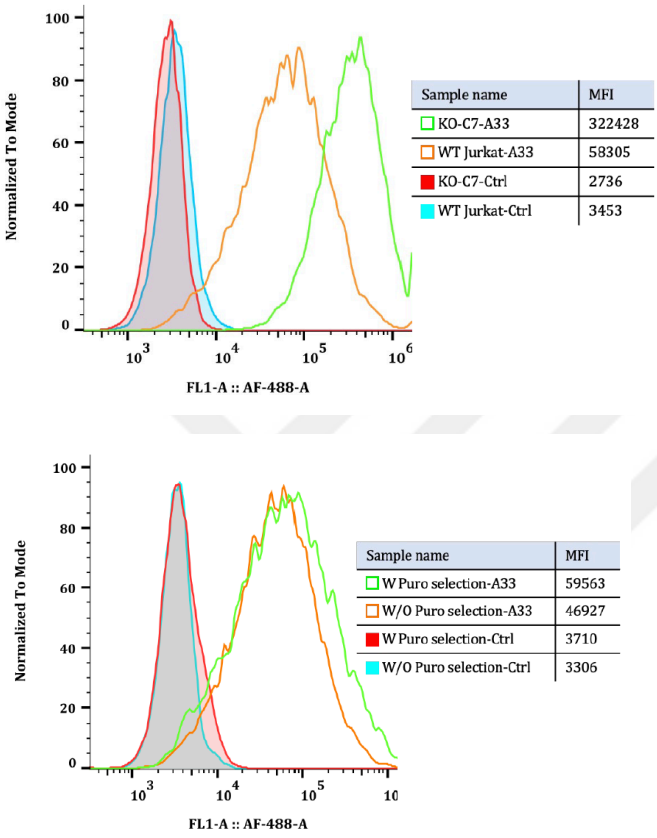

Figure 4-30. A33 cell surface staining of LRBA KO cells. WT and KO cells were stained with primary anti-hA33 antibody followed by secondary AF488-anti-goat IgG. As control cells were stained only with secondary antibody.

4.3.6. CD70

In addition to being the only ligand for CD27, CD70 has also been linked to the proliferation, differentiation, and development of antigen-specific T cells in the gut mucosa, as well as the development of Treg cells in the thymus, where it is located. It has been shown in a recent paper that CD70 is upregulated on activated T cells and inhibits

inflammatory T cell responses by bypassing immune checkpoints [95]. Having an inhibitory function, its upregulation in C7 could be a kind of compensation for CTLA-4 absence.

According to flow cytometry results, Jurkat cells express a very low level of CD70, and upregulation was only seen in C7 cells and not in the KO pool (Fig. 4-31). However, there might be benefits in following up on this receptor in patient cells for more studies.

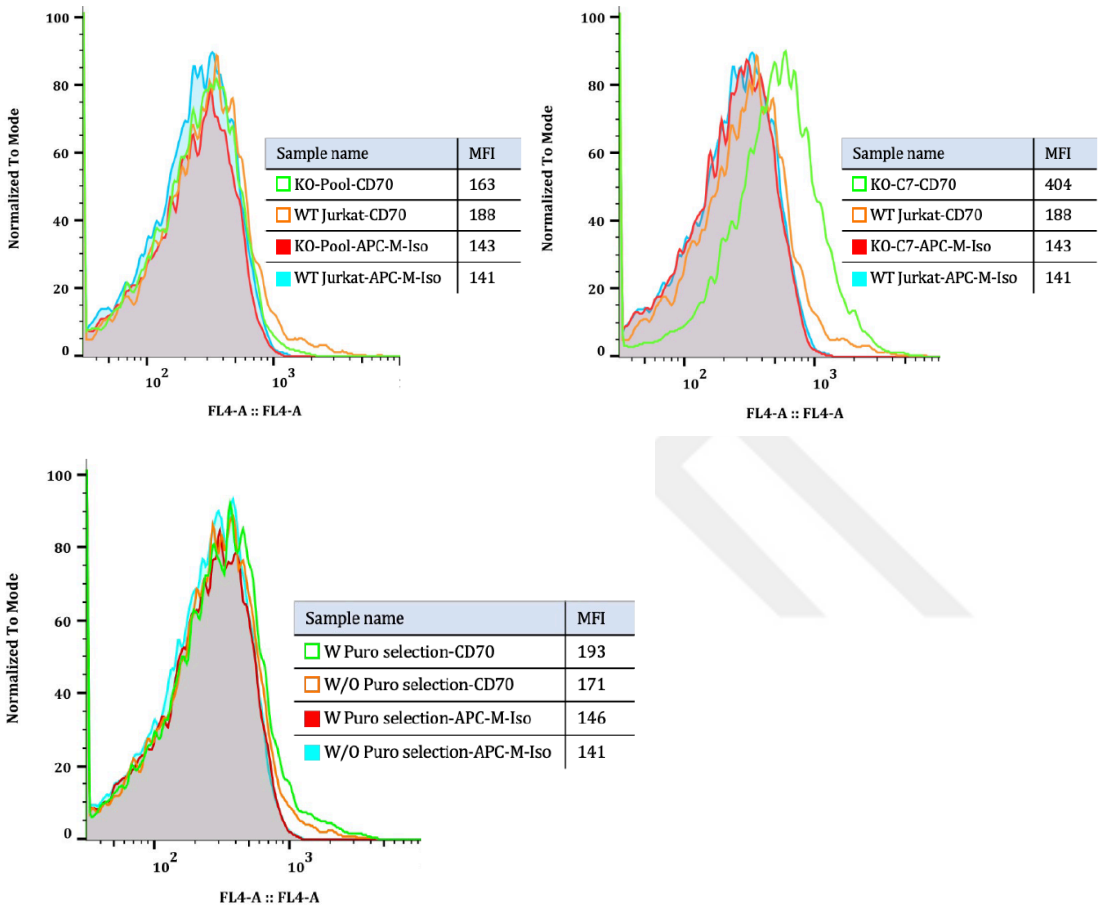

Figure 4-31. CD70 cell surface staining of LRBA KO cells. WT and KO cells were stained with APC-anti-hCD70 antibody. As control cells were stained with APC-mouse IgG isotype ctrl.

4.4. Screening the activation state of LRBA KO cells

CD148, CD154, CD70, and CD134 are among receptors that are upregulated in activated T cells. This made us curious to check other T cell activation markers like CD25 and CD69 in these cells. As shown in figure 4-32, C7 is negative for both CD25 and CD69.

KO pool with puromycin selection is slightly high for CD69 but negative for CD25. Thus, it seems that the upregulation of these receptors is not due to the activation of these cell lines.

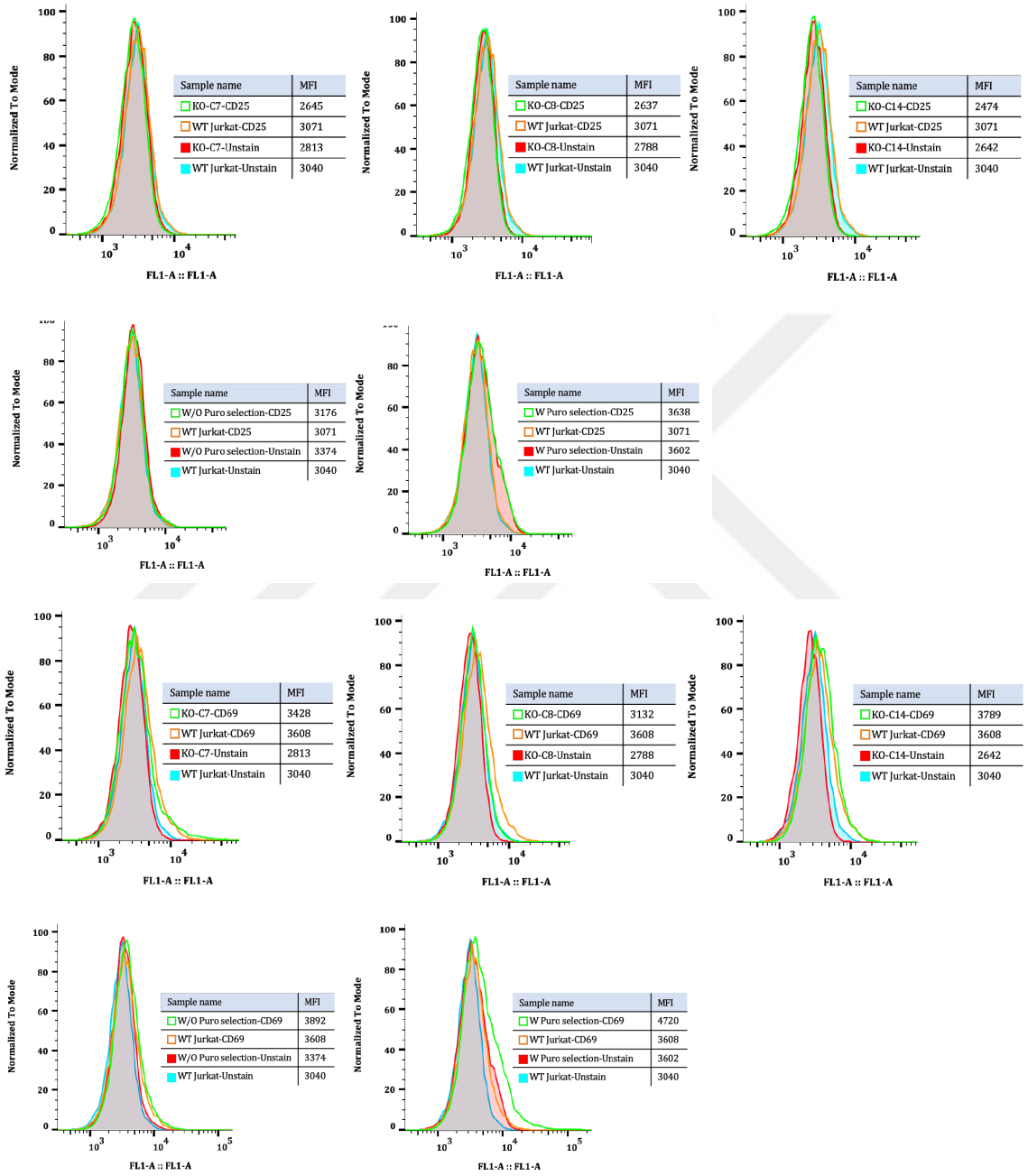

Figure 4-32. CD25 and CD69 cell surface staining for all LRBA KO cells. WT and KO cells were stained with FITC-anti-hCD25 or FITC-anti-hCD69 antibodies and as control unstained cells were used.

4.5. CTLA-4 overexpression in WT Jurkat and C7 cell line

WT Jurkat cells express endogenous CTLA-4 at a very low level, and this amount was even lower in C7 and pool LRBA KO cells (Fig.4-33). To complete our model cell for future studies, WT Jurkat and C7 were lentivirally infected with LegoiG2p-CTLA-4 plasmid to overexpress full-length CTLA-4 in these cell lines. As a control, both cell lines were infected with LegoiG2p empty plasmid. After puromycin selection, GFP percentage was checked for transduction efficiency, and all cells were more than 98% GFP positive (Fig.4-34). As expected, CTLA-4 MFI significantly decreased in the C7-CTLA-4 cell line compared to WT-CTLA-4, indicating LRBA's role in CTLA-4 rescue from lysosome degradation [25] (Fig.4-35).

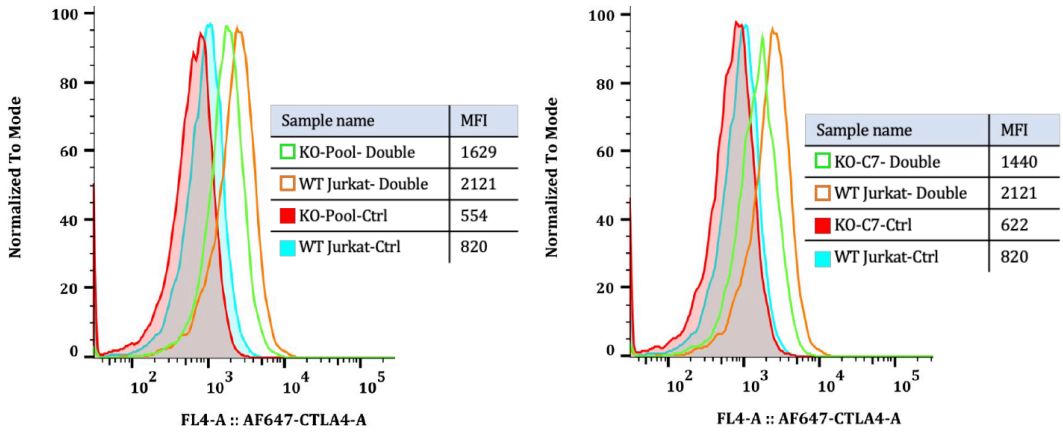

Figure 4-33. CTLA-4 endogenous expression in WT and LRBA KO cells. WT and KO cells were intracellularly stained with primary anti-hCTLA-4 antibody followed by secondary AF647-anti mouse IgG antibody. As control cells were only stained with secondary antibody.

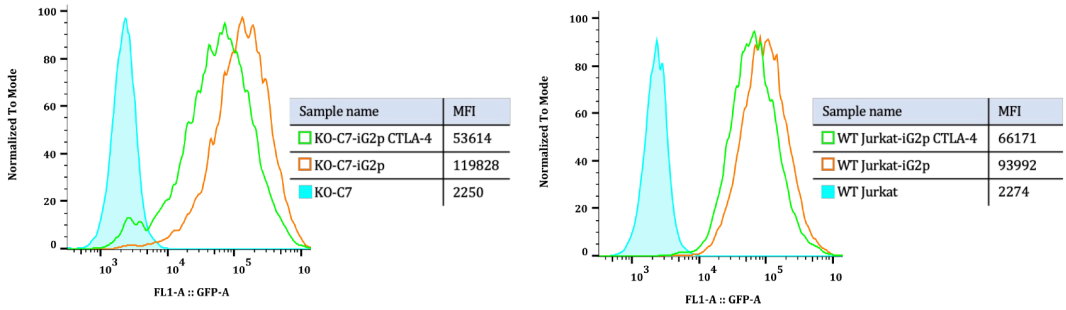

Figure 4-34. GFP expression of WT Jurkat and C7 transduced cells. Transduction efficiency was verified by GFP percentage of infected cells.

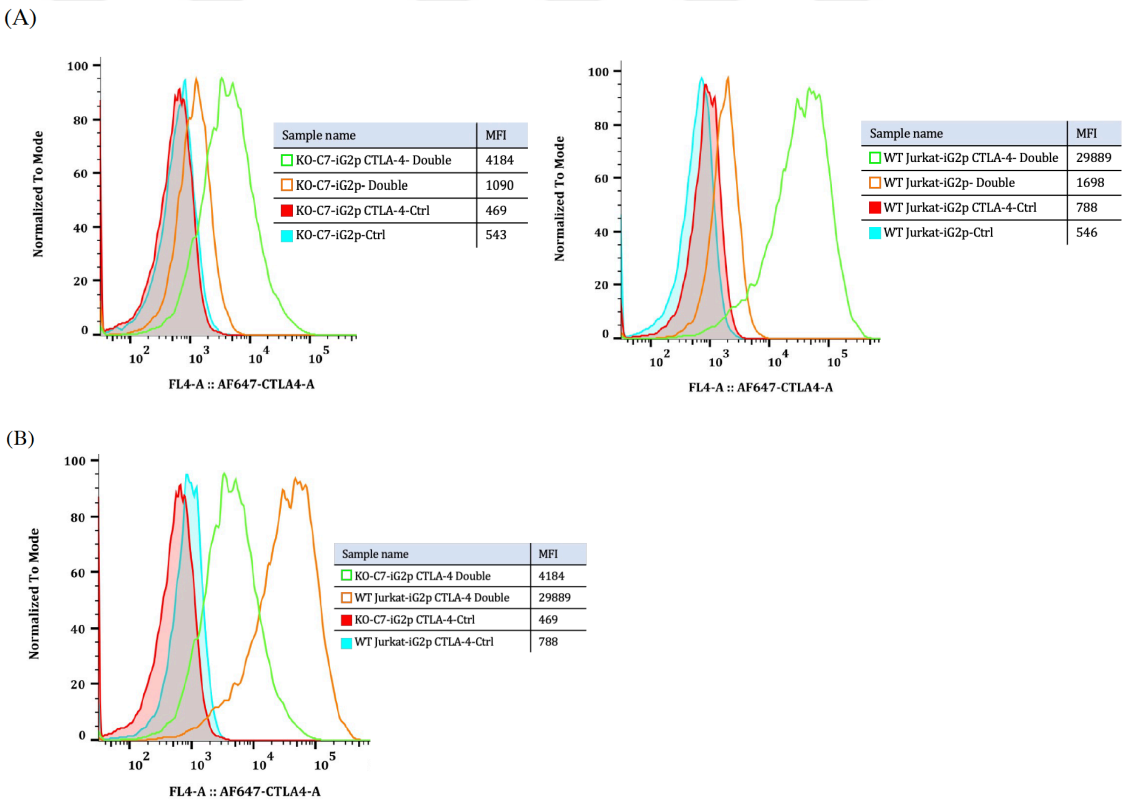

Figure 4-35. CTLA-4 total expression in WT Jurkat and C7 CTLA-4 overexpressing cells. The CTLA-4 intracellular staining was performed with primary anti-hCTLA-4 antibody followed by secondary AF647-anti mouse IgG antibody. As control cells were only stained with secondary antibody. Double: Primary and Secondary antibody staining. Ctrl: Only secondary antibody staining. A) C7-iG2p CTLA-4 compared to C7-iG2p and WT-

iG2p CTLA-4 compared to WT-iG2p. B) C7-iG2p CTLA-4 (green line) compared to WT-iG2p CTLA-4 (orange line).

5. DISCUSSION

As a member of the Beige and Chediak-Higashi (BEACH) protein family, LRBA is involved in vesicle trafficking and exocytosis within the cell. As a result of biallelic LRBA mutations, patients will develop recurrent infections and autoimmune disorders as a result of LRBA deficiency. There is no complete understanding of the underlying cause of the disorder, but it is believed that LRBA is key because it recycles CTLA-4 and shuttles membranes [60,96].

In this study we generated a cell line model to investigate cell surface proteins that are directly or indirectly interacting with LRBA protein. We used the Jurkat cell line for this purpose which is a T cell line and has the majority of signaling pathways necessary for T cell activation and responses, intact. We used CRISPR/Cas9 induced gene editing to target three different exons in the LRBA gene. Exon42 targeted cells showed the best KO efficiency, and these mutant cells were used to generate single cell clones. Among the screened single cell clones, C7, C8 and C14 were verified to be LRBA negative through flow cytometry, western blot, T7E1 assay and sequencing. To discover differentially expressed proteins on the surface of WT and C7, biotinylation assay was performed and cell surface proteins of both cell lines were isolated for mass spectrometry analysis. Proteins identified with high confidence in MS analysis, in WT and C7 lines, where compared through a statistical test to verify proteins that are significantly upregulated or downregulated in LRBA KO cells.

Flow cytometry analysis was performed to verify the proteins that are upregulated or downregulated in LRBA KO cells. All KO single clonal cells and pools were included in this analysis. However, the results from the C8 and C14 clones were not conclusive as it was not clear if the observed differences were due to LRBA absence or an artefact of the single cell cloning procedure. In addition, lentivirally generated CRISPR/Cas9 edited KO cells were continuously expressing Cas9 protein and likely off-target effects may be influencing observed phenotypes after keeping cells in culture for the duration of the experiment. Therefore, we made new KO pool cell line using the Neon transfection

method. Looking at the expression level of studied proteins in Neon transfected KO pools, along with WT and C7 seems a better approach. Table 5-1 summarizes the overall result of the studied receptors and their expression levels in LRBA positive and negative cell lines.

Among downregulated and upregulated proteins CD3 and CD4 were downregulated in not only in clone C7 but also in LRBA KO Neon transfected cell pools. An independent study of peripheral blood mononuclear cells from five patients with a homozygous mutation in the LRBA gene showed that, while three had normal levels of CD3 expression, two had higher and one had lower values than the normal range [52]. In another report, three of 19 LRBA deficient patients had reduced CD3 positive T cell counts, and one had an increase [42]. It is likely that the level of CD3 protein on the cell surface of T cells may be influencing TCR signaling and causing developmental or phenotypic defects that alter the percentage of T lymphocytes in these patients.

Different studies have investigated the effect of LRBA deficiency on CD4 levels. They show that for some LRBA deficient patients, there was a decrease in CD4 positive T cells [52,42,60,97], however, they have a normal response to stimuli compared to healthy donors [97]. These studies show that, the decrease we see in CD3 and CD4 in LRBA KO cells could be related to the absence of LRBA. However, more analysis is needed to confirm this finding and to reveal the molecular mechanism behind it.

PVRIG, which has a role in suppressing lymphocyte cytotoxic activity, might be an interesting receptor for further investigations. The whole protein level was relatively decreased in all the LRBA KO cell lines; however, it was not verified in the three LRBA deficient patients that was tested. If in fact LRBA is responsible for maintaining surface levels of PVRIG, it may be physically interacting with the cytoplasmic tail of the PVRIG protein, as it does with CTLA4. Further protein-protein interaction studies and searches for conserved interaction motifs could shed light to this hypothesis.

The phenotypes observed in LRBA deficient patients may not necessarily be recapitulated in mutant cell lines [98]. Also, not all LRBA mutations result in the same phenotype. An example would be the unexpected normal levels of CTLA-4 expression, reported in a LRBA deficient patient. The observed autoimmunity in this patient was linked to the elevated level of Th17 cells in this patient that shows CTLA-4 loss is not the only

requirement for the observed autoimmunity in LRBA deficient patients [96]. The normal CTLA-4 expression and T-reg cell function suggest that other proteins (perhaps within the PH-BEACH domain containing protein family) may compensate for the absence of LRBA and result in CTLA-4 shuttling that is required for T-reg function. Therefore, to verify one of these receptors as a biomarker in LRBA-deficient patients, they must be tested in a larger cohort of patients.

	C7	C8	C14	Pool
CD3	↓↓	↑	↑	↓↓
CD4	↓↓	↑	↑	↓↓
CD1d	↓↓	↑	↑	≅
NOTCH3	↓	≅	≅	≅
PVRIG (Surface)	↓	≅	≅	≅
PVRIG (Whole)	↓	↓	↓	↓
Sema7A	↓	≅	≅	≅
CD53	≅	↓	↓	↑
CD148	↑	↓	↓	↑
CD154	↑↑	_	_	≅
CD134	↑	_	_	≅
A33	↑↑	_	_	↑
CD70	↑	_	_	≅

Table 5-1. Summary of studied receptors in LRBA⁻ cells and their relative expression level compared to LRBA + cells. ↑: higher expression than control. ↓: lower expression than control. ≅: almost similar to control. Blue highlighted is downregulated and yellow is upregulated proteins according to MS analysis

For future studies, the expression of the identified receptors should be investigated in other LRBA KO cell lines and larger groups of patients. To verify that the variation seen in the expression level of these receptors is due to the absence of LRBA, it is important to rescue these defects through the overexpression of LRBA protein in these KO cell lines. Additionally, RNA sequencing could give a broader understanding of total differentially expressed mRNAs in LRBA KO cells. The study of different interleukins or cytokines in the presence or absence of stimulation in LRBA positive and negative cells would be beneficial in discovering new common biomarkers for LRBA deficient patients.

Our CTLA-4 overexpressing WT or KO cells is expected to be a good model for structural studies identifying the residues and post-translational modifications necessary for the interaction between LRBA and CTLA-4.

6. REFERENCE

1 Kerr WG, Heller M, Herzenberg LA. Analysis of lipopolysaccharide-response genes in B-lineage cells demonstrates that they can have differentiation stage-restricted expression and contain SH2 domains. *Proc Natl Acad Sci U S A* 1996; **93**: 3947–3952.

2 Takeuchi K, Wood H, Swank RT. Lysosomal elastase and cathepsin G in beige mice: Neutrophils of beige (chediak-higashi) mice selectively lack lysosomal elastase and cathepsin G. *J Exp Med* 1986; **163**: 665–677.

3 Faigle W, Raposo G, Tenza D, Pinet V, Vogt AB, Kropshofer H *et al.* Deficient peptide loading and MHC class II endosomal sorting in a human genetic immunodeficiency disease: The Chediak-Higashi syndrome. *J Cell Biol* 1998; **141**: 1121–1134.

4 Barrat FJ, Le Deist F, Benkerrou M, Bousso P, Feldmann J, Fischer A *et al.* Defective CTLA-4 cycling pathway in Chediak-Higashi syndrome: A possible mechanism for deregulation of T lymphocyte activation. *Proc Natl Acad Sci U S A* 1999; **96**: 8645–8650.

5 Newlon MG, Roy M, Morikis D, Hausken ZE, Coghlan V, Scott JD *et al.* The molecular basis for protein kinase A anchoring revealed by solution NMR. *Nat Struct Biol* 1999; **6**: 222–227.

6 Colledge M, Scott JD. AKAPs: From structure to function. *Trends Cell Biol* 1999; **9**: 216–221.

7 Wang J-W, Howson J, Haller E, Kerr WG. Identification of a Novel Lipopolysaccharide-Inducible Gene with Key Features of Both a Kinase Anchor Proteins and chs1/beige Proteins. *J Immunol* 2001; **166**: 4586–4595.

8 Wang JW, Gamsby JJ, Highfill SL, Mora LB, Bloom GC, Yeatman TJ *et al.* Deregulated expression of LRBA facilitates cancer cell growth. *Oncogene* 2004; **23**: 4089–4097.

9 Cullinane AR, Schäffer AA, Huizing M. The BEACH Is Hot: A LYST of Emerging Roles for BEACH-Domain Containing Proteins in Human Disease. *Traffic* 2013; **14**: 749–766.

10 Jaramillo CM, Trujillo-Vargas CM. LRBA in the endomembrane system. *Colomb Med* 2018; **49**: 236–243.

11 Medrihan L, Rohlmann A, Fairless R, Andrae J, Döring M, Missler M *et al.* Neurobeachin, a protein implicated in membrane protein traffic and autism, is required for the formation and functioning of central synapses. *J Physiol* 2009;

587: 5095–5106.

12 Nagle DL, Karim MA, Woolf EA, Holmgren L, Bork P, Misumi DJ *et al.* Analysis of the Complete. 1996; **14**: 307–311.

13 Gebauer D, Li J, Jogl G, Shen Y, Myszka DG, Tong L. Crystal structure of the PH-BEACH domains of human LRBA/BGL. *Biochemistry* 2004; **43**: 14873–14880.

14 Burgess A, Mornon JP, De saint-basile G, Callebaut I. A concanavalin A-like lectin domain in the CHS1/LYST protein, shared by members of the BEACH family. *Bioinformatics* 2009; **25**: 1219–1222.

15 Lemmon MA. Pleckstrin homology domains: Not just for phosphoinositides. *Biochem Soc Trans* 2004; **32**: 707–711.

16 Lemmon MA. Phospholipids : Regulators of Membrane Traffic and Signalling. *Biochem Soc Trans* 1999; **27**: Part 4.

17 Rebecchi MJ, Scarlata S. Pleckstrin homology domains: A common fold with diverse functions. *Annu Rev Biophys Biomol Struct* 1998; **27**: 503–528.

18 Jogl G, Shen Y, Gebauer D, Li J, Wiegmann K, Kashkar H *et al.* Crystal structure of the BEACH domain reveals an unusual fold and extensive association with a novel PH domain. *EMBO J* 2002; **21**: 4785–4795.

19 Li D, Roberts R. WD-repeat proteins: Structure characteristics, biological function, and their involvement in human diseases. *Cell Mol Life Sci* 2001; **58**: 2085–2097.

20 Smith TF, Gaitatzes C, Saxena K, Neer EJ. The WD repeat: A common architecture for diverse functions. *Trends Biochem Sci* 1999; **24**: 181–185.

21 Gámez-Díaz L, Grimbacher B. Immune checkpoint deficiencies and autoimmune lymphoproliferative syndromes. *Biomed J* 2021; **44**: 400–411.

22 McCoy KD, Le Gros G. The role of CTLA-4 in the regulation of T cell immune responses. *Immunol Cell Biol* 1999; **77**: 1–10.

23 Valk E, Rudd CE, Schneider H. CTLA-4 trafficking and surface expression. *Trends Immunol* 2008; **29**: 272–279.

24 Walker LSK, Sansom DM. The emerging role of CTLA4 as a cell-extrinsic regulator of T cell responses. *Nat Rev Immunol* 2011; **11**: 852–863.

25 Lo B, Zhang K, Lu W, Zheng L, Zhang Q, Kanellopoulou C *et al.* Patients with LRBA deficiency show CTLA4 loss and immune dysregulation responsive to abatacept therapy. *Science (80-)* 2015; **349**: 436–440.

26 Gámez-Díaz L, Neumann J, Jäger F, Proietti M, Felber F, Soulas-Sprauel P *et al.* Immunological phenotype of the murine Lrba knockout. *Immunol Cell Biol* 2017; **95**: 789–802.

27 Janman D, Hinze C, Kennedy A, Halliday N, Waters E, Williams C *et al.*

Regulation of CTLA-4 recycling by LRBA and Rab11. *Immunology* 2021; **164**: 106-119.

28 John J. O'Shea ,William E. Paul. Mechanisms underlying lineage commitment and plasticity of helper CD4+ T cells Mechanisms underlying lineage commitment and plasticity of helper CD4+ T cells. *Gerontology* 2015; **61**: 515–525.

29 Sallusto F. Heterogeneity of Human CD4+ T Cells Against Microbes. *Annu Rev Immunol* 2016; **34**: 317–334.

30 Inoue T, Moran I, Shinnakasu R, Phan TG, Kurosaki T. Generation of memory B cells and their reactivation. *Immunol Rev* 2018; **283**: 138–149.

31 Rajewsky K. Clonal selection and learning in the antibody system. Nature. 1996; **381**: 751–758.

32 Phan TG, Tangye SG. Memory B cells: total recall. *Curr Opin Immunol* 2017; **45**: 132–140.

33 Shlomchik MJ, Weisel F. Germinal centers. *Immunol Rev* 2012; **247**: 5–10.

34 Biram A, Davidzohn N, Shulman Z. T cell interactions with B cells during germinal center formation, a three-step model. *Immunol Rev* 2019; **288**: 37–48.

35 Amanna, I. J., Carlson, N. E., & Slifka, M. K. Duration of humoral immunity to common viral and vaccine antigens. *The New England journal of medicine* 2007; **357**: 1903-15.

36 Crotty S. T Follicular Helper Cell Biology: A Decade of Discovery and Diseases. *Immunity* 2019; **50(5)**:1132-1148.

37 Tangye SG, Ma CS. Molecular regulation and dysregulation of T follicular helper cells – learning from inborn errors of immunity. *Curr Opin Immunol* 2021; **72**: 249–261.

38 Alroqi, F. J., Charbonnier, L. M., Baris, S., Kiykim, A., Chou, J., Platt, C. D., Algassim, A., Keles, S., Al Saud, B. K., Alkuraya, F. S., Jordan, M., Geha, R. S., & Chatila, T. A. Exaggerated follicular helper T-cell responses in patients with LRBA deficiency caused by failure of CTLA4-mediated regulation. *The Journal of allergy and clinical immunology* 2018; **141(3)**: 1050-1059.

39 Kiykim A, Ogulur I, Dursun E, Charbonnier LM, Nain E, Cekic S *et al.* Abatacept as a Long-Term Targeted Therapy for LRBA Deficiency. *J Allergy Clin Immunol Pract* 2019; **7**: 2790-2800.

40 Azizi G, Mirshafiey A, Abolhassani H, Yazdani R, Ghanavatinejad A, Noorbakhsh F *et al.* The imbalance of circulating T helper subsets and regulatory T cells in patients with LRBA deficiency: Correlation with disease severity. *J Cell Physiol* 2018; **233**: 8767–8777.

41 Goh LK, Huang F, Kim W, Gygi S, Sorkin A. Multiple mechanisms collectively regulate clathrin-mediated endocytosis of the epidermal growth factor receptor. *J*

Cell Biol 2010; **189**: 871–883.

42 Gámez-Díaz L, August D, Stepensky P, Revel-Vilk S, Seidel MG, Noriko M *et al.* The extended phenotype of LPS-responsive beige-like anchor protein (LRBA) deficiency. *J Allergy Clin Immunol* 2016; **137**: 223–230.

43 Revel-Vilk S, Fischer U, Keller B, Nabhani S, Gámez-Díaz L, Rensing-Ehl A *et al.* Autoimmune lymphoproliferative syndrome-like disease in patients with LRBA mutation. *Clin Immunol* 2015; **159**: 84–92.

44 Sophie Mokas JRM, Cristina Garreau M-J, Fournier ´e, Robert F, Arya P, Kaufman RJ *et al.* Uncoupling Stress Granule Assembly and Translation Initiation Inhibition. *Mol Biol Cell* 2009; **20**: 2673–2683.

45 Park MY, Srivastava N, Neelam S, Youngs C. LRBA is Essential for Allogeneic Responses in Bone Marrow Transplantation. *Sci Rep* 2016; **6** : 36568.

46 Ogasawara K, Hamerman JA, Hsin H, Chikuma S, Bour-Jordan H, Chen T *et al.* Impairment of NK cell function by NKG2D modulation in NOD mice. *Immunity* 2003; **18**: 41–51.

47 Roda-Navarro P, Reyburn HT. The traffic of the NKG2D/Dap10 receptor complex during natural killer (NK) cell activation. *J Biol Chem* 2009; **284**: 16463–16472.

48 Khodosh R, Augsburger A, Schwarz TL, Garrity PA. Bchs, a BEACH domain protein, antagonizes Rab11 in synapse morphogenesis and other developmental events. *Development* 2006; **133**: 4655–4665.

49 Hansen TE, Johansen T. Following autophagy step by step. *BMC Biol* 2011; **9**: 2–5.

50 Simonsen A, Birkeland HCG, Gillooly DJ, Mizushima N, Kuma A, Yoshimori T *et al.* Alfy, a novel FYVE-domain-containing protein associated with protein granules and autophagic membranes. *J Cell Sci* 2004; **117**: 4239–4251.

51 Ichimura Y, Waguri S, Sou Y shin, Kageyama S, Hasegawa J, Ishimura R *et al.* Phosphorylation of p62 Activates the Keap1-Nrf2 Pathway during Selective Autophagy. *Mol Cell* 2013; **51**: 618–631.

52 Lopez-Herrera G, Tampella G, Pan-Hammarström Q, Herholz P, Trujillo-Vargas CM, Phadwal K *et al.* Deleterious mutations in LRBA are associated with a syndrome of immune deficiency and autoimmunity. *Am J Hum Genet* 2012; **90**: 986–1001.

53 Wang J, Lockey RF. Lipopolysaccharide-Responsive Beige-like Anchor (LRBA), a Novel Regulator of Human Immune Disorders. *Austin J Clin Immunol* 2014; **1**: 1–9.

54 Repnik U, Stoka V, Turk V, Turk B. Lysosomes and lysosomal cathepsins in cell death. *Biochim Biophys Acta - Proteins Proteomics* 2012; **1824**: 22–33.

55 Van Nierop K, Muller FJM, Stap J, Van Noorden CJF, Van Eijk M, De Groot C.

Lysosomal destabilization contributes to apoptosis of germinal center B-lymphocytes. *J Histochem Cytochem* 2006; **54**: 1425–1435.

56 Yuan XM, Li W, Dalen H, Lotem J, Kama R, Sachs L *et al.* Lysosomal destabilization in p53-induced apoptosis. *Proc Natl Acad Sci U S A* 2002; **99**: 6286–6291.

57 Mukhopadhyay S, Panda PK, Sinha N, Das DN, Bhutia SK. Autophagy and apoptosis: Where do they meet? *Apoptosis* 2014; **19**: 555–566.

58 Cagdas D, Halaçlı SO, Tan Ç, Lo B, Çetinkaya PG, Esenboğa S *et al.* A Spectrum of Clinical Findings from ALPS to CVID: Several Novel LRBA Defects. *J Clin Immunol* 2019; **39**: 726–738.

59 Lo B, Abdel-Motal UM. Lessons from CTLA-4 deficiency and checkpoint inhibition. *Curr Opin Immunol* 2017; **49**: 14–19.

60 Habibi S, Zaki-Dizaji M, Rafiemanesh H, Lo B, Jamee M, Gámez-Díaz L *et al.* Clinical, Immunologic, and Molecular Spectrum of Patients with LPS-Responsive Beige-Like Anchor Protein Deficiency: A Systematic Review. *J Allergy Clin Immunol Pract* 2019; **7**: 2379-2386.e5.

61 Abraham RT, Weiss A. Jurkat T cells and development of the T-cell receptor signalling paradigm. *Nat Rev Immunol* 2004; **4**: 301-308.

62 Gioia L, Siddique A, Head SR, Salomon DR, Su AI. A Genome-wide Survey of Mutations in the Jurkat Cell Line. *BMC Genomics* 2018;**19** : 118117.

63 Snow K, Judd W. Heterogeneity of a Human T-Lymphoblastoid. 1987; **171**: 389–403.

64 Cheng J, Haas M. Frequent mutations in the p53 tumor suppressor gene in human leukemia T-cell lines. *Mol Cell Biol* 1990; **10**: 5502–5509.

65 Marie R, Pedersen JN, Bauer DLV, Rasmussen KH, Yusuf M, Volpi E *et al.* Integrated view of genome structure and sequence of a single DNA molecule in a nanofluidic device. *Proc Natl Acad Sci U S A* 2013; **110**: 4893–4898.

66 Pistillo MP, Tazzari PL, Palmisano GL, Pierri I, Bolognesi A, Ferlito F *et al.* CTLA-4 is not restricted to the lymphoid cell lineage and can function as a target molecule for apoptosis induction of leukemic cells. *Blood* 2003; **101**: 202–209.

67 Uddin F, Rudin CM, Sen T. CRISPR Gene Therapy: Applications, Limitations, and Implications for the Future. *Front Oncol* 2020; **10**.1387.

68 Lino CA, Harper JC, Carney JP, Timlin JA. Delivering crispr: A review of the challenges and approaches. *Drug Deliv* 2018; **25**: 1234–1257.

69 Ran FA, Hsu PD, Wright J, Agarwala V, Scott DA, Zhang F. Genome engineering using the CRISPR-Cas9 system. *Nat Protoc* 2013; **8**: 2281–2308.

70 Raudvere U, Kolberg L, Kuzmin I, Arak T, Adler P, Peterson H *et al.* G:Profiler:

A web server for functional enrichment analysis and conversions of gene lists (2019 update). *Nucleic Acids Res* 2019; **47**: 191–198.

71 Choi H, Larsen B, Lin ZY, Breitkreutz A, Mellacheruvu D, Fermin D *et al.* SAINT: Probabilistic scoring of affinity purificationg-mass spectrometry data. *Nat Methods* 2011; **8**: 70–73.

72 Teo G, Choi H. SAINTexpress : Significance Analysis of INTeractome – Express Version. 2013; June 24 : 2–5.

73 Choi, H., Liu, G., Mellacheruvu, D., Tyers, M., Gingras, A. C., & Nesvizhskii, A. I. Analyzing protein-protein interactions from affinity purification-mass spectrometry data with SAINT. *Current protocols in bioinformatics* 2012, Chapter **8**, Unit8.15.

74 Barber EK, Dasgupta JD, Schlossman SF, Trevillyan JM, Rudd CE. The CD4 and CD8 antigens are coupled to a protein-tyrosine kinase (p56(lck)) that phosphorylates the CD3 complex. *Proc Natl Acad Sci U S A* 1989; **86**: 3277–3281.

75 Martin-Blanco N, Teja DJ, Bretones G, Borroto A, Caraballo M, Screpanti I *et al.* CD3ε recruits Numb to promote TCR degradation. *Int Immunol* 2016; **28**: 127–137.

76 Sommers CL, Dejarnette JB, Huang K, et al. Function of CD3 epsilon-mediated signals in T cell development. *J Exp Med*. 2000;**192(6)**:913-919.

77 Meuer SC, Schlossman SF, Reinherz EL. Clonal analysis of human cytotoxic T lymphocytes: T4+ and T8+ effector T cells recognize products of different major histocompatibility complex regions. *Proc Natl Acad Sci U S A* 1982; **79**: 4395–4399.

78 Doyle, C., Strominger, J. Interaction between CD4 and class II MHC molecules mediates cell adhesion. *Nature* 1987; **330**, 256–259.

79 Brigl M, Brenner MB. CD1: Antigen presentation and T cell function. *Annu Rev Immunol* 2004; **22**: 817–890.

80 Chen X, Wang X, Keaton JM, Reddington F, Illarionov PA, Besra GS *et al.* Distinct Endosomal Trafficking Requirements for Presentation of Autoantigens and Exogenous Lipids by Human CD1d Molecules. *J Immunol* 2007; **178**: 6181–6190.

81 López-López S, Monsalve EM, Romero de Ávila MJ, González-Gómez J, Hernández de León N, Ruiz-Marcos F *et al.* NOTCH3 signaling is essential for NF-κB activation in TLR-activated macrophages. *Sci Rep* 2020; **10**: 1–16.

82 Hosseini-Alghaderi S, Baron M. Notch3 in development, health and disease. *Biomolecules* 2020; **10**: 1–17.

83 Zhu Y, Paniccia A, Schulick AC, Chen W, Koenig MR, Byers JT *et al.* Identification of CD112R as a novel checkpoint for human T cells. *J Exp Med* 2016; **213**: 167–176.

84 Sanchez-Correa B, Valhondo I, Hassouneh F, Lopez-Sejas N, Pera A, Bergua JM *et al.* DNAM-1 and the TIGIT/PVRIG/TACTILE axis: Novel immune checkpoints for natural killer cell-based cancer immunotherapy. *Cancers (Basel)* 2019; **11**: 1–15.

85 Suzuki K, Kumanogoh A, Kikutani H. Semaphorins and their receptors in immune cell interactions. *Nat Immunol* 2008; **9**: 17–23.

86 Czopik AK, Bynoe MS, Palm N, Raine CS, Medzhitov R. Semaphorin 7A Is a Negative Regulator of T Cell Responses. *Immunity* 2006; **24**: 591–600.

87 Dunlock VE. Tetraspanin CD53: an overlooked regulator of immune cell function. *Med Microbiol Immunol* 2020; **209**: 545–552.

88 Tangye SG, Wu J, Aversa G, de VJE, Lanier LL, Phillips JH. Negative regulation of human T cell activation by the receptor-type protein tyrosine phosphatase CD148. *J Immunol* 1998; **161**: 3803–3807.

89 Lin J, Weiss A. The tyrosine phosphatase CD148 is excluded from the immunologic synapse and down-regulates prolonged T cell signaling. *J Cell Biol* 2003; **162**: 673–682.

90 Grewal IS, Flavell RA. The Role of CD40 Ligand in Costimulation and T-Cell Activation. *Immunol Rev* 1996; **1**: 85–106.

91 Blotta MH, Marshall JD, DeKruyff RH, Umetsu DT. Cross-linking of the CD40 ligand on human CD4+ T lymphocytes generates a costimulatory signal that up-regulates IL-4 synthesis. *J Immunol* 1996; **156**: 3133–40.

92 Klaus, S. J., Berberich, I., Shu, G., & Clark, E. A. CD40 and its ligand in the regulation of humoral immunity. *Seminars in immunology* 1994, ***6*(5)**, 279–286.

93 Rothfelder K, Hagelstein I, Roerden M, Blumenstock G, Hofmann M, Nuebling T *et al.* Expression of the Immune Checkpoint Modulator OX40 in Acute Lymphoblastic Leukemia Is Associated with BCR-ABL Positivity. *Neoplasia (United States)* 2018; **20**: 1150–1160.

94 Heath JK, White SJ, Johnstone CN, Catimel B, Simpson RJ, Moritz RL *et al.* The human A33 antigen is a transmembrane glycoprotein and a novel member of the immunoglobulin superfamily. *Proc Natl Acad Sci U S A* 1997; **94**: 469–474.

95 O'Neill RE, Du W, Mohammadpour H, Alqassim E, Qiu J, Chen G *et al.* T Cell–Derived CD70 Delivers an Immune Checkpoint Function in Inflammatory T Cell Responses. *J Immunol* 2017; **199**: 3700–3710.

96 De Bruyne M, Bogaert DJ, Venken K, Van den Bossche L, Bonroy C, Roels L *et al.* A novel LPS-responsive beige-like anchor protein (LRBA) mutation presents with normal cytotoxic T lymphocyte-associated protein 4 (CTLA-4) and overactive TH17 immunity. *J Allergy Clin Immunol* 2018; **142**: 1968–1971.

97 Salami F, Shariati S, Rasouli SE, Delavari S, Tavakol M, Sadri H *et al.* The Effects of Stimulation with PMA/Ionomycin on CD4+ T Cell Proliferation and Surface

CD4 Molecule Modulation of Patients with LRBA Deficiency and CVID with the Unsolved Genetic Defect. *Endocrine, Metab Immune Disord - Drug Targets* 2021; **22**: 539–544.

98 Alkhairy OK, Abolhassani H, Rezaei N, Fang M, Andersen KK, Chavoshzadeh Z *et al.* Spectrum of Phenotypes Associated with Mutations in LRBA. *J Clin Immunol* 2016; **36**: 33–45.

7. APPENDIX

APPENDIX A: Chemicals

Chemicals and Media Components	Supplier Company
2-Mercaptoethanol	Sigma, Germany
Acetic Acid	Merck, Germany
Acid Washed Glass Beads	Sigma, Germany
Acrylamide/Bis-acrylamide	Sigma, Germany
Agarose	peQLab, Germany
Ammonium Persulfate	Sigma, Germany
Ammonium Sulfate	Sigma, Germany
Ampicillin Sodium Salt	CellGro, USA
Bacto Agar	BD, USA
Bacto Tryptone	BD, USA
Boric Acid	Molekula, UK
Bradford Reagent	Sigma, Germany
Bromophenol Blue	Sigma, Germany
Chloramphenicol	Gibco, USA
D-Glucose	Sigma, Germany
Distilled water	Milipore, France
DMEM	PAN, Germany
DMSO	Sigma, Germany
DNA Gel Loading Solution, 5X	Quality Biological, Inc, USA

DPBS	CellGro, USA
EDTA	Applichem, Germany
Ethanol	Riedel-de Haen, Germany
Ethidium Bromide	Sigma, Germany
Fetal Bovine Serum (FBS)	Biological Industries, Israel
Glycerol Anhydrous	Applichem, Germany
Glycine	Applichem, Germany
HEPES	Applichem, Germany
Hydrochloric Acid	Merck, Germany
Isopropanol	Riedel-de Haén, Germany
Kanamycin Sulfate	Gibco, USA
LB Agar	BD, USA
LB Broth	BD, USA
L-Glutamine	Hyclone, USA
Liquid nitrogen	Karbogaz, Turkey
Magnesium Chloride	Promega, USA
Methanol	Riedel-de Haen, Germany
Penicillin-Streptomycin	Sigma, Germany
Phenol-Chloroform-Isoamylalcohol	Amersco, USA
PIPES	Sigma, Germany
Potassium Acetate	Merck, Germany
Potassium Chloride	Fluka, Germany
Potassium Hydroxide	Merck, Germany
Protease Tablets (EDTA-free)	Roche, Germany
ProtG Sepharose	Amersco, USA
RNase A	Roche, Germany

RPMI 1640	PAN, Germany
SDS Protein Gel Loading Pack	Fermentas, Germany
SDS Pure	Applichem, Germany
Skim Milk Powder	Fluka, Germany
Sodium Azide	Amresco, USA
Sodium Chloride	Applichem, Germany
SuperSignal Chemiluminescent Substrate	Thermo Scientific, USA
TEMED	Applichem, Germany
Tris Buffer Grade	Amresco, USA
Tris Hydrochloride	Amresco, USA
Triton X100	Promega, USA
Tween20	Sigma, Germany

APPENDIX B: Equipment

Equipment	**Company**
Autoclave	Hirayama,Hiclave HV-110,Japan
Balance	Sartorius, BP221S, Germany
	Schimadzu, Libror EB-3200 HU, Japan
Biomolecular Imager	ImageQuant LAS 4000 mini - GE Healthcare, USA
Cell Counter	Cole Parmer, USA
Centrifuge	Eppendorf, 5415D, Germany
	Hitachi, Sorvall RC5C Plus, USA
CO2 Incubator	Binder,Germany
Deepfreeze	-80oC, Forma,Thermo ElectronCorp.,USA

	-20oC,Bosch,Turkey
Electrophoresis Apparatus	Biogen Inc., USA
	Biorad Inc., USA
Electroporator	Neon Transfection System - Life Technologies, USA
Filter Membranes	Millipore,USA
Flow Cytometer	BDFACSCanto,USA
Gel Documentation	Biorad, UV-Transilluminator 2000, USA
Heater	ThermomixerComfort,Eppendorf,Germany
Hematocytometer	Hausser Scientific,Blue Bell Pa.,USA
Ice Machine	Scotsman Inc., AF20, USA
Incubator	Memmert, Modell 300, Germany
	Memmert, Modell 600, Germany
Laminar Flow	Kendro Lab. Prod., Heraeus, HeraSafe HS12, Germany
Liquid Nitrogen Tank	Taylor-Wharton,3000RS,USA
Magnetic Stirrer	VELP Scientifica, ARE Heating Magnetic Stirrer, Italy
Microliter Pipettes	Gilson, Pipetman, France
	Eppendorf, Germany
Microwave Oven	Bosch,Turkey
pH meter	WTW, pH540 GLP MultiCal, Germany
Power Supply	Biorad, PowerPac 300, USA
Refrigerator	Bosch,Turkey
Shaker Incubator	New Brunswick Sci., Innova 4330, USA
Spectrophotometer	Schimadzu, UV-1208, Japan
	Schimadzu, UV-3150, Japan
Thermocycler	Eppendorf, Mastercycler Gradient, Germany
Vortex	Velp Scientifica,Italy

APPENDIX C: Commercial Kits

Commercial Kit	Company
NucleoSpin Gel and PCR Clean-up	Macherey-Nagel, USA
Plasmid DNA purification (NucleoBond® Xtra Midi / Maxi)	Macherey-Nagel, USA
ZymoPure Plasmid Maxiprep Kit	Zymo Research, USA
Pierce™ Cell Surface Protein Biotinylation and Isolation	Thermoscientific

APPENDIX D: Antibodies

Antibody	Company	Cat. No
FITC Anti-human CD4	Biolegend	317408
FITC Anti-human CD3	Biolegend	317306
PE Anti-human NOTCH3	Biolegend	345405
PE Anti-human CD112R	Biolegend	301503
PE Anti-human CD1d	Biolegend	350305
SEMA7A Monoclonal Anti-body (MEM-150)	Invitrogen	MA1-19203
Anti-human CD148	Biolegend	328702
Anti-human CD134	Biolegend	350003
Anti-human CD53	Biolegend	325703
Anti-human CD154	Biolegend	310815
APC Anti-human CD70	Biolegend	355110
APC Mouse IgG1, κ Isotype Ctrl	Biolegend	400120
FITC Anti-human CD69	Biolegend	310903
FITC Anti-human CD25	Biolegend	356105
FITC Mouse IgG2a, κ Isotype Ctrl (FC)	Biolegend	400209
PE Mouse IgG2a, κ Isotype Ctrl (FC)	Biolegend	400213
PE Rat IgG2a, κ Isotype Ctrl	Biolegend	400507
Anti-vinculin	Biolegend	938401
HRP Goat Anti-rat IgG	Biolegend	405405
β-Actin (13E5) Rabbit mAb	Biolegend	4970
Anti-LRBA	Sigma-Aldrich	HPA023597
Anti-CTLA-4	Biolegend	349902
Anti-rabbit IgG, HRP-linked	Biolegend	7074

Human PVRIG Antibody	R&D SYSTEMS	MAB93651
Alexa Flour 647 Goat Anti-Mouse IgG	Biolegend	405322

APPENDIX E: DNA and Protein Molecular Weight Markers

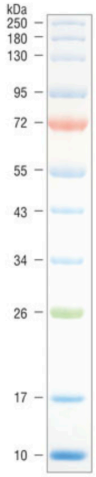

Figure 6-1. Prestained Protein Standard, Broad Range (10–250 kDa) 10–20% Tris-glycine SDS-PAGE Gel (P7719).

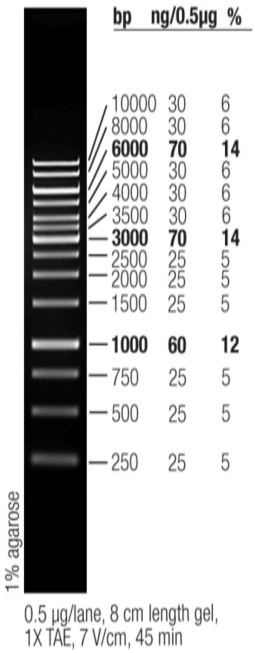

Figure 6-2. Thermo Scientific GeneRuler DNA Ladder Mix (SM0331)

APPENDIX F: Map of Plasmids

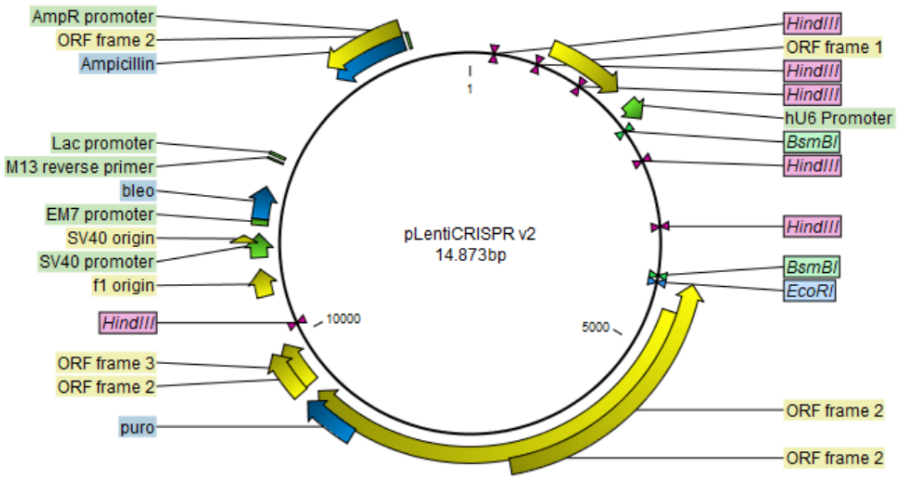

Figure 6-3. The plasmid map of LentiCRISPR V2

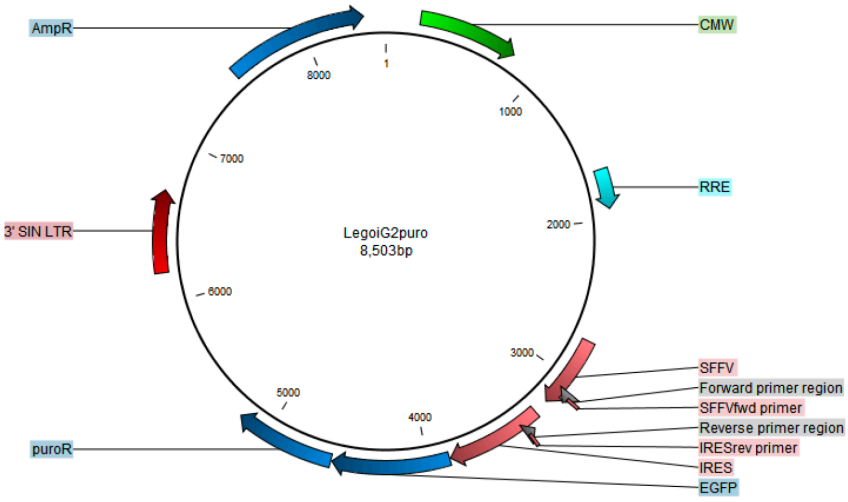

Figure 6-4. Map of Lego-iG2 Puro